The molecular mechanism of condensin in mitotic chromosome formation

Minzhe Tang

University College London

and

The Francis Crick Institute

PhD Supervisor: Frank Uhlmann

A thesis submitted for the degree of

Doctor of Philosophy

UCL

March 2022

Declaration

I, Minzhe Tang, confirm that the work presented in this thesis is my own. Where information has been derived from other sources, I confirm that this has been indicated in the thesis.

Abstract

The rearrangement of interphase chromatin into mitotic chromosomes is crucial for faithful chromosome segregation. Defects in this process may cause chromosome entanglement, decompaction, chromosome bridges during anaphase, and eventually genome instability and cell death. The key player for this process was discovered to be condensin, which is a member of the structural maintenance of chromosome (SMC) complex with a conserved pentameric ring structure. However, the exact role of condensin in mitotic chromosome formation is still under debate. Three prevalent models were proposed to explain the role of condensin in mitotic chromosome condensation, namely the diffusion capture model, the torsion-mediated compaction model, and the loop extrusion model. The diffusion capture model proposes that condensin stabilizes stochastic chromatin interactions, via sequential topological entrapment or condensin-condensin interaction, thereby forming and maintaining chromatin loops that compact chromatin. The torsion-mediated compaction model proposes that condensin introduces and maintains torsional strain that structures chromatin into a series of plectonemes, thereby compacting the chromatin. The loop extrusion model proposes that condensin and/or other DNA translocators enlarges chromatin loops anchored by condensin, thereby shrinking the chromatin lengthwise. Each model has its own weak points that still require further characterization. Therefore, my PhD project focuses on characterizing the condensin-DNA interaction *in vitro* with the hope to provide evidence for one or more of these models. Using purified fission yeast condensin, I reconstituted topological condensin loading onto DNA *in vitro*. I found that topologically loaded condensin can be subsequently unloaded from DNA in an ATP-dependent manner, recapitulating the regulated turnover of condensin on chromatin *in vivo*. Importantly, I discovered that condensin can sequentially topologically entrap two dsDNA molecules *in vitro*. Using single-molecule microscopy, I later confirmed that both the topological DNA loading and second dsDNA capture could be mediated by a single condensin complex. These observations provided a solid

ground for the diffusion capture model of mitotic chromosome assembly by condensin.

Impact Statement

Each of us is formed by trillions of cells that are produced from a single fertilised egg, which needs to undergo thousands if not millions rounds of cell division. Each one of the trillions of cells has to know exactly where it should be, and what it should do, or else we would have defects in our body or even could not be born. On the microscopic scale, each cell in our body is also an incredibly delicate and precise machine that constantly gathers and processes information, adapts to its surroundings, repairs its broken parts, consumes food to generate energy, and duplicates itself only when instructed by others. All of the information is encoded inside the DNA, and, due to the vast information it encodes, is therefore incredibly long compared to the size of our cell. There are about two metres of DNA in length for each of our cells, and that has to be packed inside a nucleus that is only 1 or a few micrometres across. To put into context, this is the same as packing a wire as long as all of the London tube lines combined into a briefcase. What's more, not only do cells have to find a way to fit all the DNA in a tiny space, but they also have to deposit exactly the same amount of it into each of its two daughter cells when they divide. Any entanglements on the DNA would impair the proper deposition of genetic information into the two new cells and cause them to either stop functioning and cause diseases or become uncontrollable and form cancers. As a result, cells have developed a robust system that packs and organises the DNA before they divide. At the heart of this system lies my protein of interest, condensin, which forms an incredibly small ring-like structure compared to the size of the DNA. However, despite decades of research, we still have very limited idea how it contributes to DNA packaging. My PhD project, therefore, focuses on investigating how these little rings are interacting with the DNA and hopefully get a clue on how cells manage to pack everything so quickly and neatly. The results of my research will not only expand our understanding on such basic biological activities, but potentially also shed light on new ways to prevent certain diseases or cancers.

Acknowledgement

I would like to thank Frank Uhlmann for giving me this opportunity to pursue my PhD in his lab, for his brilliance and guidance for me along the way, and for being a very kind person in general. Surely, I could not get this far without his support. I also would like to thank my thesis committee members, Thomas Surrey, Suzana Hadjur, and James Turner, for their outside-the-box views and suggestions on my project. I would also like to thank Maxim Molodtsov, George Pobegalov, and everyone else in the Molodtsov's lab for sharing their collaboration, specialty and reagents for single-molecule imaging. In addition, my life as a PhD student would not be as smooth as it was without the support from the student teams at the Crick and the Crick science and technology platforms (STPs), especially the structural biology STP, the genomics sequencing STP, and the fermentation STP.

I am immensely grateful for all the support from the present and past members of the Chromosome Segregation Lab. Thank you very much Higashi sensei, for always being there (literally), for your innovative idea, and for your sense of humour. Thank you very much Minamino sensei, for all the companying chats and for your sharing of knowledge, Japanese words, and lab reagents, especially G50 spin columns. I couldn't thank you enough, Celine, for basically babysitting everyone in the lab regarding both experimental details as well as logistics, admin, and paperwork. Thank you, Martina and Sam, for sharing so much experience and new techniques regarding the single-molecule microscopy, and for always offering to let me use the when it's free. And I thank everyone else for their company and help with experiments and paper works.

I would like to thank my parents, Xiaoniu and Jiarong, and my grandparents, Zengying and Shurong, for their endeavours over the past 20 years to raise me and to guide me. Without their love, support, and constructive criticism, I could not be who I am now. And I am very grateful for my fiancée, Qingxin, for your love, understanding, and support that help me get back on track whenever I am lost or confused. Having you by my side is the luckiest thing that ever happened to me.

Table of Contents

Table of figures

Abbreviations

ATP	adenosine triphosphate
ADP	adenosine triphosphate
ADP.BeF_3	adenosine triphosphate paired with BeF_3
BSA	bovine serum albumin
cDNA	coding DNA
CSM	complete supplement mixture
CV	column volume
ddH_2O	double distilled water
dNTP	deoxynucleotide triphosphates
dsDNA	double stranded DNA
DTT	1,4- dithiothreitol
EtOH	ethanol
FACS	fluorescence assisted cell sorting
FRET	fluorescence resonance energy transfer
IP	immunoprecipitation
PCR	polymerase
PEG	polyethylene glycol
PMSF	Phenylmethanesulfonylfluoride
pN	pica-Newton
rpm	revolutions per minute
SDS	Sodium dodecyl sulphate
SDS-PAGE	SDS containing (denaturing) polyacrylamide gel electrophoresis
SMC	structural maintenance of chromosome

ssDNA	single stranded DNA
TAE	Tris – Acetate – EDTA (buffer)
TCA	trichloroacetic acid
YNB	yeast nitrogen base
YPD	yeast extract peptone with 2 % (w/v) dextrose
YPR	yeast extract peptone with 2 % (w/v) raffinose

Chapter 1. Introduction

1.1 Introduction to condensin

1.1.1 Mitotic chromosomes are organised by condensin

Each cell must pack an incredible length of DNA into a tiny volume such as the nucleus. This is especially problematic for equal genome segregation during mitosis, where any entanglement between chromatin would prevent separation between chromatids. Each interphase chromatin must be properly folded and distinguished from each other to form mitotic chromosomes, while remaining attached with its sister chromatid counterpart until segregation at anaphase. The formation of mitotic chromosomes was initially modelled as a hierarchical assembly of nucleosomes, where the nucleosomes pack onto each other to form fibres, which then pack themselves into thicker fibres iteratively (Schalch et al. 2005; Woodcock and Ghosh 2010). However, this nucleosome-based hierarchical folding model was challenged by the observation that nucleosome-depleted *Xenopus* extract supported mitotic chromosome reconstitution from mouse sperm DNA, with only slightly larger chromosome widths (Shintomi et al. 2017). Furthermore, the idea of any continuous proteinaceous scaffold that holds the mitotic chromosome in place was challenged by the chromosome micromanipulation experiment showing that nuclease treatment alone was sufficient to break apart the mitotic chromosome (Poirier and Marko 2002). This suggests that the continuity of the mitotic chromosome is maintained by DNA, whereas proteins only maintain ‘crosslinks’ *in cis* on chromatin.

So, what are these ‘crosslinking’ proteins and how do they work? The essential protein factors for chromosome organisation were identified to be the SMC (structural maintenance of chromosome) complexes, including condensin, cohesin, and SMC5/6 complexes (Uhlmann 2016; Jeppsson et al. 2014; Hirano 2012). SMC complexes are structurally conserved ring-shaped protein complexes and are found across all domains of life. While the irreplaceable role of cohesin during mitosis is holding the sister chromatid together until separase

cleavage at anaphase, that of condensin is to organise and individualise chromosomes for efficient chromosome segregation. Consistently, condensin mutations results in uncompacted, entangled chromosomes which lead to mis-segregation of chromosomes in eukaryotic cells or anucleate cells in *E. coli* (Niki et al. 1991; Saka et al. 1994). Temperature-sensitive condensin strains are defective in chromatin length compaction as well as rDNA loop condensation (D'Ambrosio et al. 2008). The *in vitro* reconstitution of mitotic chromosome from *Xenopus* sperm nuclei using purified proteins identified condensin as the essential factor (Shintomi, Takahashi, and Hirano 2015). This confirms the pivotal role of condensin in mitotic chromosome formation.

1.1.2 The overall structure of condensin

Condensin is a pentameric ring-like complex, formed predominantly by its two SMC subunits, Cut3^{Smc4} and Cut14^{Smc2} (The fission yeast subunit names in the main text are followed by the more commonly known budding yeast names in the superscript). Each SMC subunit consists of long coiled coils, flanked by a hinge domain, which dimerises with its other SMC partner, and an ABC-type ATPase head domain, whose dimerization depends on ATP and DNA binding, a process commonly called the "head engagement". The hinge dimerization interactions are believed to be stable, whereas the ATPase heads are often seen separated from their binding partner due to the lack of ATP and/or DNA, as revealed by EM images and AFM images (Anderson et al. 2002; J. K. Ryu et al. 2020). Connecting the two ATPase heads is the condensin kleisin subunit Cnd2^{Brn1}, which consists of N- and C-terminal structured domains that are flanked by a long flexible unstructured linker. The N-terminal domain of the Cnd2^{Brn1} forms a bundle of α-helices, which binds to the coiled coils adjacent to ATPase head of Cut14^{Smc2}. The C-terminal domain of Cnd2^{Brn1} forms a cap-like structure that binds to the bottom of Cut3^{Smc4} ATPase head domain. The unstructured region of the Cnd2^{Brn1} associates with two HEAT repeat subunits Cnd1^{Ycs4} and Cnd3^{Ycg1}, each consisting of a series of helix-loop-helix motifs in parallel to form an overall hook-shaped structure (Figure 1.1).

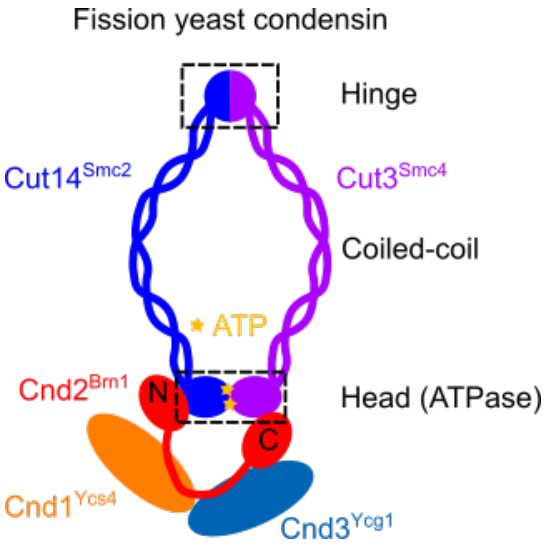

Figure 1.1 Schematic of the overall structure of fission yeast condensin

Although these two HEAT repeat subunits are structurally similar and each bind to both Cnd2^{Brn1} and DNA, the proposed functions for Cnd1^{Ycs4} and Cnd3^{Ycg1} are different. Since Cnd1^{Ycs4} binds to the corresponding position on the kleisin subunit as the cohesin loader Mis4^{Scc2}, it is regarded as the loader of the condensin complex, *i.e.* the factor required for condensin to topologically associate with DNA. On the other hand, Cnd3^{Ycg1} was reported as the anchor position of condensin due to its high affinity to DNA (Kschonsak et al. 2017).

The overall structure of condensin was visualised in many EM and AFM analyses (Anderson et al. 2002; Yoshimura et al. 2002; J. K. Ryu et al. 2020). Structures and movies derived from these studies showed flexible coiled coils of condensin that resulted in an equilibrium between the “open” and “closed” conformations. In the open conformation, the coiled coils of condensin are extended, and the hinge is positioned far apart from the ATPase head. When switching to the closed conformation, condensin zips up and bends the coiled coils, bringing the hinge closer to the ATPase heads (Lee et al. 2020). In contrast to cohesin, whose bending position (also known as the “elbow”) is around the middle of the coiled coils, resulting in the hinge folding directly on top of the ATPase head (Bürmann et al. 2019; Higashi et al. 2020; Shi et al. 2020), the “elbow” of condensin is closer to the hinge, so that the hinge can only be folded back onto the coiled coils of condensin (Lee et al. 2020; Shaltiel

et al. 2021; Lee, Rhodes, and Löwe 2021). The transition between open and closed conformations of condensin seems nucleotide-dependent based on structural comparison between Apo- and ATP-bound condensin ATPase head structures (Lee et al. 2020; Lee, Rhodes, and Löwe 2021). Direct visualisation using AFM confirms that in the presence of ATP, the closed conformation is favoured over the open conformation, though condensin can already shift between open and closed conformations in the absence of ATP (J. K. Ryu et al. 2020).

In contrast to yeast, two or more versions of the condensin complex are present in higher eukaryotes. In *Xenopus*, condensin I contains the homologs of the same subunits as described above, and it is the dominant driver of mitotic chromosome compaction. Condensin II has its own versions of kleisin and HEAT repeat subunits, CAP-H2, CAP-D3, and CAP-G2, and contributes differently to mitotic chromosome condensation (Ono et al. 2003). In *C. elegans*, a variant of condensin complex is essential to the down regulation of gene expression of both sex chromosomes in hermaphrodites (Csankovszki, Petty, and Collette 2009), from which it derives its name, the dosage compensation complex (DCC). Interestingly, in *C. elegans*, the DCC differs from the canonical condensin I by only one subunit. Such a small difference in subunit composition resultes in very different localisation and function between the two complexes: while the DCC exclusively localises to the sex chromosome and functions in suppression of gene expression, condensin I and II bind throughout the genome for chromosome compaction and individualisation in mitosis.

1.2 Models of mitotic chromosome formation

How condensin mediates mitotic chromosome formation remains elusive. Many models are proposed to link condensin behaviour *in vitro* to its function in mitosis *in vivo*, which are described in detail below.

1.2.1 The torsion-mediated compaction model

This model proposes that the supercoils introduced by condensin contribute to DNA packaging and compaction (Hirano 2014). This model proposes that condensin introduces positive supercoiling, potentially in the form of positive crossing of the linker DNA between nucleosomes. As the positive supercoiling spread along the chromosome, the chromatin would start forming plectonemes, which restrains the Brownian motion of the chromatin and thereby compacts the chromosome. The supercoiling activity would also naturally bring the condensin and perhaps also topoisomerase II to the axis of the chromosome, as observed in immunostaining studies (Maeshima and Laemmli 2003).

This model is supported by the observation that topoisomerase I mutation, which impairs relaxation of torsional stress within the chromatin, suppressed the condensin deletion phenotype in *E. coli* (Sawitzke and Austin 2000). This confirms the role of torsional strain in chromosome compaction. In addition, the ATP-dependent positive supercoiling activity of eukaryotic condensin is dependent on the phosphorylation by mitotic kinases such as the mitotic cyclin-dependent kinases and Aurora kinases (Kimura and Hirano 1997; Kimura et al. 1998; 1999; St-Pierre et al. 2009). Moreover, the positive supercoiling also provides a possible solution to the chromosome individualisation and decatenation problem (Baxter et al. 2011): since the supercoiling can only spread *in cis*, condensin cannot accidentally entangle two chromatids. On a different note, since transcription requires negative supercoils to facilitate DNA melting at the promoter region, condensin-dependent positive supercoiling might also provide an explanation to transcription down-regulation during mitosis (Hirano 2014).

The main issue associated with the torsion-mediated compaction model is whether the positive supercoiling activity of condensin is strong enough to reconfigure chromatin *in vivo*, especially in the presence of many other chromatin-associated proteins. Even if condensin can positively supercoil chromatin *in vivo*, how is such torsional stress maintained through the course of mitosis, especially in the presence of abundant topoisomerases? These

questions need to be addressed before considering the torsion-mediated compaction model as a viable mechanism for chromosome compaction.

1.2.2 The loop extrusion model

The loop extrusion model proposes that condensin complexes function as chromatin loop anchors, while condensin or other proteins reel in chromatin fibres to enlarge those loops (Nasmyth 2001; Alipour and Marko 2012). This model avoids the necessity of maintaining a torsional strain on the genomic DNA. At the same time, it keeps the *in cis* spreading property – once started from a single position on a piece of DNA, a chromatin loop can only enlarge by reeling in DNA from the same DNA molecule. Once a piece of chromatin is reeled into the loop, this piece of chromatin is free from entanglement. The result is that chromatin entanglements become concentrated between extruded chromatin loops, which serve as decatenation substrate for topoisomerase II (Charbin, Bouchoux, and Uhlmann 2014).

The loop extrusion model became the spotlight of SMC research in recent years after the observation that condensin and cohesin promote loop formation on naked lambda DNA (Ganji et al. 2018; Terakawa et al. 2017; Davidson et al. 2019). The time-resolved high-C data from chicken cells and *B. subtilis* showing a gradual increase of sequence non-specific long-range contacts as cells progress through cell division was also interpreted as the result of loop extrusion by SMC complexes (Xindan. Wang et al. 2017; Gibcus et al. 2018). Computer simulations confirmed the theoretical feasibility of the loop extrusion model (Banigan et al. 2020). However, it is still debated on whether loop extrusion alone is fast enough to organise mitotic chromosome within the limited time window from prophase till metaphase. In addition, loop extrusion simulations failed to reproduce the experimentally observed reduction of chromatin motility in mitosis compared to interphase, suggesting that loop extrusion alone might not be sufficient to explain mitotic chromosome organisation by condensin (Gerguri et al. 2021).

Another unresolved question regarding the loop extrusion model is whether condensin or other SMC complexes can loop extrude physiological chromatin substrates *in vivo*, especially in the presence of various roadblocks such as transcription and replication machineries. The loop extrusion activities of SMC proteins are only efficiently observed on naked DNA substrates against very low forces (Ganji et al. 2018; Davidson et al. 2019), whereas *in vivo* genomic DNA is coated by histones and other chromatin binding proteins. The high-C data showing juxtaposed chromosome arms in *S. subtilis* was interpreted to support the notion that loop-extruding SMC complexes can bypass large chromatin-bound complexes *in vivo*, such as transcription and DNA replication machineries (Xindan. Wang et al. 2017), despite the lack of evidence for *in vitro* loop extrusion activities of bacterial SMC complexes. Direct observation using single-molecule microscopy suggests that loop-extruding SMC complexes by themselves can bypass obstacles even larger than its ring size *in vitro* (Kong et al. 2020; Pradhan et al. 2021). However, if the obstacle bypass also happens *in vivo* during condensin loop extrusion, this would potentially mean that the DNA loop extruded by condensin is no longer free from entanglement (since condensin can simply bypass the entangled regions of DNA), negating the loop extrusion-dependent chromosome decatenation and individualisation by condensin. Therefore, whether condensin can bypass roadblocks *in vitro* and *in vivo* requires additional investigation.

The observation of loop extrusion activity of single condensin molecules led to the hypothesis that condensin loop extrusion is the sole driving force for chromatin loop formation during mitosis, and that condensin localises to the chromosome axis due to the collision and blockage between converging loop-extruding condensin complexes. However, loop-extruding condensin was observed to bypass each other (E. Kim et al. 2020), questioning the mechanism of condensin axial localisation as explained by loop extrusion. Moreover, though it cannot loop extrude, condensin with impaired DNA binding at the kleisin-Cnd3^{Ycg1} region could still localise to the chromosome axis, as well as compact and individualise chromosomes in the *in vitro* chromosome reconstitution assay (Ganji et al. 2018; Kinoshita, Kobayashi, and Hirano 2015; Kinoshita et al.

2022). This further questions whether loop extrusion by condensin is the sole driving force for condensin localisation to the chromosome axis and for chromosome condensation. As a result, it is likely that axial localisation of condensin employs a different mechanism or requires additional factors.

Another puzzle regarding the loop extrusion model is the mechanism for loop initiation and enlargement. Given their elongated, flexible ring structure and low ATPase activity (Kimura and Hirano 1997; St-Pierre et al. 2009; J. K. Ryu et al. 2020), SMC complexes were thought unlikely to be DNA translocators by themselves. Therefore, initial attempts attributed the drivers of loop enlargement to DNA / RNA polymerases (Lengronne et al. 2004; Busslinger et al. 2017). While transcription and DNA replication might contribute to chromatin loop formation in interphase and S-phase, the mitotic chromosomes formed *in vitro* or *in vivo* do not strictly require these polymerases (Shintomi, Takahashi, and Hirano 2015; Laura Vian et al. 2018). With recent experimental evidence that purified SMC complexes extrude loops in single-molecule experiments, and that such loops are extruded in step sizes close to the size of the SMC ring (J.-K. Ryu et al. 2020; Terakawa et al. 2017), SMC complexes are proposed to drive loop extrusion *in vitro.* Many models have been proposed to explain the loop extrusion activities by SMC complexes (Higashi and Uhlmann 2022). Please see Section 1.3.5 for detailed introductions.

Interestingly, even though condensin and cohesin are structurally very similar complexes, their loop extrusion activities *in vitro* are different. Condensin is a one-sided loop extruder, whereas cohesin is a two-sided loop extruder. In other words, once bound to DNA and initiated loop extrusion, condensin can only reel in DNA from one side (J.-K. Ryu et al. 2020; Kong et al. 2020), whereas cohesin reels in DNA from both sides (Y. Kim et al. 2019; Davidson et al. 2019). So why do these two structurally similar complexes behave differently? Comparing condensin with cohesin, the most significant difference is the loader association to kleisin subunits. This association is transient in case of cohesin, whereas that for condensin is stable (Rhodes et al. 2017; Murayama and Uhlmann 2014; Kimura and Hirano 1997). This raises the possibility that the stability of loader association with the kleisin determines the mode of loop

extrusion (Higashi et al. 2021). Another possibility is that the condensin Ycg1/kleisin module, more commonly referred to as the “safety-belt”, binds DNA so tightly that it might function as a loop anchor (Kschonsak et al. 2017). Then, DNA can only be reeled in or released from the other condensin-DNA contacts during loop extrusion. Consistently, “safety-belt” mutations impaired the ability to anchor the extruded DNA loops by *S. cerevisiae* condensin (Ganji et al. 2018). On the other hand, this model assumes that the counterpart in cohesin, the Scc3/kleisin module, binds DNA less stably, which is not directly confirmed.

1.2.3 The diffusion-capture model

As introduced above, the torsion-mediated compaction model and the loop extrusion model both require active motor activities of SMC complexes to organise chromatin. Such motor activities would be antagonised by all DNA-binding proteins (Kong et al. 2020; Pradhan et al. 2021). Given that SMC complexes are very poor ATPases, only hydrolysing two ATPs per molecule per second, it would be difficult to imagine how mitotic chromosomes can be efficiently formed *in vivo* by torsion-mediated compaction or loop extrusion alone. Furthermore, both of these models fail to explain the formation of condensin clusters that have been observed *in vivo* (Gerguri et al. 2021). An alternative to those proactive models is a more passive model, the diffusion-capture model, which proposes that condensin merely stabilizes the contacts between distant chromatin fragments that arise by Brownian motion, thereby restricting the Brownian motion of the chromatin and eventually condensing the chromatin (Cheng et al. 2015). Condensin could stabilise chromatin contacts through physical DNA binding. At the same time, condensin and cohesin can topologically entrap DNA within their ring-shape structures, which raises the possibility that condensin could stabilize chromatin interactions via topological DNA entrapment (Murayama and Uhlmann 2014; Cuylen, Metz, and Haering 2011).

The diffusion capture model assumes minimal functions from condensin and other SMC complexes. In this model, condensin stabilises chromatin contacts

via either sequential binding to two DNAs or via condensin-condensin interactions between DNA-bound condensin complexes. Nevertheless, this model surprisingly well recapitulates many aspects of the chromatin condensation in mitosis, including terms of degree of compaction, the speed of compaction, the change in chromosome motility (Cheng et al. 2015; Gerguri et al. 2021). Perhaps most importantly, the diffusion-capture model does not require a high ATPase turnover from the SMC complexes to compact chromosome (Cheng et al. 2015). In addition, the association of condensin to chromosome is very dynamic, with a half-life of only three minutes on the chromatin (Thadani et al. 2018). Such a fast turnover would severely impair and delay the chromosome condensation in the loop extrusion model and the torsion-mediated compaction model, since both rely on the processivity of condensin on chromatin.

Due to the randomness of chromatin contacts, it is difficult for individual condensin to distinguish between *cis* and *trans* interactions. Therefore, how can the diffusion-capture model individualise chromosomes from each other, especially during G2 to metaphase, when two sister chromatids are held closely together by cohesin? Computer simulations suggest that given a small bias towards *cis* interactions due to the physical structure of the chromatin polymer, the diffusion-capture model, with a reasonable rate of dynamic turnover, can achieve chromosome individualisation (Cheng et al. 2015). However, the extent to which such simulations reflect the physiological conditions is unclear.

Another missing piece from the diffusion-capture model is the ability of condensin to maintain chromatin contacts. High-C data from different organisms show condensin-mediated chromatin contacts in mitosis (Gibcus et al. 2018; Xindan. Wang et al. 2017). In addition, *in vitro* assays hinted at the ability of condensin to tether two DNAs together (Terakawa et al. 2017). However, the ability of condensin to mediate DNA-DNA interaction was never directly investigated. The related SMC complex, cohesin, was observed to sequentially topologically entrap dsDNA and then ssDNA *in vitro* (Murayama et al. 2018), raising the question whether condensin might also be able to sequentially topologically entrap two DNAs to stabilize chromatin contacts.

1.3 Mechanisms of condensin-DNA interactions

Having introduced three models for how condensin might act in mitotic chromosome formation, I now introduce the currently available evidence of how condensin engages with DNA, that are relevant when discussing distinctions between these models.

1.3.1 The temporal and spatial regulation of condensin binding to chromatin *in vivo*

The temporal localisation of condensin on chromatin has been studied extensively. Generally, as a result of phosphorylation by cyclin-dependent kinase, Polo kinase, and Aurora kinases, condensin is activated and becomes chromatin-bound during mitosis (Kimura et al. 1999; St-Pierre et al. 2009; Nakazawa et al. 2011). In addition, different organisms use slightly different mechanisms for tight temporal control of chromatin association by condensin. In budding yeast, the expression level of the Ycg1 subunit was shown to fluctuate throughout the cell cycle, peaking only at mitosis to support maximum condensin activity (Doughty, Arsenault, and Benanti 2016). In higher eukaryotes, condensin II remains nuclear in interphase, and become chromatin bound as early as prophase. The condensin I complex on the other hand is excluded from the nucleus in interphase and could only access the chromatin after nuclear envelope break down in prometaphase (Hirota et al. 2004; Ono et al. 2004).

While the majority of condensin functions in chromatin compaction and individualisation during mitosis after receiving activating phosphorylation (Aono et al. 2002), a small population of condensin contributes to genome organisation during interphase. In budding yeast, the condensin ChIP-Chip signals revealed unaltered condensin binding sites between interphase and mitosis along chromosome arm regions (D'Ambrosio et al. 2008), hinting at a role of condensin in chromatin organisation throughout the cell cycle. Indeed, condensin depletion causes global deregulation of transcription in both

interphase and mitosis in budding yeast (Lancaster et al. 2021). In fission yeast, the small fraction of condensin that remain chromatin-bound during G2 phase restrains chromatin motility and prevents DNA damage at active transcription sites (Kakui et al. 2020).

The chromatin binding sites of condensin were extensively studied. In budding yeast, condensin localises primarily to centromere regions and the promoter regions of actively transcribed genes, such as the tRNA gene promoters, which form a minimal condensin recruitment sequence (D'Ambrosio et al. 2008; B.-D. Wang et al. 2005). A similar pattern was observed in fission yeast and human cells, whose proper condensin association depends on transcription during mitosis (Sutani et al. 2015). How can a non-sequence-specific DNA binding protein like condensin localise to specific regions of the chromosome? One theory proposes that the open chromatin at the promoters of highly transcribed genes serves as loading sites for SMC proteins. Indeed the loading of cohesin was shown to depend on the histone remodeller, RSC, for both its remodelling activity that opens up an nucleosome-free region as well as its physical recruitment of the cohesin loader, $Mis4^{Scc2}$/$Ssl3^{Scc4}$ (Muñoz et al. 2019; Muñoz, Passarelli, and Uhlmann 2020). Given that condensin also colocalises with the cohesin loader and active gene promoters in budding yeast (D'Ambrosio et al. 2008), it is likely that condensin loading onto chromatin also requires nucleosome-free regions and indeed fission yeast RSC is required for fission yeast condensin loading onto chromosome *in vivo* (Toselli-Mollereau et al. 2016). During mitosis in Chicken DT40 cells, condensin disrupts topologically associated domains (TADs) formed during interphase and promotes long-range interactions by stabilising DNA loops that are apparently randomly positioned along each chromosome arms (Gibcus et al. 2018). Condensin II binds first onto chromatin in prometaphase and stabilises loops that grow to 400 kbp in size in metaphase, thereby compacting the chromatin axially. After nuclear envelope breakdown, condensin I binds to the loops formed by condensin II to create nested loops that further condense the chromatin widths. A similar division of labour between condensin I and II was also observed in *ex vivo* chromosome reconstitution assay using *Xenopus* egg extracts (Shintomi,

Keishi, Hirano, Shintomi, and Hirano 2011), suggesting that such nested loops are probably conserved across higher eukaryotes that harbours both versions of condensin.

1.3.2 Roles of the two HEAT repeat proteins of condensin

Different roles of the two HEAT repeat subunits of condensin were studied in the chromosome reconstitution assay using the *Xenopus* egg extract (Kinoshita, Kobayashi, and Hirano 2015). Condensin lacking CAP-D2 (homolog of Cnd1^{Ycs4}) failed to bind efficiently to the chromatin and assemble the chromosome axis, leaving behind only a mesh of DNA. On the other hand, condensin lacking CAP-G (homolog of Cnd3^{Ycg1}) could dynamically bind to chromatin and assemble a chromosome axis but with somewhat impaired chromosome width compaction. Such phenotype is similar to the chromosome assembled *in vitro* without histones (Shintomi et al. 2017). Taken together, CAP-D2 (Cnd1^{Ycs4}) is responsible for condensin loading onto and localisation to the chromosome axis, while the CAP-G (Cnd3^{Ycg1}) is important for width-wise condensation by an unknown mechanism.

1.3.3 The ATPase of condensin is essential for condensin function

Condensin was shown to hydrolyse ATP in a DNA-dependent manner, implying an interplay between ATPase heads of condensin and DNA (Kimura and Hirano 1997; St-Pierre et al. 2009; Yoshimura et al. 2002). At the same time, the positive supercoiling activity of condensin was highlighted, especially because such activity is dependent on the phosphorylation of condensin complex by mitotic kinases (Kimura and Hirano 1997; St-Pierre et al. 2009). As described earlier, this positive supercoiling activity of condensin was proposed to contribute to genome reorganisation during mitosis (Hirano 2014). Nevertheless, the mechanism of the positive supercoiling remained enigmatic.

The ATPase of condensin is essential for chromatin organisation. In budding yeast, mutations of condensin ATPase impaired its binding to chromatin as well

as chromosome segregation (Thadani et al. 2018; Palou et al. 2018). Mutations in the condensin ATPase altered the turnover of condensin on chromatin, resulting in condensation defects in budding yeast. Consistently, the *in vitro* chromosome reconstitution experiments showed that the ATP-binding mutation prevented condensin binding to chromatin, while the ATP-hydrolysis mutation supported chromatin localisation of condensin but not formation of mitotic chromosomes (Kinoshita, Kobayashi, and Hirano 2015).

ATPase is important for condensin activities *in vivo* and *in vitro*. Among the three proposed models of condensin Section 1.2, the requirement for level of condensin ATPase activity is different. For the loop extrusion model, the condensin population has to traverse the entire lengths of chromatin at least once to form the mitotic chromosome, requiring a high rate of ATP hydrolysis, consistent with calculations from simulations (Higashi et al. 2021). The requirement of ATP hydrolysis for the diffusion capture model is relatively low, since condensin only requires at most two rounds of ATPase cycle to topologically tether between two pieces of chromatin. The ATPase requirement for the torsion-mediated compaction model is very difficult to estimate, due to the lack of molecular details or proposed mechanisms for condensin-mediated supercoiling of DNA or chromatin. Finally, since condensin rapidly turnover on chromatin, the processivity of all three models discussed above is low in general. As a result, the estimated ATPase requirement above represents only a lower bound of the actual ATP hydrolysis requirement for each model,

Two interesting non-lethal condensin ATPase mutations were characterised in human haploid cells (Elbatsh et al. 2019). While the Smc2 L1085V mutation produced fuzzy and seemingly less condensed chromosomes, the Smc4 L1191V mutation produced longitudinally hyper-condensed chromosomes, reminiscent of the phenotypes produced by the condensin II-specific and condensin I-specific depletion in HeLa cells, respectively (Ono et al. 2004). The Smc2 L1085V mutation impairs both DNA compaction and loop extrusion initiation, whereas Smc4 L1191V mutation promotes DNA compaction, even though both mutations reduce the ATPase activity and chromatin recruitment of

condensin (Elbatsh et al. 2019). This suggests that the two ATPase of condensin have different contributions in condensin functions.

Consistent with differences between the two condensin ATPase domains, the two ATPase site on condensin were shown to bind ATP at different stages of the ATPase cycle (Hassler et al. 2019; Lee et al. 2020). Initially, Cnd1^{Ycs4} bridges the two SMC ATPase heads and physically blocks ATPase head engagement. Subsequent ATP binding to the Cut3^{Smc4} disrupts this interaction, allowing the head engagement with Cut14^{Smc2}. The engaged heads now can bind a second ATP molecule, which disrupts the interaction between N-terminus of the kleisin and the coiled coil of Cut14^{Smc2}.

This model is also consistent with the FRET measurement from cohesin DNA loading experiments (Higashi et al. 2020). The cohesin ATPase heads were kept apart by the addition of cohesin loader (counterpart of Cnd1^{Ycs4}), consistent with the loader bridging between ATPase heads in the initial state. Similarly, ATP binding releases the N-terminus of kleisin from Smc3 (counterpart of Cut14^{Smc2}). Taken together, similar subunit rearrangements were observed at the beginning of the ATPase cycles of condensin and cohesin, potentially indicating a universally conserved ATPase cycle for all SMC proteins. However, this model lacks the description of condensin subunit rearrangement in the presence of DNA. So, in the next section, I use the better characterised subunit rearrangements of cohesin DNA loading reaction as a reasonable reference for condensin-DNA interaction during the condensin loading reaction.

1.3.4 Mechanism of condensin loading onto DNA, inferred from cohesin studies

Condensin was found to topologically entrap DNA *in vivo* (Cuylen, Metz, and Haering 2011). However, the mechanism of DNA entry into the condensin ring remained elusive. Recently posted condensin-DNA gripping structures are remarkably similar to cohesin DNA-gripping structures (Shaltiel et al. 2021; Lee, Rhodes, and Löwe 2021; Higashi et al. 2020; Shi et al. 2020), hinting at a

shared loading mechanisms between cohesin and condensin. The DNA loading mechanism of cohesin introduced below can therefore be reasonably extrapolated to condensin.

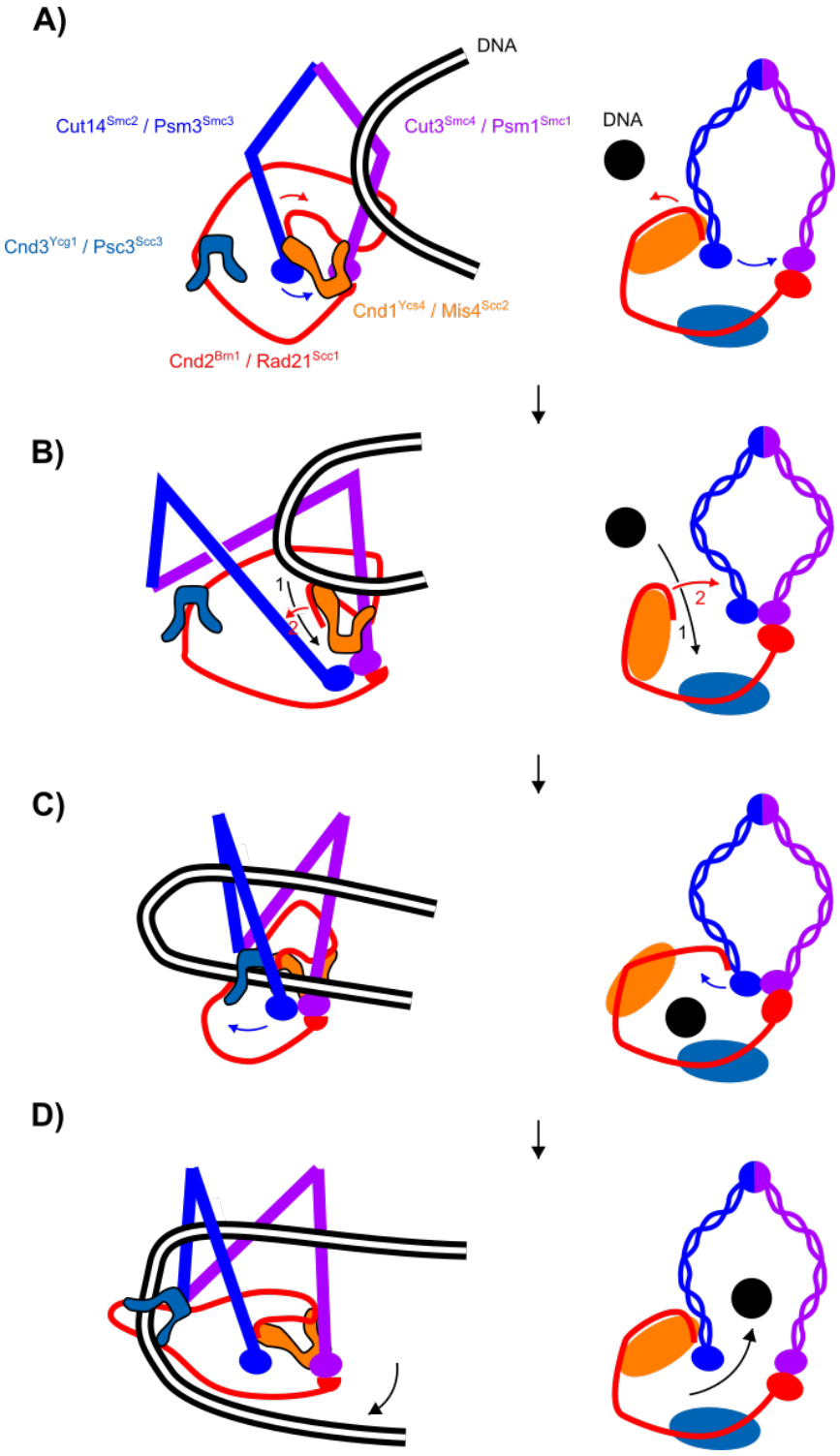

Figure 1.2 Schematic of topological entry mechanism by condensin or cohesin

The left column is the schematic representation that mimics the actual structure. The right column is more abstract and only illustrates the topological relationships between condensin and DNA. The DNA is shown as a black dot to represent a DNA double helix perpendicular to the plane of the illustration.
A) Condensin ring is initially closed. Upon ATP binding, the "N-gate" opens (orange arrow) while the ATPase head engages (blue arrow). The subunits are labelled in a "fission yeast condensin name$^{\text{budding yeast condensin name}}$ / fission yeast cohesin name$^{\text{budding yeast cohesin name}}$" format.
B) DNA passes the "N-gate" (black arrow noted with "1") and then "N-gate" is closed by loader complex (orange arrow noted with "2").
C) Now the gripping state forms. ATP hydrolysis results in head disengagement (blue arrow).
D) The DNA can now pass between the two ATPase head and enter the SMC lumen (black arrow).

To understand the mechanism of DNA loading by cohesin, one must establish where the DNA enters the cohesin ring. Two different models were proposed for cohesin loading onto DNA, namely the hinge-opening model and the kleisin-opening model. The hinge-opening model proposes that cohesin opens its hinge dimerization interface for DNA entry. This model was supported by the genetic studies on interface fusions in budding yeast (Gruber et al. 2006). While the fusion that closed either Smc3-kleisin or kleisin-Smc1 interface was tolerated, the rapamycin-induced closure of hinge resulted in cell lethality. Consistently, after neutralising positive charges at the hinge, cohesin still binds and spreads along the chromatin, but cannot topologically entrap mini-chromosomes *in vivo* (Srinivasan et al. 2018). However, given that cohesin loading depends on ATP hydrolysis (Murayama and Uhlmann 2014), the hinge-opening model lacks a substantial evidence regarding how the hinge opening is coupled to ATP hydrolysis at the ATPase heads.

Alternatively, the kleisin-opening model proposes that the DNA enters the cohesin ring via the interface between N-terminus of kleisin and Smc3 (counterpart of Cut14^{Smc2} in cohesin), also known as the "N-gate" (Higashi et al. 2020). As introduced in Section 1.3.3, ATP binding to the ATPase head opens

the kleisin-Smc3 interface (Figure 1.2 A). The unstructured tail of the kleisin N-terminus (also known as the “N-tail”) guides the incoming DNA towards the ATPase head, gradually bending the DNA as it approaches the ATPase heads (Figure 1.2 B). As the DNA sits on top of the engaged ATPase head, the cohesin loader complex (counterpart of Cnd1^{Ycs4} in cohesin) undergoes substantial conformational changes to close the “N-gate” while simultaneously contacting the engaged heads, forming a positively charged channel that embraces the DNA. The DNA sensor double lysine residues on Smc3 contact both the DNA and the loader. In addition, the hinge is folded down towards the head while also contacting the Scc3 (Ycg1 counterpart in cohesin) that is stacked against the cohesin loader (Figure 1.2 C). After ATP hydrolysis, the ATPase heads disengage, and the loader is free to return to its original extended conformation. Now the DNA is free to pass between the ATPase heads and into the cohesin lumen, completing topological entry (Figure 1.2 D). This model provides a mechanism that couples ATP-hydrolysis with topological DNA entry for cohesin, with experimental evidence from cohesin supporting the outlined steps up until the DNA gripping state (Higashi et al. 2020). Although the direct structural evidence from the cohesin post-ATP-hydrolysis state is missing, the structure of the disengaged, ATP-free condensin ATPase heads bridged by its loader Ycs4 is consistent with this model (Lee et al. 2020).

1.3.5 Mechanisms of condensin-mediated loop extrusion

Condensin extrudes DNA loops in an asymmetric manner *in vitro*, meaning that condensin holds onto one side of the loop (*i.e.* the “anchor”) and only reels in DNA from the other side of the loop (*i.e.* the “motor”) (Ganji et al. 2018; Golfier et al. 2020). The Cnd3^{Ycg1}-Cnd2^{Brn1} was proposed as the “anchor” due to its strong DNA affinity as well as its importance in maintaining extruded loops (Kschonsak et al. 2017; Ganji et al. 2018).

If condensin extrudes loops with random directionality in vivo, DNA organised by condensin via asymmetric loop extrusion would lead to un-extruded DNA gaps along 25 % of the genome, which would compromise organisation of

mitotic chromosomes (Banigan et al. 2020). Instead, it was proposed that a pair of condensin can work as a two-sided loop extruder or that loop-extruding condensin complexes can randomly switch the loop extrusion direction to ensure complete extrusion of DNA. Indeed, loop-extruding condensin could bypass each other *in vitro*, producing a Z-loop that functions as a two-sided loop extruder (E. Kim et al. 2020). The exact mechanism of the collision and bypass between two condensin complexes is unclear.

The rate of loop extrusion is also under debate. The consensus is that for each ATP hydrolysis cycle, condensin can reel in DNA not longer than the length of its coiled coils. The exact number of base pairs reeled in per cycle will depend on DNA density per length, which in turn depends on the tension felt by either the doubly tethered DNA *in vitro* or the chromatin *in vivo* (Terakawa et al. 2017; J. Ryu et al. 2021).

Despite direct observation of single condensin loop extrusion events *in vitro*, the exact mechanism of condensin loop extrusion (i.e. the mechanism of the "motor") is still under debate (Ganji et al. 2018; Banigan and Mirny 2020). Currently proposed models are summarised below.

The tethered inchworm model proposes that the two ATPase heads of the condensin bind to the two HEAT repeat subunits respectively. Each head-HEAT repeat pair forms an independent DNA binding site and therefore could "walk" along the DNA driven by the ATP hydrolysis-dependent head engagement and disengagement. The hinge, on the other hand is the "anchor". Lacking direct experimental evidence, this model remains speculative (Nichols and Corces 2018).

The loop capture model proposes that condensin pseudo-topologically entraps a DNA loop in the open conformation and then squeeze the loop towards the ATPase head, thereby driving loop enlargement. This model was based on the observed equilibrium of open and closed conformation of condensin that couple the nucleotide state of the ATPase heads to the conformational changes of the coiled coil and the hinge (Lee et al. 2020).

A similar model, the scrunching model, proposes that, rather than the closing of coiled coil, it is the moving of the hinge that brings the DNA closer towards the ATPase heads, thereby driving the loop enlargement (J. K. Ryu et al. 2020). However, it does make several assumptions that remain untested. Firstly, this model assumes a change in DNA affinity at the hinge in response to ATP-hydrolysis at the ATPase heads. While the cryo-EM structure of the cohesin hinge in the DNA-gripping state did indicate a slight change in conformation (Shi et al. 2020), the change in DNA affinity at the hinge was not directly observed. Secondly, this model assumes that, after the hinge releases the DNA, and the coiled coils return to the elongated conformation for the second round of loop extrusion, the previously extruded loops are temporarily held (presumably by the ATPase head) to prevent the loop slipping back. More importantly, this model assumes that, every time when the hinge extends out to grab the DNA (to reel it in), the hinge can grab onto the same DNA on the same side of the loop. Note that, if the hinge grabs onto the different side of the loop, then the previously extruded loops would be lost. Given that condensin can bind a second DNA while moving along the first DNA (Terakawa et al. 2017), making it unclear if and how does condensin distinguishes *cis* DNA versus *trans* DNA during loop extrusion.

Recently available cryo-EM structures of DNA-gripping cohesin and the details of cohesin loading mechanism inspired the Brownian ratchet model of loop extrusion by SMC complexes (Higashi et al. 2020; 2021). This model proposes that topological loading reaction and loop extrusion reaction are fundamentally the same in terms of DNA binding sequence as well as the subunit rearrangements prior to and after the DNA-gripping state. The difference between the two reactions is the DNA movement after resolution of the DNA-gripping state. In contrast to the loading reaction where DNA is released from the SMC ATPase head-Mis4^{Scc2} (cohesin counterpart of Cnd1^{Ycs4} of condensin) module into the SMC-kleisin compartment after DNA-gripping step (Figure 1.2 D), the loop extrusion reaction occurs when the DNA somehow remains bound to the SMC ATPase head-Mis4^{Scc2} module even after ATP hydrolysis and head

disengagement (Figure 1.3 A). Then as the Mis4^{Scc2} switches back to extended

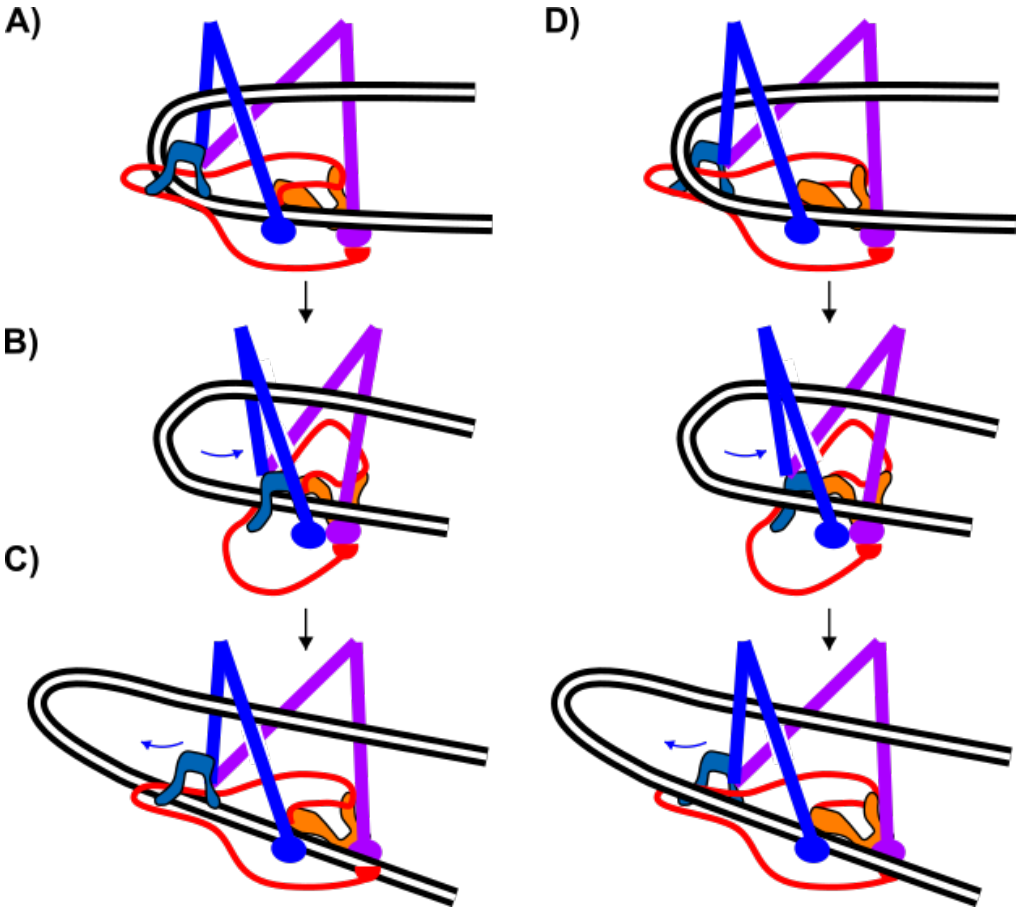

Figure 1.3 Brownian ratchet model of loop extrusion

The pseudo-topological Brownian ratchet model is depicted in (A) (B) and (C). The non-topological Brownian ratchet model is depicted in (D).
A) After gripping state, DNA does not pass through the ATPase head domain after ATP hydrolysis. Hinge module swings away and pulls out DNA.
B) New ATP binding induces the next DNA gripping state, where the hinge module swings back towards the ATPase heads (blue arrow).
C) ATP hydrolysis allows the hinge module to swing away and again pulls out DNA (blue arrow).
D) The non-topological Brownian ratchet model. A DNA loop is simply docked onto the condensin, without passing through the "N-gate". ATP induces similar condensin DNA-gripping state. The movement of the hinge module drives loop enlargement via similar mechanism as the pseudo-topological model.

conformation when the ATPase head disengages, the stacking interaction between Mis4^{Scc2} and Psc3^{Scc3} (cohesin counterpart of Cnd3^{Ycg1} of condensin) is lost, allowing the hinge-Psc3^{Scc3} to swing away and pull DNA out of the ATPase head module, driving the loop enlargement. The hinge-Psc3^{Scc3} module then releases the DNA and, upon another ATP binding, the hinge-Psc3^{Scc3} module again stacks with the cohesin loader at the engaged ATPase heads (Figure 1.3 B), where it binds again to the DNA and begins the next cycle of loop extrusion (Figure 1.3 C).

The “anchor” in this model is proposed to be the region near the “elbow” on the coiled coils, where DNA-protein crosslinking mass spectrometry showed consistent DNA binding throughout the ATPase cycle (Higashi et al. 2020). Mostly backed up by experimental evidence, this model suggests a possible solution to the loop extrusion directionality – since the DNA remains bound to the ATPase head-loader module, the hinge can only fold back and grab the DNA on the same side of the extruded loop. Like other models, the Brownian rachet model also makes a few assumptions that require further examination. Firstly, this model assumes that the hinge remains bound to Psc3^{Scc3} after resolution of the DNA-gripping state. Although the bulk FRET data is consistent with a stable binding between hinge and Psc3^{Scc3} (Higashi et al. 2021), such association is not captured in EM or AFM analyses (Anderson et al. 2002; J. K. Ryu et al. 2020; Yoshimura et al. 2002; Lee et al. 2020). Although these contrasting observations could be explained by the difference in sample preparation for FRET and structural analyses, the hinge-Psc3^{Scc3} binding dynamics requires further experimental confirmation. Secondly, the Psc3^{Scc3}-hinge module is assumed to release the DNA after resolution of DNA-gripping state. This assumption is consistent with the biophysical calculations based on biochemically measured Psc3^{Scc3}-DNA affinity. Nevertheless, a more direct measurement of the DNA binding dynamics at this module is needed to further verify this assumption. Finally, this model assumes a DNA loop is accommodated inside the SMC ring, therefore also termed as the pseudo-topological Brownian ratchet model. However, it was recently observed that loop extrusion of a covalently closed cohesin could still bypass obstacles larger

than its ring size (Pradhan et al. 2021), challenging any model that requires topological or pseudo-topological DNA entrapment for loop extrusion. To reconcile this, an alternative version of the Brownian ratchet model was proposed, where DNA is organised outside the ring, therefore termed as the non-topological model (Figure 1.3 D) (Higashi and Uhlmann 2022). In this alternative model, the DNA loop is pre-formed via Brownian motion and then the condensin docks onto the tip of the DNA loop, thereby forming a structure very similar to DNA-gripping state, except that the DNA is on the outside of the complex. Similar to the pseudo-topological Brownian ratchet model, the movement of the hinge module induced by ATP binding and hydrolysis at the heads drives loop extrusion. If the choice between the pseudo- and non-topological DNA topologies is random, then half of the condensin population might employ the pseudo-topological Brownian ratchet model whilst the other half adopts the non-topological mechanism, consistent with the 50 % bypass efficiency in the case of condensin (Pradhan et al. 2021). In summary, although the Brownian ratchet model is mostly consistent with experimental data, its validity remains to be tested.

1.4 Aims and outline of this thesis

Even though a topic of intense study, the mechanism of condensin-mediated chromosome compaction during mitosis is still unclear. Specifically, the very mechanism of how condensin interacts with chromosomal DNA that ultimately leads to formation of mitotic chromosome formation is under debate. Each of the three models of condensin-mediated chromosome formation introduced above, namely the loop extrusion model, the torsion-mediated compaction model and the diffusion capture model, has its merits and limitations. The structural similarities between the condensin and the cohesin complex prompt me to hypothesize that condensin, similar to cohesin, also organises DNA via topological entrapment and perhaps topological DNA-DNA tethering. However, such DNA entrapment activities were never rigorously demonstrated for condensin. This project aims to biochemically characterise the interaction between the purified condensin complex and DNA, specifically probing whether

condensin complexes can topologically interact with DNA. The results from this project will hopefully shed light on the mechanism of condensin-DNA interaction with implications for condensin functions in mitosis *in vivo*.

Since condensin complexes was never purified in my PhD lab, I started with establishing purification protocol of the condensin complexes, followed by adapting and developing biochemical assays to probe topological interactions between condensin and DNA in bulk biochemical experiments. These are described in Chapter 3. Using budding yeast as the expression host, I purified the fission yeast condensin complex and validated the ATPase and DNA binding affinities of the purified condensin with respect to previously available biochemical data of condensin from other species. Topological loading of condensin onto DNA was for the first time directly biochemically observed and characterized. A DNA-gripping state of condensin in the presence of a non-hydrolysable ATP analogue was also observed and exhibited distinct characteristics compared to topologically loaded condensin. Interestingly, topologically loaded condensin was capable of topologically entrapping a second dsDNA substrate in an ATP-dependent manner.

After observing topological condensin-DNA interactions in the bulk biochemical assays, I then wondered whether a single condensin complex is sufficient to entrap one or two or more DNA molecules. For this aim, I reconstituted condensin-DNA reactions inside a flow cell under the single-molecule fluorescence microscope, which is described in Chapter 4. There, I observed that a single condensin was capable of topologically entrapping one or two DNA molecules.

Finally, these results and their wider inferences are discussed in Chapter 5.

Chapter 2. Materials and Methods

2.1 Yeast Techniques

These techniques were required to generate and validate the *S. cerevisiae* strains, especially condensin overexpression strains, used in this thesis.

2.1.1 Quick yeast genomic DNA preparation

S. cerevisiae were plated on YPD agar plate or minimum selection media agar plate overnight. A small amount of cells was scooped from the patch using 10 µl loop and swirled in 100 µl lysis buffer (0.6 M Lithium acetate, 1 % SDS) and heated to 70 ^{o}C for 10 mins. 300 µl absolute ethanol was added to the cell suspension and then centrifuged at 14,000 g for 3 mins to pellet the DNA. Supernatant was aspirated and the pellet were air dried at room temperature for 30 mins. 100 µl ddH_2O was added and vortexed to resuspend the pellet before centrifuging at 14,000 g for 1 min. The supernatant, now containing the extracted yeast genomic DNA, was transferred to a clean tube and stored at -20 ^{o}C until use.

2.1.2 Yeast transformation

S. cerevisiae were grown in 50 ml either rich medium (YPD) or selective medium (YNB supplemented with 2 % glucose, and CSM omitting the selective marker) and shaken at 25 ^{o}C overnight until exponential growing phase (OD_{600} around 0.8). The culture was then back diluted to OD_{600} 0.2 and was allowed to grow for another 2 to 3 hrs. Then the cells in 50 ml culture were spun down at 3500 rpm 4 ^{o}C 3 min, transferred to 1.5 ml Eppendorf tube, and washed once with 1 ml ddH_2O and once with 1 ml freshly made TEL buffer (10 mM Tris/HCl pH 7.5, 1 mM EDTA pH 8.0, 0.1 M Lithium Acetate). The cells were then resuspended in 100 µl TEL buffer. 50 µl cell suspension were mixed with 1 µg digested integrative plasmid or 500 ng integrative PCR product or 300 ng centromeric plasmid, 50 µg Salmon Sperm DNA, and 300 µl TELP buffer (10

mM Tris/HCl pH 7.5, 1 mM EDTA pH 8.0, 0.1 M Lithium Acetate, 40 % PEG-3350) and vortexed for 10 sec. The mixture was incubated at 25 ^{o}C for 2.5 – 3 hrs before heat shocked at 42 ^{o}C for 15 min. The cells were spun down at 6000 g for 1 min. The supernatant was aspirated and the cell pellet was resuspended in 1 ml 2 M sorbitol. 0.1 ml suspension was plated onto the selective plate and the rest was spun down again and resuspended in 100 µl 2 M sorbitol before plated onto the selective plate and incubated at 25 ^{o}C for 3 days.

2.1.3 Glycerol stocks for indefinite storage

Yeast strains were grown on YPD or YNB agar plate at 25 ^{o}C for 1 to 2 days. Then the cells were scrapped from the plate and resuspended in 1 ml 15 % glycerol in 2 ml cryogenic tubes and stored at -80 ^{o}C.

To use the stock, scrape around 5 to 10 µl of cell suspension and plate onto YPD or YNB agar plate at 25 ^{o}C or 30 ^{o}C for 1 to 2 days.

2.1.4 FACS (Fluorescence assisted cell sorting)

0.5 – 1 OD_{600} units of *S. cerevisiae* cells were collected and fixed in ice-cold 70 % EtOH on ice for 1 hrs. Then cells were pelleted and resuspended in Tris/RNase buffer (50 mM Tris/HCl pH 7.5, 0.1 mg/ml RNase A) and incubated at 37 ^{o}C overnight. The cells were pelleted again and resuspended in FACS solution (0.2 M Tris/HCl pH7.5, 211 mM NaCl, 78 mM $MgCl_2$) supplemented with 0.5 mg/ml propidium iodide solution. Cells were briefly sonicated, diluted 20- to 50-fold in 50 mM Tris/HCl pH7.5 before passing into FACS Calibre machine and analysed using FlowJo.

2.1.5 Small-scale protein A tag pull down using IgG beads

2.1.5.1 Cell growth and induction of protein overexpression

S. cerevisiae strains were grown in 50 ml of YPR cultures overnight at 25 ^{o}C or 30 ^{o}C to OD_{600} between 0.7 – 1.0 before 5 ml 20 % galactose solution was added to induce protein overexpression for 4 to 5 hours. Cells were collected by

centrifugation, resuspended with 1 ml ddH_2O and transferred to cell breaker tubes. Cells were pelleted and supernatant aspirated before frozen at -80 ^oC.

2.1.5.2 Native soluble protein extract preparation from S. cerevisiae using glass beads and beads shocker

The cell pellet was thawed on ice and resuspended in 0.5 ml ice cold Lysis buffer (40 mM Tris/HCl pH7.5, 300 mM NaCl, 10 % glycerol, 2 mM DTT, 1 mM PMSF, 1x cOmplete (Merck 5056489001), 2 µg/ml RNase A). Roughly 0.5 ml glass beads (Merck G4649) were added and the tube was shaken in beads shocker with 28 cycles of 2500 rpm 60 sec on and 90 sec off. The lysate was checked for lysis efficiency under the microscope.

Using a flame-heated needle to poke two holes at the bottom of the beads shocker tubes and fit the tube inside a 2 ml Eppendorf tube. No more than two tubes were placed inside a 50 ml Falcon tube and centrifuged at 1000 rpm 4 ^oC 5 min to collect the lysate. Another 0.5 ml Lysis buffer was added to the lysate before centrifuge at 21,000 g, 4 ^oC for at least 30 min. The supernatant was collected and transferred to a clean tube.

2.1.5.3 Protein A-tagged protein pull down using IgG beads

Unless specified otherwise, all centrifugation steps in this section were performed at 4 ^oC and 500 g for 10 sec. Then each tube was rotated 180^o in the rotor and centrifuged again for 10 sec to aggregate beads at the bottom of each tube.

40 µl Rabbit IgG-Agarose beads suspension (Merck A2909) was added to the supernatant in the clean tube. The tube was rotated on a wheel at 4 ^oC for at least 2 hours before centrifuging to collect beads. The beads were washed three times by resuspending in 1 ml Wash buffer (40 mM Tris/HCl pH7.5, 300 mM NaCl, 10 % glycerol, 2 mM DTT) and centrifuging to collect the beads. Finally, the beads were resuspended in 60 µl Laemmli sample buffer (2X) (120 mM Tris/HCl pH7.5, 4 % SDS, 20 % glycerol, 0.02 % bromophenol blue, 1 %

(v/v) β-mercaptoethanol) and boiled for 5 min. 10 µl to 20 µl samples were loaded on SDS-PAGE gel for analysis.

2.1.6 Total protein extraction using TCA

1.5 to 2 OD_{600} units of *S. cerevisiae* cells were collected by centrifuging at 8000 g, 4 ^{o}C for 1 min inside the cell breaker tube. Supernatant was aspirated and the cell pellet was resuspended in 0.5 ml 20 % TCA (v/v) and incubated on ice for at least 30 min. Then cells were pelleted and resuspended in 0.5 ml 1 M Tris base (not pH'ed). Cells were pelleted again and resuspended in 50 µl Laemmli sample buffer (2X) (120 mM Tris/HCl pH7.5, 4 % SDS, 20 % glycerol, 0.02 % bromophenol blue, 1 % (v/v) β-mercaptoethanol). The cell suspension was boiled at 99 ^{o}C for 5 min before adding 100 µl glass beads (Merck G4649). Cells were lysed using FastPrep *S. cerevisiae* program at 4 ^{o}C.

Using a flame-heated needle to poke two holes at the bottom of the beads shocker tubes and fit the tube inside a 1.5 ml Eppendorf tube. No more than two tubes were placed inside a 50 ml Falcon tube and centrifuge at 1000 rpm 4 ^{o}C 5 min to collect the protein extract in 2X Laemmli sample buffer. 8 µl to 10 µl of sample was loaded on SDS-PAGE gels for Western blotting analysis.

2.2 Biochemical techniques

This section begins with some basic biochemical techniques leading to purification protocol of *S. pombe* condensin in *S. cerevisiae*. Later, this section describes the two main biochemical assays used to probe condensin-DNA interactions, namely, the condensin loading assay by condensin pull down and the condensin loading assay using dsDNA beads substrates. These assays and their variations allowed me to identify a topological DNA-DNA tethering activity of *S. pombe* condensin.

2.2.1 Western blotting

Protein samples were separated by SDS-PAGE. The gel was briefly rinsed in tap water before assembling the transfer cassette. 1 L of wet transfer buffer (25 mM Tris/HCl pH 7.5, 192 mM Glycine, 0.05 % SDS, 20 % methanol) was poured into a tray. The cassette was placed black side down inside the tray. On top of the black side was the following in this order: pre-wet black sponge, pre-wet filter paper, gel, nitrocellulose membrane, pre-wet filter paper, pre-wet black sponge. Then the transparent side of the cassette was folded back, sandwiching everything inside. The cassette was then placed inside a transfer tank filled with wet transfer buffer, with transparent side facing the positive side. The transfer was performed at 4 ^{o}C at 600 V 400 mA 150 min. Then the membrane was recovered and rinsed briefly with Ponceau S solution to visualise the transferred protein. Then the membrane was washed once with water and twice with PBSAT buffer (0.2 % Tween 20 (v/v) in phosphate buffered saline solution) before incubated with 10 ml Milk (0.5 % Fat-free milk (w/v) dissolved in phosphate buffered saline solution) at 4 ^{o}C overnight or at room temperature for at least 1 hour. The membrane was washed again with 30 ml PBSAT buffer twice before adding Milk containing the antibody at room temperature for at least 1 hour. Then the membrane was washed with 30 ml PBSAT buffer at room temperature for 20 min three times. If needed, the Milk containing the secondary antibody was incubated with the membrane at room temperature for at least1 hour and washed three times with PBSAT buffer as before. Then the membrane is placed on plastic film or Saran wrap before 0.2 ml to 0.8 ml of ECL Western Blotting substrate (prepared by mixing two solutions 1:1 according to Thermo Scientific 32106). Another piece of plastic or Saran wrap was placed on top and the membrane is exposed to X-ray film in the dark for 10 sec to 15 min depending on signal strength.

2.2.2 BSA purification

To remove higher molecular weight contaminants from commercial BSA, BSA powder was dissolved in 3 ml BSA buffer (20 mM Tris/HCl pH7.5, 150 mM

NaCl, 10 % glycerol, 2 mM DTT) to final concentration of 50 mg/ml. The solution was injected into a 2 ml loop and then loaded onto Superdex 200 pg 16/600 (Cytiva) column pre-equilibrated with BSA buffer. The sample was passed through the column in the BSA buffer. 1 ml fractions were collected and analysed on SDS-PAGE. Peak fractions were pooled, concentrated in VivaSpin concentrator to 70 mg/ml, and then aliquoted and flash frozen in liquid nitrogen and stored at -80 ^{o}C until use.

2.2.3 3C protease purification

E. coli strain harbouring the expression plasmid was streaked on LB agar plate supplemented with 25 µg/ml chloramphenicol and 100 µg/ml ampicillin and incubated at 37 ^{o}C overnight. Single colony was picked to inoculate 50 ml LB +AMP +CHL (LB media supplemented with 25 µg/ml chloramphenicol and 100 µg/ml ampicillin) and shaken at 37 ^{o}C over the day before inoculating 2 L LB +AMP +CHL while shaking at 37 ^{o}C until OD_{600} reaches 0.6. Then the media was cooled down to room temperature and IPTG was added to 0.1 mM final concentration and the culture was further shaken at 20 ^{o}C overnight for protein expression. On the next day, the cells were collected using centrifugation and washed once with water. The cell pellet can be stored at -20 ^{o}C for 1-2 weeks before use. The cell pellet was resuspended in 30 ml lysis buffer (30 mM HEPES pH7.5, 135 mM NaCl, 2 mM DTT, 0.5 mM PMSF, 1X cOmplete (Merck 5056489001)) before sonicated in an ice bath for 5 cycles of power 14.5, 30 sec ON, 2 min OFF. The lysate was centrifuged at 30,000 rpm in JA20 rotor at 4 ^{o}C for 30 min and the supernatant was taken and incubated with 5 ml GSH-Sepharose beads (pre-equilibrated in lysis buffer) at 4 ^{o}C for 2 hours. The beads were then poured back onto the gravity column (BioRed 7321010). The beads were washed five times with 20 ml lysis buffer. Then the beads were incubated with 5 ml lysis buffer supplemented with 10 mM GSH (made from glutathione powder (Merck G4626)) at 4 ^{o}C for 10 min and again with 5 ml lysis buffer supplemented with 10 mM GSH at 4 ^{o}C for 10 min to completely elute the 3C protease. The eluate was dialysed against 2 L 3C buffer (25 mM HEPES pH7.5, 150 mM NaCl, 15 % glycerol, 2 mM DTT) overnight. The dialysed

sample was concentrated using VivaSpin concentrator (Fisher Scientific 10774797) to 4 mg/ml, before loaded onto Superdex 200 (pre-equilibrated in 3C buffer). The sample was passed through the column with 0.2 ml/min flow rate and 0.25 ml fractions were collected and analysed by SDS-PAGE. Peak fractions were pooled and concentrated to 1 mg/ml using VivaSpin concentrator. The concentrate was aliquoted and flash frozen in liquid nitrogen and stored at -80 ^{o}C until use.

2.2.4 Condensin purification

2.2.4.1 Cell growth, induction of overexpression, and collection and lysis

Plasmids containing *S. pombe* condensin five wild-type subunits (or their variants) under the control of Gal1-10 bi-directional promoter were integrated into a Δpep4 *S. cerevisiae* at LEU2, ADE2, and TRP1 loci. Galactose inducible strain was plated freshly on YPD agar plate at 25 ^{o}C for 1 to 2 days until a patch was grown. A bit of cells were taken from the patch to inoculate 50 ml YPD media and shaken in 250 ml conical flask overnight at 25 ^{o}C. On the next day, the culture was back diluted to maintain OD_{600} between 0.1 to 1. Then about 20 OD_{600} units of cells were collected to inoculate the large 2.2 L YPR cultures in 5 L conical flasks to achieve OD_{600} around 1 in the next morning. Then 200 ml 20 % galactose were added per each 2.2 L YPR culture to induce protein overexpression. The cells were allowed to grow for another 3 to 5 hours at 25 ^{o}C. The cells were collected by centrifugation, washed once with ice cold water, and resuspended in 30 ml to 50 ml lysis buffer (40 mM Tris/HCl pH7.5, 300 mM NaCl, 10 % glycerol, 2 mM DTT, 1 mM PMSF, 1x cOmplete (Merck 5056489001), 2 µg/ml RNase A). The cell suspension was then added to liquid nitrogen drop by drop to make popcorn. Popcorn was then grinded to powder in freezer mill to lyse the cells. The powder was thawed on ice and supplemented with additional 50 ml to 100 ml lysis buffer and incubated or stirred at 4 ^{o}C for at least 1 hour.

2.2.4.2 IgG pull down and 3C elution

Then the lysate was centrifuged at 35,000 rpm in 45Ti (105,000 g) 4 °C 45 min. Carefully avoiding the top white layer and the bottom brown unstable precipitate, the supernatant was taken out into a Duran bottle. 1 ml to 3 ml Rabbit IgG-Agarose beads (Merck A2909), i.e. 2 ml to 6 ml beads slurry, was packed on a gravity column (BioRed 7321010) and washed with 5 ml wash buffer (40 mM Tris/HCl pH7.5, 300 mM NaCl, 10 % glycerol, 2 mM DTT) before resuspended in 5 ml wash buffer. The beads suspension was poured into the Duran bottle containing the supernatant and the bottle was sealed and rolled on a roller at 4 °C for at least 2 hours.

The supernatant was then poured back to the gravity column to pack the beads. The beads were washed once with 20 ml wash buffer, then washed twice with 10 ml wash buffer containing 10 mM $MgCl_2$ and 1 mM ATP, and finally washed six times with 20 ml wash buffer. The beads were then resuspended in 15 ml to 30 ml wash buffer, transferred into a 50 ml Falcon tube, supplemented with 2 µg/ml RNase A, 1 µg/ml 3C protease and rolled at 4 °C overnight.

On the next day, the contents inside the Falcon tube was poured onto the gravity column again and the flow through, i.e. the eluted condensin complex, was collected in a new clean Falcon tube.

20 µl samples were taken from the flow throughs at each washing step or for the final elution step for SDS-PAGE analysis.

2.2.4.3 Heparin and size exclusion chromatography

HiTrap Heparin HP 1 ml column (Cytiva 10288944) was washed with 10 CV of ddH_2O to remove ethanol, then equilibrated with 5 CV Heparin A buffer (20 mM Tris/HCl pH7.5, 100 mM NaCl, 10 % glycerol, 2 mM DTT), 5 CV Heparin B buffer (20 mM Tris/HCl pH7.5, 1M NaCl, 10 % glycerol, 2 mM DTT), and then with 5 CV buffer containing 80 % Heparin A buffer and 20 % Heparin B buffer. Then the eluted protein was injected onto the Heparin column using a sample pump with an air sensor as the stopper. The column was washed with 10 CV

buffer containing 80 % Heparin A buffer and 20 % Heparin B buffer at 0.6 ml/min. The flow through of the sample injection and column wash was collected in a 100 ml beaker. Then the protein was eluted using a 20 CV linear gradient starting at 20 % Heparin B (80 % Heparin A) and finishing at 100% Heparin B (0 % Heparin A). 0.5 ml fractions were collected using a fraction collector in a 96 deep well plate. After analysing each fractions on the SDS-PAGE, peak fractions were pooled and concentrated to 0.75 ml or 1.25 ml using VivaSpin concentrator (Fisher Scientific 10774797).

If fluorophore labelling was required, the concentrated protein was supplemented with 1 mM SNAP-Alexa 647 (NEB) or other indicated fluorophores at room temperature for 4 hours.

Then the concentrated protein was injected onto a 0.5 ml or 1 ml loop before passing through the Superose 6 Increase 10/300 GL column (Cytiva GE29-0915-96) that was pre-equilibrated in size exclusion buffer (20 mM Tris/HCl pH7.5, 200 mM NaCl, 10 % glycerol, 2 mM DTT). The column was run at 0.3 ml/min and 0.25 ml fractions were collected. The fractions were analysed by SDS-PAGE followed by Coomassie staining and, in the case of fluorescence labelled condensin, in-gel fluorescence scanning. Peak fractions were pooled and concentrated using VivaSpin concentrator to around 1 mg/ml, corresponding to around 1.5 μM condensin. Proteins were aliquoted and flash frozen in liquid nitrogen and stored at -80 ^{o}C until use.

2.2.5 Condensin loading assay by condensin immunoprecipitation

2.2.5.1 Preparation of pBlueScript dsDNA

Supercoiled, relaxed circular, nicked, or linear dsDNA used in this assay was prepared from pBlueScript as described in (Murayama and Uhlmann 2014).

2.2.5.2 Preparation of pBlueScript ssDNA

F' *E. coli* (NEB C2992H) was transformed with pBlueScript II SK (+) according to manufacturer instructions. A single colony was picked to inoculate 500 ml LB supplemented with 100 µg/ml Ampicillin and shaken vigorously at 37 °C until OD_{600} reaches 0.05. Then 0.5 ml of M13KO7 helper phage (NEB) was added to the culture and shaken vigorously at 37 °C for additional 90 mins. Kanamycin was added to final concentration of 70 mg/L and the culture was shaken overnight. The culture was centrifuged at 7500 rpm in Sorvall GS3 rotor for 10 mins. The supernatant was recovered and mixed with 14.6 g NaCl and 20 G PEG6000 until fully dissolved. The supernatant was gently stirred at 4 °C for 1.5 hours before centrifuging at 6500 rpm in Sorvall GS3 rotor at 4 °C for 20 mins. The supernatant was discarded carefully before centrifuging again at 6500 rpm in Sorvall GS3 rotor at 4 °C for 2 mins. The supernatant was carefully removed using pipette. The pellet was resuspended in 8 ml 10:1 TE solution (10 mM Tris/HCl pH7.5, 1 mM EDTA pH8.0), transferred into a 2059 tube, and centrifuged at 8000 rpm in Sorvall SS34 (using an adaptor with ~2 ml H_2O inside) for 1 min. The supernatant was recovered and mixed with 2 ml 20 % PEG6000 2.5 M NaCl, mixed well and stood at room temperature for 5 mins before centrifuging at 8000 rpm in Sorvall SS34 for 10 min. The supernatant was carefully discarded and pellet was resuspended in 1 ml 10:1 TE solution. 0.4 g $CsCl_2$ was dissolved in the suspension and the suspension was transferred into 2 ml Hitachi quick-seal tube. The tube was filled to the top using a solution made by dissolving 0.4 g $CsCl_2$ in 1 ml 10:1 TE solution. The tube was heat-sealed and centrifuged at 120,000 rpm for 3 hours at 20 °C in a Hitachi 120VT rotor. The phage particle formed a dense band with a high refractive index. A needle attached to a 1 ml syringe was used to carefully puncture the tube 5 mm below the band. The tube was then punctured at the top with another needle to make an airhole. Then the first needle was extended to the bottom of the band and the band was carefully withdrawn into the syringe. The recovered phage particle was dialysed against 1 L 10:1 TE solution overnight. The phage solution was diluted two times with 10:1 TE

solution and then mixed gently with 1/5 volume of Tris-saturated phenol before centrifuged at 15000 rpm for 5 mins. The aqueous phase was recovered, diluted 2 times with 10:1 TE and aliquoted 0.4 ml aliquots. The solution was phenol/chloroform extracted twice and washed once with chloroform. The aqueous phase containing the DNA was precipitated by adding 1 ml 0.3 M sodium acetate dissolved in 100 % ethanol and stored at -20 ^{o}C for at least 2 hours. The solution was centrifuged and the resulting pellet washed with 1 ml 100 % ethanol twice. After evaporating the ethanol, the DNA pellet was dissolved in 0.3 ml 10:1 TE solution in total. The concentration of the resulting ssDNA was measured using NanoDrop, aliquoted and stored at -20 ^{o}C until use.

2.2.5.3 Conjugation of dynabeads with anti-PK antibodies

To prepare beads enough for x number of samples, x*10 µl Dynabead^{TM} Protein A (ThermoFisher Scientific 10002D) magnetic beads were first washed twice with 1 ml PBSA-BSA (5 mg/ml BSA dissolved in phosphate-buffered saline solution and then passed through a 0.22 µm filter) in a Costar tube (Fisher Scientific 3207). Then the beads were resuspended in x*100 µl PBSA-BSA supplemented with x*3 µl 1 mg/ml anti-V5 mouse antibody (BioRed MCA1360G) and rotated on a wheel at 4 ^{o}C for 1 to 2 hours (not more than 2 hours). Then the beads were washed twice with 1 ml PBSA-BSA and twice with 1 ml wash buffer (40 mM Tris/HCl pH 7.5, 500 mM NaCl, 10 % glycerol, 0.5 mM TCEP, 0.01% IGEPAL) before resuspended in x*100 µl wash buffer.

2.2.5.4 Condensin loading reaction

For each sample, 75 nM of purified condensin was mixed in 15 µl loading buffer (40 mM Tris/HCl pH 7.5, 50 mM KCl, 10 % glycerol, 1 mM TCEP, 3 mM $MgCl_2$, 0.3 mg/ml BSA) containing 1 mM ATP and 90 ng pBlueScript plasmid prepared as described in previous sections, unless specified otherwise, in a Costar tube. The reaction was incubated at 30 ^{o}C for 30 min unless indicated otherwise. 1.5 µl reactions was taken and mixed with 9 µl Laemmli sample buffer (2X) (120 mM Tris/HCl pH7.5, 4 % SDS, 20 % glycerol, 0.02 % bromophenol blue, 1 %

(v/v) β-mercaptoethanol) as the “10 % protein input” sample. 1.5 µl reactions was taken and mixed with 9 µl DNA elution buffer (35 mM Tris/HCl pH7.5, 50 mM NaCl, 0.75 % SDS, 20 mM EDTA pH8.0, 2 mg/ml proteinase K) as the “10 % DNA input” sample. 100 µl wash buffer was then added to the remaining 12 µl loading reaction to completely quench the reaction.

2.2.5.5 Condensin IP

For each sample, quenched condensin loading reaction was mixed with 100 µl magnetic beads suspension prepared previously and rotated on a wheel at 4 ^{o}C for 2 hours. Then the beads were washed three times with 1 ml wash buffer and once with 1 ml pre-equilibration buffer (40 mM Tris/HCl pH 7.5, 100 mM NaCl, 10 % glycerol, 5 mM $MgCl_2$, 0.5 mM TCEP, 0.01% IGEPAL).

2.2.5.6 Further processing for loading reaction

Following condensin IP in section 2.2.5.5, the beads were resuspended in 0.8 ml pre-equilibration buffer, and then split to analyse DNA and protein compositions remaining bound to the beads. For DNA sample, 0.5 ml beads suspension was taken, beads collected, supernatant aspirated, and beads were resuspended in 10 µl DNA elution buffer and incubated at 50 ^{o}C for at least 20 min to completely recover DNA from the beads. The DNA samples were then separated on 0.7 % TAE agarose gel before staining with GelRed dissolved in 150 mM NaCl solution. For protein sample, 0.25 ml beads suspension was taken, beads collected, supernatant aspirated, and beads were resuspended in 10 µl Laemmli sample buffer (2X) and boiled at 99 ^{o}C for 5 min. The protein samples were separated on 4-12 % Tris-Gly SDS-PAGE and stained by Coomassie.

2.2.5.7 DNA linearisation after condensin loading reaction

Following condensin IP in section 2.2.5.5, the beads were resuspended in 0.1 ml pre-equilibration buffer, collected again and resuspended in 10 µl NEB2.1 buffer (10 mM Tris/HCl pH7.5, 50 mM NaCl, 10 mM $MgCl_2$, 0.1 mg/ml BSA) with

or without 1 µl ScaI-HF (NEB) and shaken at 18 °C for 1 hour. Then 10 µl 1M buffer (10 mM Tris/HCl pH7.5, 1M NaCl, 10 mM $MgCl_2$, 0.1 mg/ml BSA) was added to adjust the salt concentration. Then 12.5 µl suspension was taken as the DNA samples (50 % of total reaction) and 6.25 µl suspension was taken as the protein samples (25 % of total reaction). For these samples, both supernatant and beads were separated and both supernatant and beads were processed as described above for DNA and protein samples.

2.2.6 Condensin gripping assay by condensin immunoprecipitation

2.2.6.1 Preparation of 124bp dsDNA fragment

124 bp dsDNA fragment was amplified from pBlueScript using Taq polymerase PCR (Qiagen) according to manufacturer protocol. The product was loaded onto a 0.7 % TAE agarose gel containing 1:10,000 GelRed. The band was cut and purified using NucleoSpin Gel Purification and PCR Cleanup kit (Takarabio 740609).

2.2.6.2 Conjugation of dynabeads with anti-PK antibodies

To prepare beads enough for x number of samples, x*10 µl Dynabead™ Protein A (ThermoFisher Scientific 10002D) magnetic beads were first washed twice with 1 ml PBSA-BSA (5 mg/ml BSA dissolved in phosphate-buffered saline solution and then passed through a 0.22 µm filter) in a Costar tube (Fisher Scientific 3207). Then the beads were resuspended in x*100 µl PBSA-BSA supplemented with x*3 µl 1 mg/ml anti-V5 mouse antibody (BioRed MCA1360G) and rotated on a wheel at 4 °C for 1 to 2 hours (not more than 2 hours). Then the beads were washed twice with 1 ml wash buffer (40 mM Tris/HCl pH 7.5, 500 mM NaCl, 10 % glycerol, 0.5 mM TCEP, 0.01% IGEPAL) and twice with 1 ml pre-equilibration buffer (40 mM Tris/HCl pH 7.5, 100 mM NaCl, 10 % glycerol, 5 mM $MgCl_2$, 0.5 mM TCEP, 0.01% IGEPAL) before resuspended in x*100 µl pre-equilibration buffer.

2.2.6.3 Condensin gripping reaction

For each sample, 75 nM of purified condensin was mixed in 15 µl gripping buffer (40 mM Tris/HCl pH 7.5, 50 mM KCl, 10 % glycerol, 1 mM TCEP, 3 mM $MgCl_2$, 0.3 mg/ml BSA) containing 1 mM UltraPure ADP (2B Scientific ADP100-2), 0.5 mM $BeSO_4$, 2.5 mM NaF and 90 ng 124bp dsDNA, unless specified otherwise, in a Costar tube. The reaction was incubated at 30 ^oC for 30 min unless indicated otherwise. 1.5 µl reactions was taken and mixed with 9 µl Laemmli sample buffer (2X) (120 mM Tris/HCl pH7.5, 4 % SDS, 20 % glycerol, 0.02 % bromophenol blue, 1 % (v/v) β-mercaptoethanol) as the “10 % protein input” sample. 1.5 µl reactions was taken and mixed with 9 µl DNA elution buffer (35 mM Tris/HCl pH7.5, 50 mM NaCl, 0.75 % SDS, 20 mM EDTA pH8.0, 2 mg/ml proteinase K) as the “10 % DNA input” sample. 100 µl pre-equilibration buffer was then added to the remaining 12 µl loading reaction to completely quench the reaction.

2.2.6.4 Condensin IP and further processing

For each sample, quenched condensin loading reaction was mixed with 100 µl magnetic beads suspension prepared in section 2.2.6.2 and rotated on a wheel at 4 ^oC for 2 hours. Then the beads were washed three times with 1 ml pre-equilibration buffer and then resuspended in 0.8 ml pre-equilibration buffer. The beads were then split to analyse DNA and protein compositions remaining bound to the beads and processed as described in section 2.2.5.6.

2.2.7 Condensin loading using dsDNA beads substrate

2.2.7.1 Preparation of digoxygenin labelled linear dsDNA fragment

Two triply digoxygenin labelled primers (IDT) were used to PCR amplify a 5 kb fragment from pEGFP-C1 (CloneTech), according to CloneAmp manufacturer protocol. The product was loaded onto a 0.7 % TAE agarose gel containing 1:10,000 GelRed. The band was cut and purified using NucleoSpin Gel Purification and PCR Cleanup kit (Takarabio 740609).

2.2.7.2 Preparation of DNA-beads substrate

To prepare beads-DNA substrates for x number of samples, x*10 µl Dynabeads™ Protein G (ThermoFisher Scientific 10004D) was washed two times with 1 ml PBSA-BSA (5 mg/ml BSA dissolved in phosphate and resuspended in x*100 µl, rotated on a wheel at 4 °C. In the meantime, x*100 ng purified DNA was mixed with x*0.3 µg anti-DIG antibody (Abcam ab420) and x*2 µl DBB (DNA binding buffer: 40 mM Tris/HCl pH7.5, 50 mM NaCl, 5 % glycerol, 1 mM EDTA pH8.0, 1 mM TCEP, 0.5 mg/ml BSA) at room temperature for at least 30 min before adding to beads suspension and rotated further at 4 °C for at least 1 hour (3 hours is recommended). Then the beads were washed three times with 1 ml wash buffer (40 mM Tris/HCl pH 7.5, 500 mM NaCl, 10 % glycerol, 0.5 mM TCEP, 0.01% IGEPAL), once with 1 ml pre-equilibration buffer (40 mM Tris/HCl pH 7.5, 100 mM NaCl, 10 % glycerol, 5 mM $MgCl_2$, 0.5 mM TCEP, 0.01% IGEPAL) and finally resuspended in x*100 µl pre-equilibration buffer. The suspension was then aliquoted into 100 µl in new Costar tubes. The beads were collected and supernatant was aspirated just before use. (Avoid drying of beads!)

2.2.7.3 Condensin loading or gripping onto DNA

For each sample, beads were resuspended in 15 µl loading buffer (40 mM Tris/HCl pH 7.5, 50 mM KCl, 10 % glycerol, 1 mM TCEP, 3 mM $MgCl_2$ or 20 mM EDTA pH8.0, 0.3 mg/ml BSA) containing 150 nM condensin and 1 mM ATP, unless stated otherwise. The tube containing the reaction was shaken at 800 rpm at 30 °C in a thermomixer for 30 min and the beads were manually resuspended by tapping every 5 to 10 min to avoid aggregation at the bottom of the tube. Then the beads were collected and 1.5 µl sample were taken from the supernatant as the “10 % unbound” protein sample. The rest of the supernatant was aspirated. For each sample, the beads were washed three times with 1 ml wash buffer, once with 1 ml pre-equilibration buffer.

2.2.7.4 Further processing for normal loading or gripping reaction

Following condensin loading or gripping in section 2.2.7.3, beads were resuspended in 1 ml pre-equilibration buffer. 0.7 ml suspension were taken, beads collected, supernatant aspirated as the protein sample (“70 % beads”). 0.25 ml suspension were taken, beads collected, supernatant aspirated as the DNA sample (“25 % beads”). Protein and DNA samples were then processed and analysed as described in section 2.2.5.5.

2.2.7.5 Cut the beads-tethered DNA after condensin loading or gripping

Following condensin loading and washing in section 2.2.7.3, the beads were resuspended in 0.1 ml pre-equilibration buffer, collected again and resuspended in 10 µl NEB2.1 buffer (10 mM Tris/HCl pH7.5, 50 mM NaCl, 10 mM $MgCl_2$, 0.1 mg/ml BSA) with or without 1 µl ScaI-HF (NEB) and shaken at 18 ^oC for 1 hour. Then 10 µl 1M buffer (10 mM Tris/HCl pH7.5, 1M NaCl, 10 mM $MgCl_2$, 0.1 mg/ml BSA) was added to adjust the salt concentration. Then 14 µl suspension was taken as the DNA samples (70 % of total reaction) and 5 µl suspension was taken as the protein samples (25 % of total reaction). For these samples, both supernatant and beads were separated and both supernatant and beads were processed as described above for DNA and protein samples.

2.2.7.6 Condensin second DNA capture

After 30 min 30 ^oC incubation of condensin with DNA-beads substrate as described in section 2.2.7.3, 1.5 µl sample were taken from the supernatant as the 10 % first-loading unbound protein sample (“10 % 1UBP”). The rest of the supernatant was aspirated and beads were washed three times with 1 ml pre-equilibration buffer, once with 0.3 ml pre-loading buffer (40 mM Tris/HCl pH 7.5, 50 mM KCl, 10 % glycerol, 1 mM TCEP, 3 mM $MgCl_2$, 0.01 % IGEPAL), and finally resuspended in 0.1 ml pre-loading buffer. The beads were collected, supernatant aspirated, and then the beads were resuspended in 15 µl loading buffer containing 1 mM ATP and 100 ng pBlueScript dsDNA plasmid or ssDNA plasmid. The reaction was shaken at 30 ^oC for 30 min as described in section

2.2.7.3, unless indicated otherwise. 1.5 µl sample were taken from the supernatant as the 10 % second-loading unbound DNA sample (10 % 2UBD). 3.75 µl sample were taken from the supernatant as the 25 % second-loading unbound protein sample (25 % 2UBP). The rest of the supernatant was aspirated. For each sample, the beads were washed three times with 1 ml wash buffer, once with 1 ml pre-equilibration buffer and finally resuspended in 1 ml pre-equilibration buffer. 0.7 ml suspension were taken, beads collected, supernatant aspirated as the protein sample (“70 % beads”). 0.25 ml suspension were taken, beads collected, supernatant aspirated as the DNA sample (“25 % beads”). Protein and DNA samples were then processed and analysed as described in section 2.2.5.5.

2.2.7.7 Condensin unloading from DNA

After condensin loading onto DNA-beads substrate, washed with wash buffer and pre-equilibration buffer as described in section 2.2.7.3, or condensin second DNA capture, washed with wash buffer and pre-equilibration buffer as described in section 2.2.7.6 the beads were resuspended in 15 µl unloading buffer (40 mM Tris/HCl pH 7.5, 135 mM NaCl, 10 % glycerol, 1 mM TCEP, 3 mM $MgCl_2$ or 20 mM EDTA pH8.0, 0.3 mg/ml BSA) containing 1 mM ATP unless stated otherwise. The tube containing the reaction was shaken at 30 ^{o}C in a thermomixer for 30 min as described in section 2.2.7.3. 10.5 µl suspension was taken as the protein sample (70 % of total reaction) and 3.75 µl suspension was taken as the DNA sample (25 % of total reaction). The supernatant and beads fraction of these samples were separated, processed and analysed as described in section 2.2.5.5.

2.2.8 Southern blotting

2.2.8.1 Capillary transfer and DNA crosslinking

The sample DNA was separated on an agarose gel. The gel was stained with GelRed and imaged by GelDoc. The agarose gel was rocked in 100 ml 0.25 M HCl at room temperature for 30 min for depurination. The gel was then rinsed

briefly with 100 ml ddH_2O twice. Then the gel was rocked in 100 ml transfer buffer (0.5 M NaOH, 1.5 M NaCl) at room temperature for 20 min twice. 800 ml transfer buffer was poured into a container. A glass plate was placed on top of the container. Two long filter paper, pre-wet with transfer buffer, was stacked on top of the glass plate, with both ends immersed in the transfer buffer. The gel was placed upside down on the filter paper and air bubble repelled carefully. The Hybond XL membrane (Cytiva RPN303S) was cut to gel size and pre-wet with transfer buffer before placed on top of the gel, air bubbles repelled. Four thin strips of Saran were placed to cover maximum 3 mm of the edge of the membrane and the gel below to prevent short circuit of the transfer buffer. Two more pieces of dry filter paper, cut to gel size, were placed on top of the membrane directly. Finally a stack of tissue was added on top of the filter paper and a moderate weight (in this case, a metal block) was placed on top. The transfer setup was left overnight for efficient transfer.

On the next day, the setup was disassembled, and the top right corner of the membrane was cut to indicate the top right side of the original DNA gel. The membrane was rinsed briefly in 2x SSC (ten times diluted 20X SSC (0.3 M sodium citrate, 3 M NaCl, pH adjusted to 7.5)) and dried at room temperature. Then the membrane was irradiated with 120,000μJ UV in Stratagene UV1800 to crosslink DNA.

2.2.8.2 Hybridization and detection using radioisotope labelled probes

To make the radioisotope labelled probe, 350bp to 2kb non-radioisotope labelled probe was first made using Taq PCR followed by gel purification. The non-radioisotope labelled probe was kept at -20 ^oC until use.

The membrane was placed inside a radioactive-proof roller bottle, DNA side up. 10 ml QuickHyb (Agilent 201220) was added to the roller bottle and pre-hybridize the membrane at 68 ^oC for at least 1 hour. In the meantime, the radioisotope labelled probes were made from 25ng of the non-radioisotope labelled probes using the Prime-It Random Primer Labelling kit (Agilent 300385) according to manufacturer manual, supplemented with 5 μl [α-P^{33}] dCTP

(Hartmann srf-205). The product was then passed through a G-50 spin column (Cytiva 27533001) to remove excess radioactive nucleotides and enzymes to make the final radioisotope labelled probe. Note the radioisotope labelled probes must be made fresh on the day.

The probe was then mixed with Salmon Sperm DNA to blot the membrane, and the membrane was washed according to the QuickHyb manufacturer protocol.

Then the membrane was wrapped inside the Saran wrap and exposed to phosphor imager plate overnight before scanned on Typhoon laser-scanner.

2.2.8.3 Hybridization and detection using digoxygenin labelled probes

The digoxygenin labelled probe was made by GoTaq PCR. Specifically, 3 ng of plasmid DNA, 1 µl of 10µM each PCR primer, 5 µl 10x GoTaq Buffer, 1 µl dNTPs (10mM each), 2 µl 1mM digoxygenin-11-dUTP (Merck 11093088910), and 0.3 µl GoTaq (Promega M7841) was mixed in a PCR tube and filled to 50 µl using ddH_2O. The template was amplified in a thermocycler and the product was separated on an agarose gel and purified using NucleoSpin Gel Purification and PCR Cleanup kit (Takarabio 740609) and stored at -20 ^oC before use. If stripping of membrane and re-probing is required, use alkali-labile digoxygenin-dUTP (Merck 11573152910) to make the probe.

The following protocol is adapted and practically modified from a protocol from MIT open courseware: https://ocw.mit.edu/courses/biology/7-13-experimental-microbial-genetics-fall-2003/labs/Southern_blotting_v2.pdf

Hybridization buffer was made freshly according to the following protocol. Add 1 g of Blocking Reagent to 10 ml Maleic Acid Buffer (0.1 M Maleic Acid, 0.15 M NaCl, pH adjusted to 7.5 using NaOH) and 55 ml ddH_2O. Microwave to dissolve completely before adding 25 ml 20x SSC. Keep hybridization buffer at 68 ^oC until use.

The crosslinked membrane was rocked in 30 ml Hybridization Buffer at 68 ^oC for 3 hours and then discarded. Note that to reduce background, the DNA side should face down, care must be taken to ensure no bubble is on the DNA side

of the membrane, and the membrane should be kept wet throughout this protocol unless mentioned otherwise. 300 ng of digoxygenin labelled probe was mixed with 100 µl Hybridization buffer and boiled at 99 ^{o}C for 20min and immediately cool on ice for at least 5 min. The probe was then mixed well with 70 ml fresh Hybridization Buffer (kept at 68 ^{o}C) before adding to the membrane and incubated overnight at 68 ^{o}C.

The membrane was washed twice in 50 ml 2x SSC, 0.1 % SDS and once with 40 ml 0.2x SSC, 0.1 % SDS at room temperature for at least 30 min each.

Then the membrane was washed briefly in 20 ml Wash buffer (0.3 % TWEEN-20 dissolved in Maleic Acid buffer) before rocked in 50 ml Blocking buffer (1 % Blocking reagent (w/v) dissolved in Maleic Acid buffer by microwaving) at room temperature for at least 1 hour before discarded. Then 3 µl Sheep anti-digoxygenin-AP Fab (Merck 11093274910) was mixed well with 30 ml Blocking buffer before adding to the membrane and rocked at room temperature for at least 30 min. The membrane was washed with 40 ml Wash buffer at room temperature for 30 min twice. The membrane was then rinsed briefly in Detection buffer (0.1 M Tris/HCl pH7.5, 0.1 M NaCl) before assembly of detection cassette.

To assemble the cassette, the membrane was placed on a plastic wrap, DNA side up. Excess amount of ready-to-use CSPD solution (Merck 11755633001) was quickly added to membrane drop wise to cover the membrane. Then the second plastic wrap was placed on top of the membrane. Excess CSPD solution was squeezed out as much as possible and no bubble should be trapped inside. The membrane was exposed to X-ray film between 1 hour to overnight for different dynamic ranges.

2.2.8.4 Stripping membrane for reblotting

The membrane was washed twice with 50 ml 0.2 M NaOH, 0.1 % SDS at room temperature for at least 30 min each. The membrane was then rinsed briefly in 50 ml 2x SSC before incubating in Hybridization buffer at 68^{o}C for pre-hybridization.

For radioisotope labeled probes, the membrane was left inside the Saran wrap for a few days before stripping to allow spontaneous decay of radioisotopes.

For DIG-labeled probes, the stripping of membrane is most effective with probes made using alkali-labile DIG dUTP.

2.3 Single-molecule imaging techniques

This section describes the experimental details of the single-molecule analysis of DNA-bound condensins with or without second DNA capture.

2.3.1 Preparing and set up the microfluidic flow channel

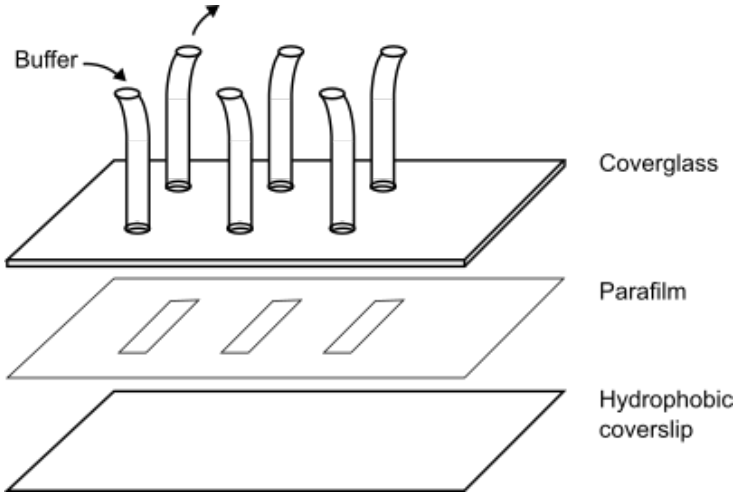

Figure 2.1 Microfluidic flow cell assembly

The Cover glass was drilled to fit the inlet and outlet tubing, which were fixed tightly using epoxy glue. The flow channels were cut out from the parafilm that was sandwiched between cover glass and coverslip. The parafilm was slightly melted to adhere to both cover glass and coverslip and create water-tight channels.

The hydrophobic coverslips were made as described in (Molodtsov et al. 2016). The cover glass was drilled with holes that matches the outer diameter of the flexible plastic tubing. The parafilm was cut to size of the cover glass and flow channels were cut out. Then the parafilm was sandwiched between cover glass and the hydrophobic coverslip and was heated briefly on a 95 ^{o}C heat block to

adhere tightly to both the cover glass and the coverslip. Plastic tubing was cut to appropriate lengths and tethered onto the cover glass using epoxy glue. Please see Figure 2.1 for illustration of the final microfluidic flow cells.

The flow cell was mounted onto the commercial Nikon microscope. The outlet tubing was connected to a Syringe pump (Harvard Apparatus) for flow control. All experiments were performed at room temperature.

2.3.2 Passivation and λ-DNA tethering inside the microfluidic flow channel

The λ-DNA was labeled at both ends by Klenow fragment end filling using dATP, dCTP, dGTP, and digoxygenin-11-dUTP (Merck 11093088910) in the provided buffer, followed by cleanup using G-50 spin column. The flow cell was washed with Binding Buffer (40 mM Tris/HCl pH 7.5, 50 mM NaCl, 2 mM EDTA pH 8.0), incubated in 10 μg/ml Sheep anti-digoxygenin-AP Fab (Merck 11093274910) for 15 min. Then the flow cell surface was passivated using 1 % Pluronic F-127 and finally in 0.7 mg/ml BSA solution. Then the digoxygenin-labeled λ-DNA was introduced at low flow rate (< 10 μl/min) in the presence of Sytox Orange to mildly stretch the λ-DNA while tethering onto the surface. The flow cell was observed under the Nikon's TIRF microscope and the doubly tethered λ-DNA was inspected for quality control.

2.3.3 Condensin loading onto λ-DNA

Alexa 647-condensin was introduced into the flow cell in reaction buffer (40 mM Tris/HCl pH7.5, 5 % glycerol, 0.5 mM TCEP, 1 % glucose, 2 mM Trolox, 0.7 mg/ml BSA) supplemented with 3 mM $MgCl_2$, 50 mM NaCl, 1 mM ATP and incubated for 5 min. Then excess condensin was washed off using reaction buffer supplemented with 50 mM NaCl. The flow cell was re-equilibrated in reaction buffer supplemented with 0.5 M NaCl, 500 nM Sytox orange, glucose oxidase and catalase and excited using 561 nm and 647 nm laser to observe both DNA and Alexa 647-condensin, respectively.

2.3.4 Second DNA capture following condensin loading

Alexa 647-condensin was introduced into the flow cell in reaction buffer (40 mM Tris/HCl pH7.5, 5 % glycerol, 0.5 mM TCEP, 1 % glucose, 2 mM Trolox, 0.7 mg/ml BSA) supplemented with 3 mM $MgCl_2$, 50 mM NaCl, 1 mM ATP and incubated for 5 min. The excess condensin was washed off using reaction buffer supplemented with 50 mM NaCl. Then 3 ng of supercoiled pBlueScript plasmid was introduced into the flow cell in reaction buffer (40 mM Tris/HCl pH7.5, 5 % glycerol, 0.5 mM TCEP, 1 % glucose, 2 mM Trolox, 0.7 mg/ml BSA) supplemented with 3 mM $MgCl_2$, 50 mM NaCl, 1 mM ATP and incubated for 5 min. The excess plasmids were washed off using reaction buffer supplemented with 50 mM NaCl. Finally, the flow cell was re-equilibrated in reaction buffer supplemented with 0.5 M NaCl, 500 nM Sytox orange, glucose oxidase and catalase and excited using 488 nm and 561 nm laser or 561 nm and 647 nm laser to observe either the MFP 488-labelled pBlueScript and all DNA simultaneously or all DNA and Alexa 647-condensin simultaneously.

To visualise the second dsDNA substrate separately from the λ-DNA, supercoiled pBlueScript plasmid was labeled by MFP488 using the Label IT® Nucleic Acid Labeling Kit, MFP488 (Mirus MIR 7100) according to manufacturer's protocol. The labelling efficiency was then measured from the absorbance spectrum at 260 nm and 501 nm.

2.3.5 Image acquisition and analysis

The microscope was purchased from Nikon company. The Alexa 647 signal from labeled condensin was excited with a 647 nm laser. The Cytox Orange (DNA dye) signal was excited with a 561 nm laser. The MFP488 signal from labeled second DNA plasmid was excited with a 488 nm laser. All lasers illuminated the sample through an SR HP Apo TIRF 100xH NA=1.49 WD=120 μm objective using an angle between 58 to 60 degrees to achieve the Highly Inclined and Laminated Optical sheet (HILO) mode. The HILO mode positions the laser beam in a way that only a thin slice of the volume close to the

coverslip surface is illuminated, thereby removing the background from the bulk buffer on top of the surface. Movies were recorded on NIS-Elements provided by the Nikon company using 16-bits HDR camera settings in the dual camera acquisition mode. The nd2 files generated by the NIS-Elements were later analysed using Fiji. Due to the flexibility both condensin and the tethered λ-DNA, the photobleaching plots were generated by measuring the mean intensity of the entire square area cropped around the λ-DNA over time.

Chapter 3. Biochemical reconstitution of *S. pombe* condensin loading onto DNA

As mentioned in Section 1.2, the mechanism of condensin-mediated chromosome formation is still under debate. Current studies focused on mainly the loop extrusion aspect of the condensin-DNA interaction. However, the topological condensin-DNA interactions were not comprehensively examined. Given that cohesin, a complex structurally very similar to condensin, can topologically entrap one dsDNA and then one ssDNA, it is reasonable to suspect that condensin could perform similar topological DNA-DNA tethering reactions. This part of the thesis therefore aims to rigorously examine whether condensin can topologically entrap one or more DNA. I began with establishing an expression and purification protocol for functional *S. pombe* condensin using *S. cerevisiae* cells. Then I probed the condensin interaction with one DNA substrate. Finally I explored the possibility of condensin-mediated topological DNA-DNA tethering activity.

3.1 Purification of *S. pombe* condensin complexes

From plasmids containing genomic sequences of *S. pombe* condensin subunits (kindly provided by Yasutaka Kakui), cDNA sequences for the five subunits of the fission yeast condensin complex and a budding yeast *GAL4* gene were cloned into three integrative plasmids under the control of bidirectional *GAL1-10* promoters (pGal) (Figure 3.1 A). The three plasmids were then sequentially integrated into an *S. cerevisiae* strain with Δpep4 background that has less protease activity so that the overexpressed condensin complex is better protected at the first affinity purification step. The resulting budding yeast strains were grown in YPR and co-expression of the fission yeast condensin subunits was induced by addition of raffinose to final concentration of 2 %. After 4 hours of induction, the cells were harvested and lysed using a freezer mill. Condensin was affinity purified using Rabbit IgG-Agarose beads, followed by Heparin column, and finally by size exclusion chromatography using Superose 6 column

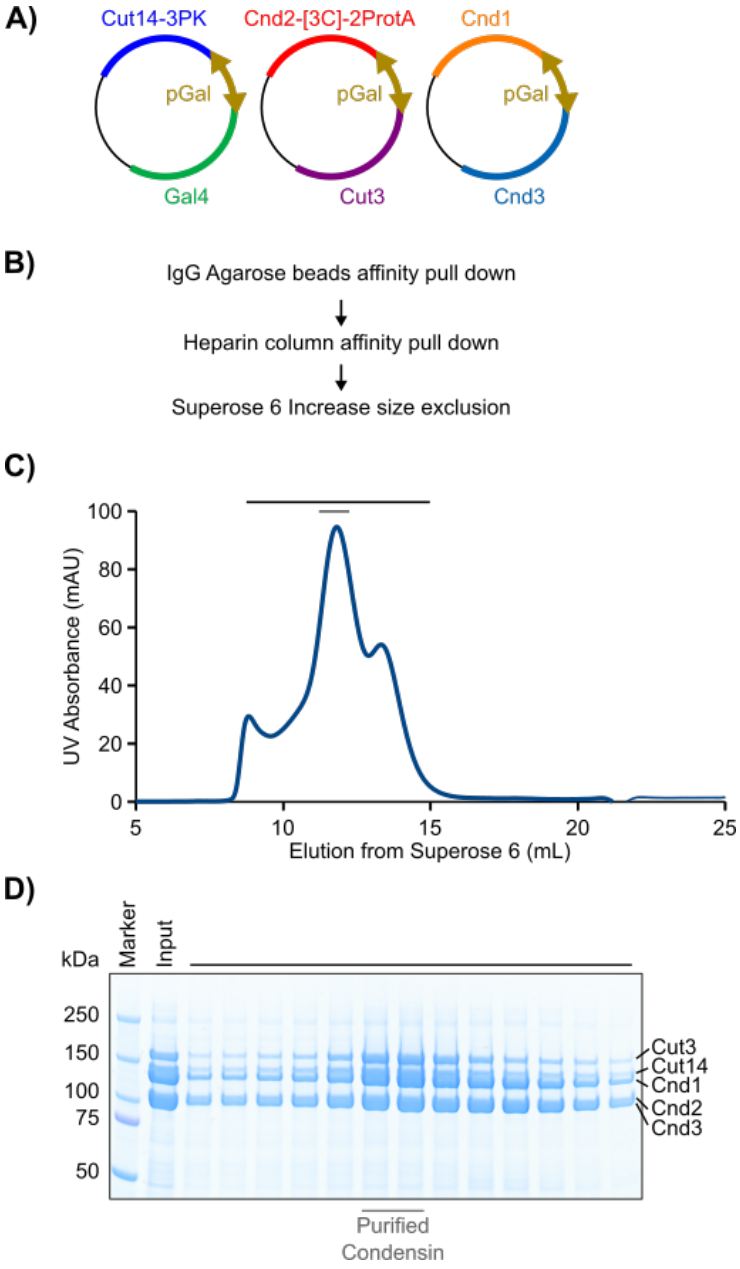

Figure 3.1 Purification of fission yeast condensin

A) Schematic of the three plamsids that were integrated into budding yeast genome for co-overexpression of the five subunits of fission yeast condensin complex.

B) Three-step purification strategy for fission yeast condensin purification.

C) Chromatogram of the size exclusion chromatography of condensin on Superose 6 Increase column.

D) SDS-PAGE analysis of the fractions marked by the black line. The grey lined fractions were pooled and concentrated as the purified condensin complex.

(Figure 3.1 B). Please see more details in materials and methods section. The final size exclusion step showed a stable condensin complex eluting at the expected elution volume (Figure 3.1 C) (St-Pierre et al. 2009). Peak fractions of the size exclusion step were sampled and analysed on 4-12 % Tris-Glycine SDS-PAGE, which showed high purity and stoichiometric complex at the main peak and a kleisin-HEAT repeats sub-complexes at the peak eluting later (Figure 3.1 D).

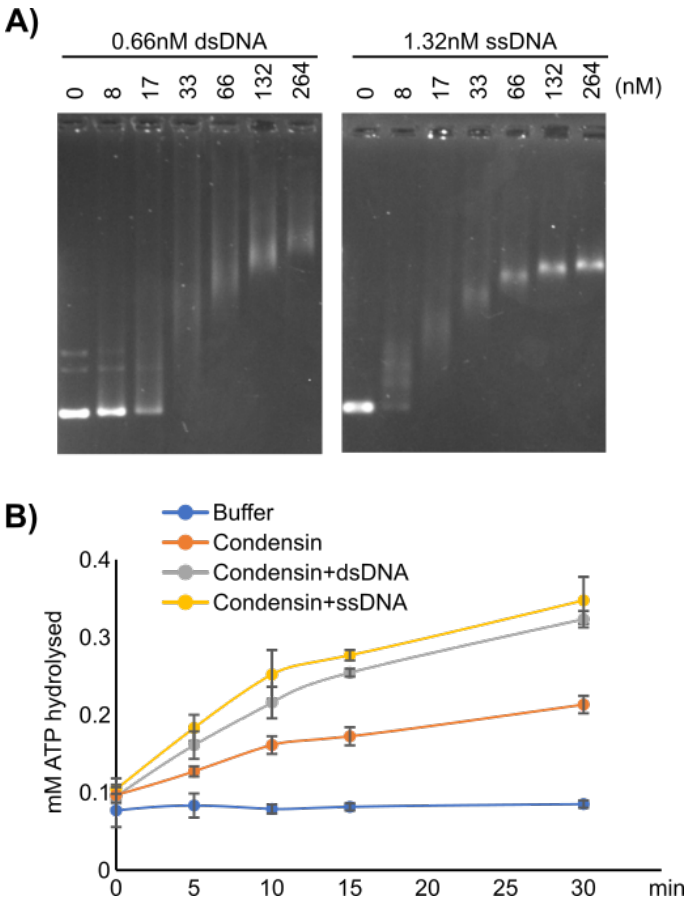

Figure 3.2 Confirmation of activities of the purified fission yeast condensin

A) EMSA (electrophoresis mobility shift assay) of increasing concentrations of condensin binding to either 0.66 nM supercoiled circular dsDNA or 1.32 nM circular ssDNA.

B) ATPase activity of condensin in the absence or presence of 3.3 nM circular dsDNA or 6.6 nM circular ssDNA.

I then confirmed the expected activities of my purified fission yeast condensin by ATPase assay and EMSA. The purified condensin complex could bind either dsDNA or ssDNA, with a slight preference towards the ssDNA (Figure 3.2 A). The fission yeast condensin also showed ATPase activity that was stimulated by either dsDNA or ssDNA (Figure 3.2 B), consistent with previous reports (Kimura et al. 1999; St-Pierre et al. 2009; Yoshimura et al. 2002). These observations confirmed that my purified fission yeast condensin is of adequate quality for further biochemical characterisation.

3.2 Condensin binds to DNA in a salt-resistant manner

Budding yeast condensin was observed to bind topologically to mini-chromosomes *in vivo* (Cuylen, Metz, and Haering 2011). Additionally, cohesin, a close relative of condensin, was shown to topologically load onto DNA *in vivo* and *in vitro* (Ivanov and Nasmyth 2005; Murayama and Uhlmann 2014; Minamino et al. 2018). A common observation of such topological DNA loading reactions is a salt-resistant DNA association that is stimulated by ATP; therefore, I explored whether my purified condensin can bind DNA in a salt-resistent manner *in vitro*. I adapted previously described, topological cohesin loading assay to condensin. Briefly, the condensin was incubated with a supercoiled dsDNA substrate in the presence of either EDTA, Buffer (denoted as “ddH_2O”), or ATP for 30 mins before immunoprecipitation by magnetic beads pre-coupled with anti-PK antibodies. The beads were washed with high-salt buffer to disrupt direct protein-DNA interactions and finally the beads were split to analyse DNA and protein contents (Figure 3.3 A). The high-salt resistant DNA binding by condensin was stimulated by ATP (Figure 3.3 B). As a control, the amount of immunoprecipitated condensin was consistent across all conditions, so that the DNA recovered from the beads can be directly compared. I conclude that condensin can bind to supercoiled dsDNA in a salt-resistant manner.

Similar to cohesin (Murayama and Uhlmann 2014), the condensin loading reaction was also dependent on low-salt conditions during the initial incubation,

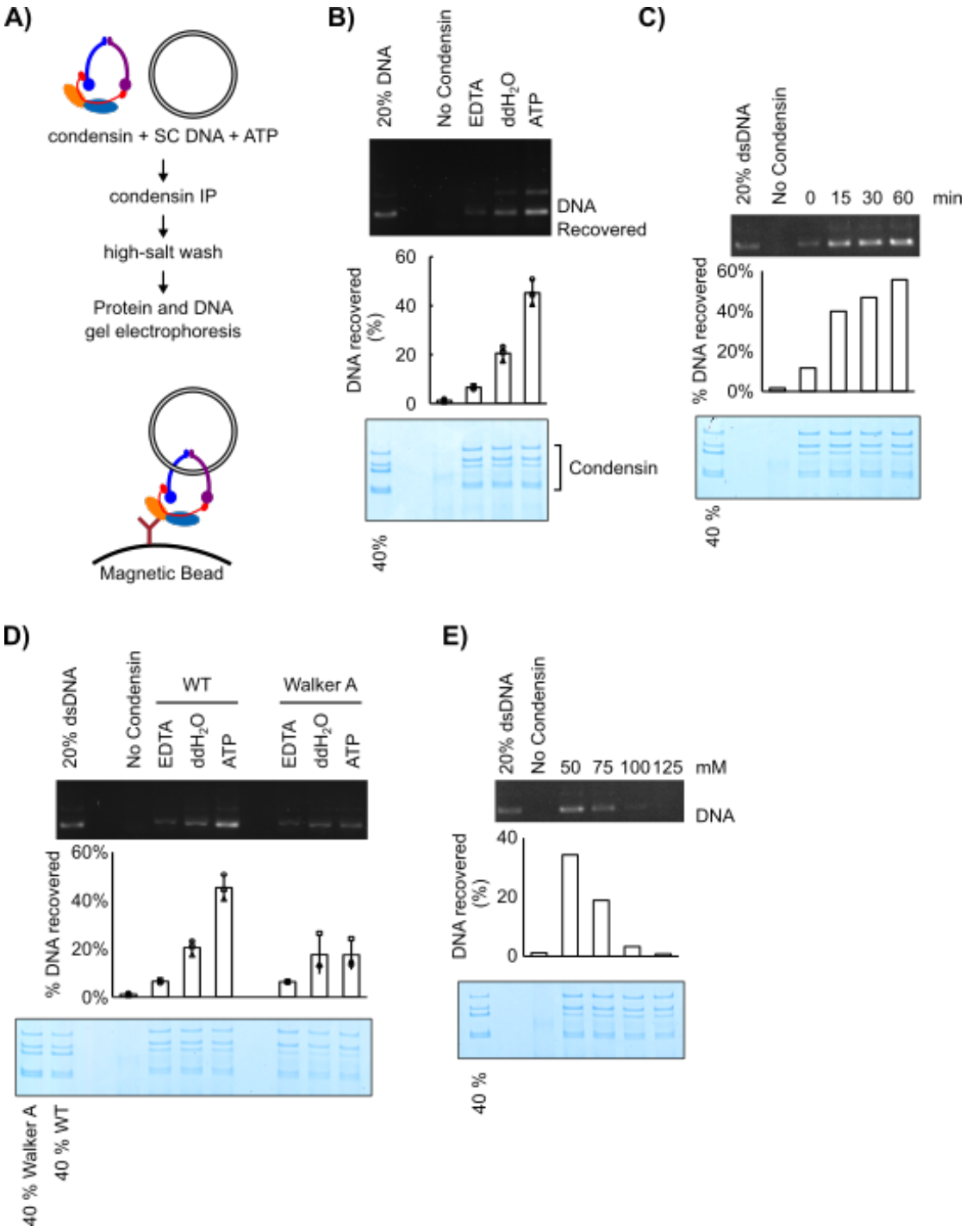

Figure 3.3 Condensin binds dsDNA in a salt-resistant, ATP-dependent manner

A) Condensin loading assay based on (Murayama and Uhlmann 2014).
B) Condensin loading assay. Top: 0.8 % TAE-Agarose analysis on the DNA recovered from magnetic beads in condensin loading assay. Middle: quantification of DNA contents from three biological repeats of the condensin loading assay. Error bars indicate sample standard deviations. Bottom: 4-12 %

Tris-Glycine SDS-PAGE analysis of the protein recovered from magnetic beads in condensin loading assay.
C) Condensin loading assay using supercoiled dsDNA in the presence of ATP with different incubation times.
D) Comparison between wild-type condensin and a double Walker A mutant condensin in the condesin loading assay.
E) Condensin loading reaction performed at the indicated salt concentrations.

before the high-salt wash - as the salt concentration increased during the initial incubation, less DNA was recovered from the condensin IP following high-salt wash (Figure 3.3 E).

To further establish the role of ATPase activity of condensin in the DNA loading assay, I monitored the condensin loading onto supercoiled dsDNA over time (Figure 3.3 C). Under these experimental conditions, the amount of DNA loaded onto condensin increased rapidly over the first 15 min and gradually plateaued after 30 min. This trend is remarkably similar to the observed ATP hydrolysis of condensin, suggesting that the condensin loading reaction could be coupled to ATP hydrolysis. Additionally, the ATP-stimulation of condensin loading onto DNA is completely lost when I mutated both Walker A motifs on the condensin head ATPase (Figure 3.3 D). These observations confirmed that the salt-resistant condensin loading onto DNA is dependent on ATP.

Next, I compared condensin loading in the presence of ATP but onto DNA substrates with different topologies. The supercoiled (SC), nicked (NC), or relaxed (RC) dsDNA substrates was recovered with similar efficiencies, whereas no linear (L) dsDNA substrate was recovered (Figure 3.4 A). These results suggest that condensin can only bind to circular dsDNA substrates in a salt-resistant manner, but not linear DNA substrates, suggesting that condensin binds to dsDNA in a topological manner.

Interestingly, condensin could also load onto circular ssDNA (ss) substrate in a salt-resistant manner. I then confirmed that the condensin loading onto ssDNA is also ATP-dependent (Figure 3.4 B). Taken together, fission yeast condensin

can bind to DNA substrates in a salt-resistant manner, as long as the circular DNA substrate remains covalently closed.

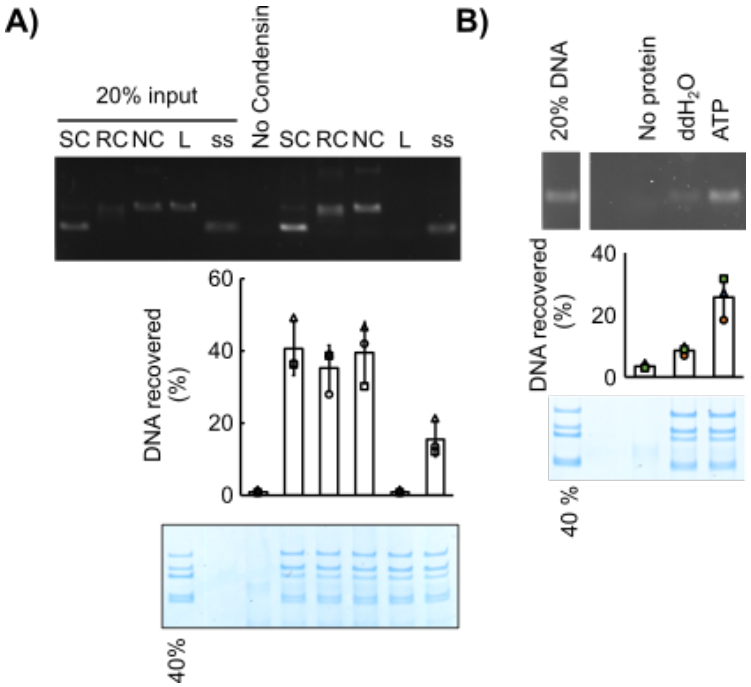

Figure 3.4 Condensin loading onto DNA with different topologies

A) Condensin loading onto different DNA substrates in the prescence of ATP. SC, supercoiled circular dsDNA. RC, relaxed circular dsDNA. NC, nicked circular dsDNA. L, linear dsDNA. ss, circular ssDNA.
B) Condensin loading onto circular ssDNA substrate is dependent on ATP.

3.3 Condensin topologically loads onto DNA

Previous data using different DNA topologies potentially means that the ATP-dependent salt-resistant condensin loading onto DNA might be topological. To confirm the topological nature between the DNA and the loaded condensin, I linearised the supercoiled dsDNA substrate after the condensin loading assay using restriction enzyme ScaI. I then adjusted to middle-salt conditions (250 mM NaCl) and monitored the distribution of the DNA and protein with or without restriction enzyme treatment (Figure 3.5 A left). The predicted outcome of this experiment is that if condensin binds to DNA only via high-salt resistant, direct protein-DNA interaction, then DNA should remain bound to the condensin in the

presence or absence of the restriction digestion. On the other hand, if condensin binds to DNA topologically, then the linearised DNA substrate would be lost whereas the circular DNA substrate would remain bound to condensin. Indeed, while the intact dsDNA plasmid remains bound to condensin on the beads, all the linearised dsDNA is released into the supernatant (Figure 3.5 A right), proving that condensin interacts with the dsDNA substrate topologically.

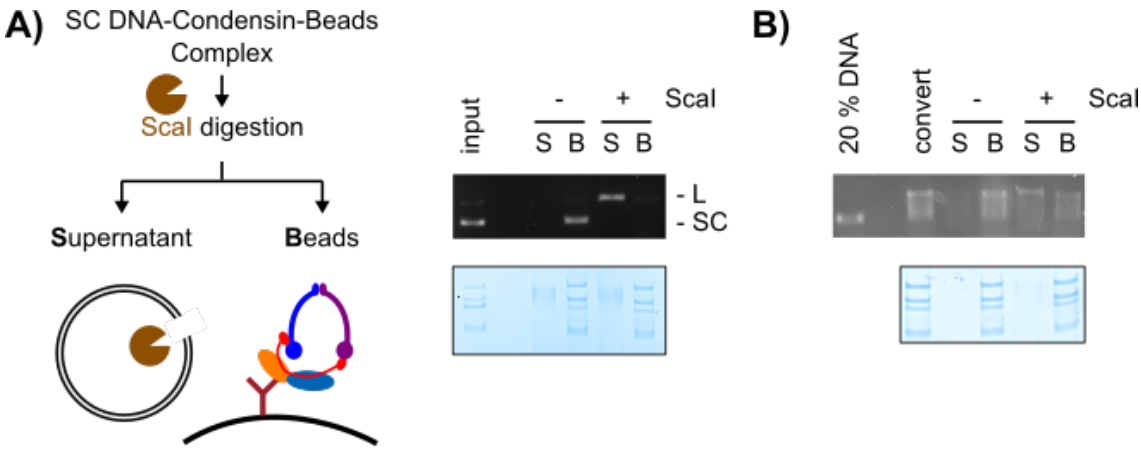

Figure 3.5 Condensin binds to DNA topologically

A) Schematic (left) and the result (right) of dsDNA linearisation after condensin loading assay. S, supernatant. B, beads fraction. L, linearised plasmid. SC, supercoiled plasmid.
B) Condensin loaded onto ssDNA topologically. After condensin loading onto primer-annealed circular ssDNA substrate, the ssDNA was converted into dsDNA and then treated with either ScaI or buffer only.

What about the topology of the ATP-dependent salt-resistant ssDNA loading? To probe the topology of the loaded ssDNA, after loading using the primer-annealed circular ssDNA, I used T4 DNA polymerase to convert the loaded circular ssDNA into dsDNA and then treated with the restriction enzyme ScaI. After linearisation, the converted dsDNA (from ssDNA) was effectively released from beads-tethered condensin (Figure 3.5 B), indicating that the ssDNA was originally loaded in a topological manner. Taken together, condensin can topologically load onto any covalently closed DNA substrate.

3.4 Condensin forms a DNA gripping state in the presence of ADP.BeF_3

Cohesin was previously shown to form a “DNA gripping state” in the presence of a short linear dsDNA and non-hydrolysable ATP analogues (such as ADP.BeF_3) and cryo-EM structures were solved using either wild type cohesin or Walker B mutant cohesin that could still bind to but not hydrolyse ATP (Higashi et al. 2020; Shi et al. 2020). Given that the complete DNA loading reaction requires ATP hydrolysis (Murayama and Uhlmann 2014), the observed “DNA gripping state” of cohesin using non-hydrolysable ATP analogues must have formed prior to ATP hydrolysis during the cohesin loading reaction. Recent articles posted on bioRxiv also reported similar DNA-gripping structures by budding yeast condensin using non-hydrolysable ATP analogues such as ADP.BeF_3 (Shaltiel et al. 2021; Lee, Rhodes, and Löwe 2021). To investigate whether the fission yeast condensin forms a similar DNA gripping state prior to topological loading, I modified the condensin loading reaction as stated below. The DNA substrate was changed to a short 124 bp linear dsDNA. And both IP and wash steps were performed in a middle-salt buffer (Figure 3.6 A left). Consistent with previous results using linearised dsDNA plasmids, the short linear dsDNA following incubation in the presence of ATP or ADP could not be retained by beads-tethered condensin after IP and wash steps (Figure 3.6 A right). Strikingly, ADP.BeF_3 supported the recovery of short linear dsDNA after middle-salt IP and wash, suggesting a stronger condensin-DNA interaction that is reminiscent of the DNA-gripping state formed by cohesin. Although the ADP.BeF_3 supported the recovery of 124 bp dsDNA under middle-salt conditions, the 124 bp dsDNA is lost after high-salt (500 mM NaCl) IP and wash (Figure 3.6 B).

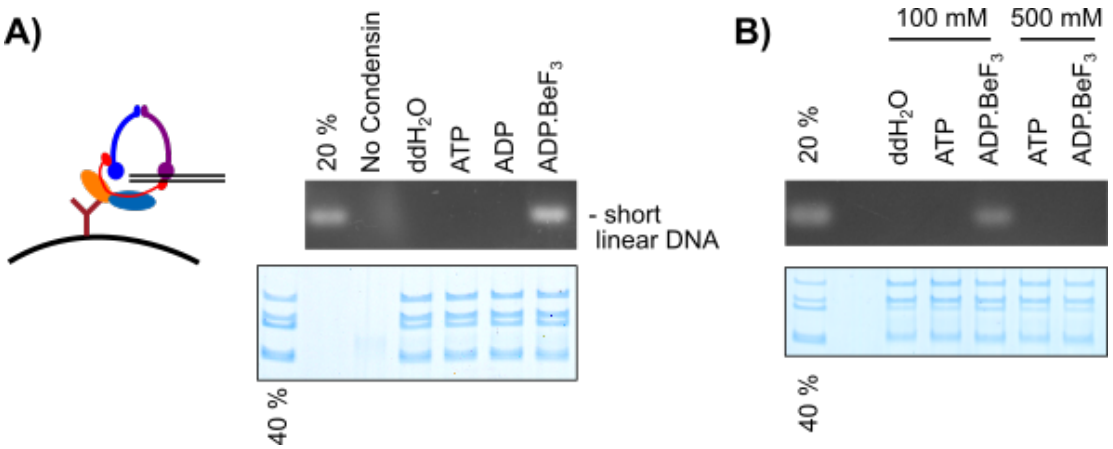

Figure 3.6 Condensin forms a DNA-gripping state

A) Condensin can grip short linear dsDNA in the presence of ADP.BeF_3. Left: Schematic of modified condensin loading reaction to probe condensin DNA-gripping state. Right: after washing with middle salt buffer, only ADP.BeF_3 loaded short linear dsDNA is recovered from the beads-tethered condensin. B) After gripping reaction, condensin was Immunoprecipitated and washed using either middle-salt buffer (100 mM NaCl) or high-salt buffer (500 mM NaCl). ATP loaded DNA cannot retain linear dsDNA in either case. ADP.BeF_3 induced DNA gripping by condensin could resist middle-salt buffer but not high-salt buffer.

The loss of condensin interaction with the 124 bp dsDNA following high-salt washes has two potential explanations: 1) high-salt conditions could weaken the condensin-DNA interactions that held the 124 bp dsDNA in place. 2) high-salt conditions might disrupt the condensin conformation that held the 124 bp dsDNA. These two possibilities could not be easily distinguished.

As a complementary approach to observe condensin loading onto DNA, I developed an additional assay to measure condensin loading onto DNA. I utilised a 5 kbp linear dsDNA substrate, doubly tethered onto magnetic beads via digoxygenin – anti-digoxygenin antibody interactions (Figure 3.7 A left). The beads-tethered dsDNA was incubated with condensin in the presence of a series of different nucleotides. Then the beads were washed with high-salt buffer (500 mM NaCl) before the protein and DNA contents were analysed.

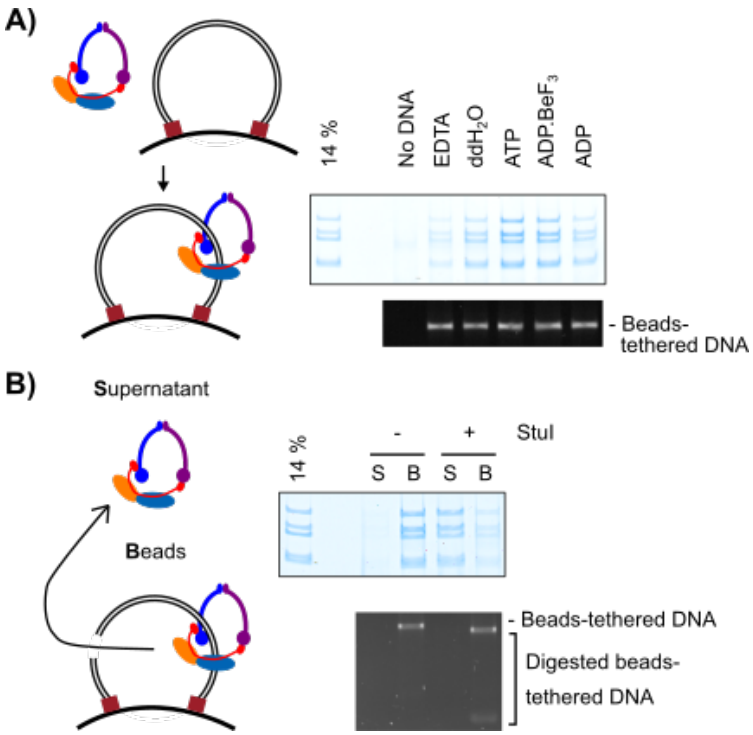

Figure 3.7 Condensin topologically bound to beads-tethered dsDNA

A) Left: Schematic of the condensin loading assay using beads-tethered dsDNA. dsDNA was doubly tethered onto magnetic beads via digoxygenin – anti-digoxygenin antibody interactions, thereby forming a closed topology. Condensin was incubated with the beads-tethered dsDNA and washed with high-salt buffer to remove condensin that only interacted with the beads-tethered dsDNA electrostatically. Right: The condensin loading onto beads-tethered dsDNA after high-salt wash.
B) Left: Schematic of the StuI cleavage of beads-tethered dsDNA after condensin loading onto dsDNA by ATP. If the condensin loading onto the new DNA substrate were also topological, the condensin would only be released when the beads-tethered dsDNA was cleaved. Right: Condensin was released from beads-tethered dsDNA only after the dsDNA was cleaved by StuI.

The amount of dsDNA on the beads were consistent between samples so that condensin recovery could be directly compared (Figure 3.7 A right). Consistent with the condensin IP loading assay, the recovery of condensin on the beads-tethered dsDNA was stimulated by ATP. To confirm the topological nature of the loading with this substrate, I cleaved the beads-tethered dsDNA using StuI

after condensin loading and high-salt washes (Figure 3.7 B left). Again, consistent with the topological mechanism of loading, condensin remained stably bound to intact beads-tethered dsDNA but was released from beads-tethered dsDNA once the DNA was cleaved by StuI (Figure 3.7 B right).

Interestingly, the condensin loaded with ADP.BeF_3 onto this topologically constrained dsDNA substrate resisted washing with high-salt buffer (Figure 3.7 A right). This suggests that loss of the 124 bp short linear dsDNA in condensin IP gripping assay under high-salt wash (Figure 3.6 B) was due to loss of electrostatic interaction between the condensin and the gripped dsDNA, while the topologically restrained DNA was retained within the topological enclosure that forms part of the DNA gripping state. This idea is consistent with the recent structures mentioned above (Shaltiel et al. 2021; Lee, Rhodes, and Löwe 2021), which showed that the dsDNA was tightly bound inside the positively charged channel formed between the dimerising ATPase heads and the condensin loader Ycs4 (the budding yeast equivalent of Cnd1). Taken together, similar to cohesin, condensin can be induced by ADP.BeF_3 to form a DNA-gripping state that is more salt-resistant than ATP loaded condensin.

3.5 ATP loaded condensin can unload from DNA in an ATP-dependent manner

Condensin has a high turnover rate on chromatin (Thadani et al. 2018; Gerlich et al. 2006). The dynamics of condensin is thought to be crucial to its function in genome organisation during mitosis (Cheng et al. 2015; Gerguri et al. 2021). To observe condensin dynamics after topological loading, I loaded condensin onto beads-tethered dsDNA, washed with high-salt buffer, then further incubated the beads in middle-salt (135 mM NaCl) buffer, before again observing the condensin distribution between supernatant and beads fractions (Figure 3.8 A). While the beads-tethered dsDNA remained in the beads fraction under all the conditions, the condensin distribution was dependent on the conditions of the second incubation. Without Mg^{2+} in the buffer, most condensin remained bound to the beads-tethered dsDNA. In the presence of ATP, most of the condensin

was released into the supernatant fraction. This suggests that topologically loaded condensin can unload itself from DNA in an ATP-dependent manner. To further confirm the role of the ATP in the unloading reaction, I monitored condensin unloading over time (Figure 3.8 B). Whereas little unloading was observed in the presence of EDTA, addition of ATP stimulated condensin unloading over time, with the highest unloading rate over the first 5 mins of the unloading reaction, which then plateaued after 15 mins. These kinetics are again reminiscent of the condensin ATP hydrolysis rate measured over time (Figure 3.2 B).

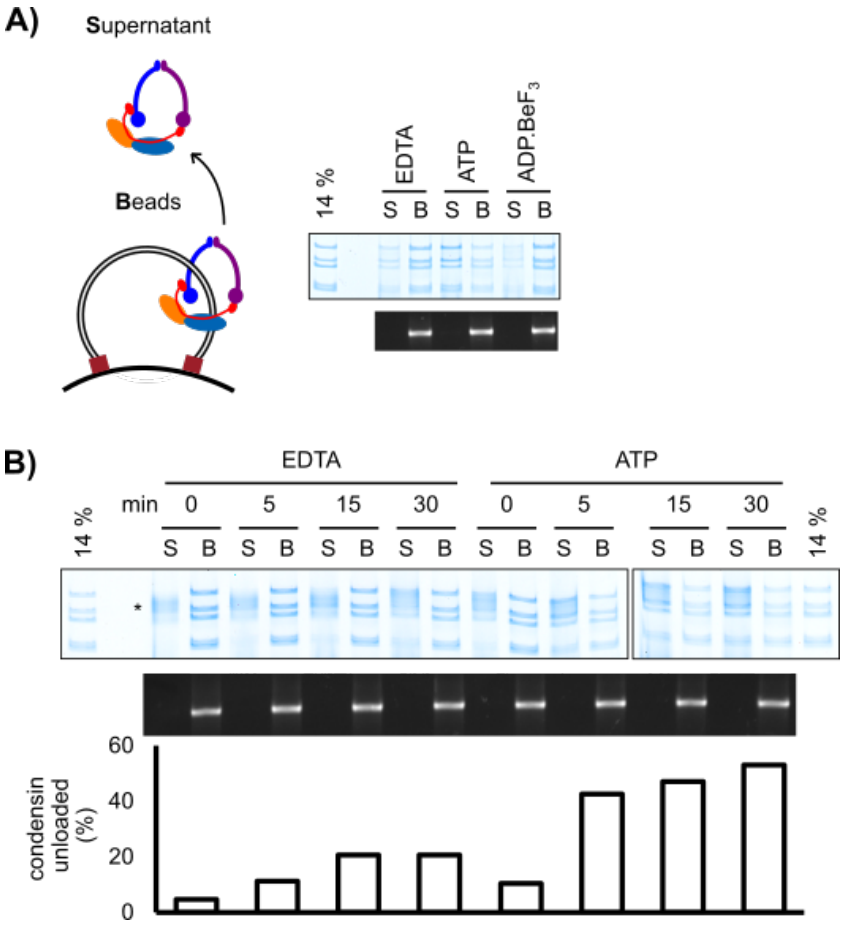

Figure 3.8 Topologically loaded condensin can unload from DNA in an ATP-dependent manner.

A) Left: Schematic of the unloading reaction. Right: ATP-dependent condensin unloading from beads-tethered dsDNA

B) Time course experiment of condensin unloading from beads-tethered dsDNA

C) Condensin unloading after condensin loading with either ATP or ADP.BeF$_3$

Interestingly, topologically loaded condensin did not unload from DNA in the presence of ADP.BeF_3 (Figure 3.8 A), suggesting that ATP binding alone cannot support the condensin unloading reaction – ATP hydrolysis is required for condensin unloading from dsDNA.

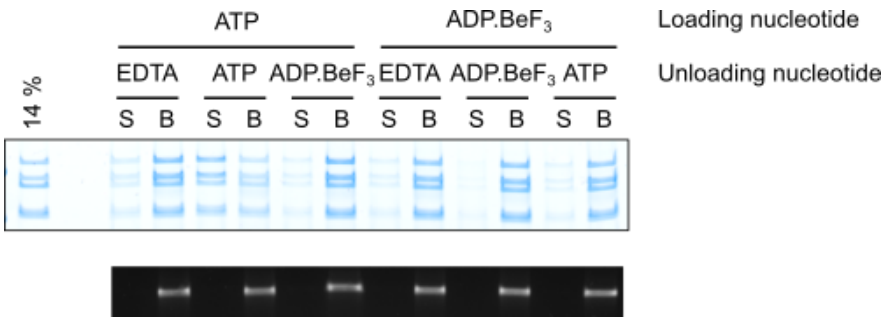

Figure 3.9 Condensin loading using either ATP or ADP.BeF_3 followed by unloading

Condensin was first loaded onto beads-tethered dsDNA using either ATP or ADP.BeF_3. The beads were washed with high-salt buffer before re-equilibrate in middle-salt buffer in the presence of EDTA (without Mg^{2+}), ATP (with Mg^{2+}), or ADP.BeF_3 (with Mg^{2+}). Supernatant (S) was separated from beads (B) before gel electrophoresis analyses.

To directly compare the difference between topologically loaded condensin by ATP and DNA-gripping condensin by ADP.BeF_3, I performed unloading reactions following either ATP-stimulated topologically loading or ADP.BeF_3-induced DNA-gripping state formation (Figure 3.9). The ATP loaded condensin could unload in the presence of ATP but not ADP.BeF_3. On the other hand, the ADP.BeF_3-induced DNA-gripping condensin could not be unloaded even after the reaction was supplemented with additional ATP. This suggests that the ADP.BeF_3 trapped the condensin ATPase heads in the engaged state, where nucleotide exchange with the surrounding environment is inhibited.

Taken together, although both ATP and ADP.BeF_3 induced high-salt resistant binding of condensin onto beads-tethered dsDNA, the dsDNA was held very differently between these two kinds of binding modes. ATP-stimulated topologically loaded condensin can unload itself from the DNA, which again requires ATP hydrolysis. The ADP.BeF_3-induced DNA-gripping condensin

cannot be unloaded from the DNA by any means, possibly because the ATPase heads are trapped in the head engaged state and nucleotide exchange with the surroundings is physically blocked.

3.6 dsDNA loaded condensin can sequentially bind to a second DNA substrate in a salt-resistant manner

Single-molecule observations of condensin on DNA curtains suggest that condensin can interact with two pieces of DNA (Terakawa et al. 2017). To

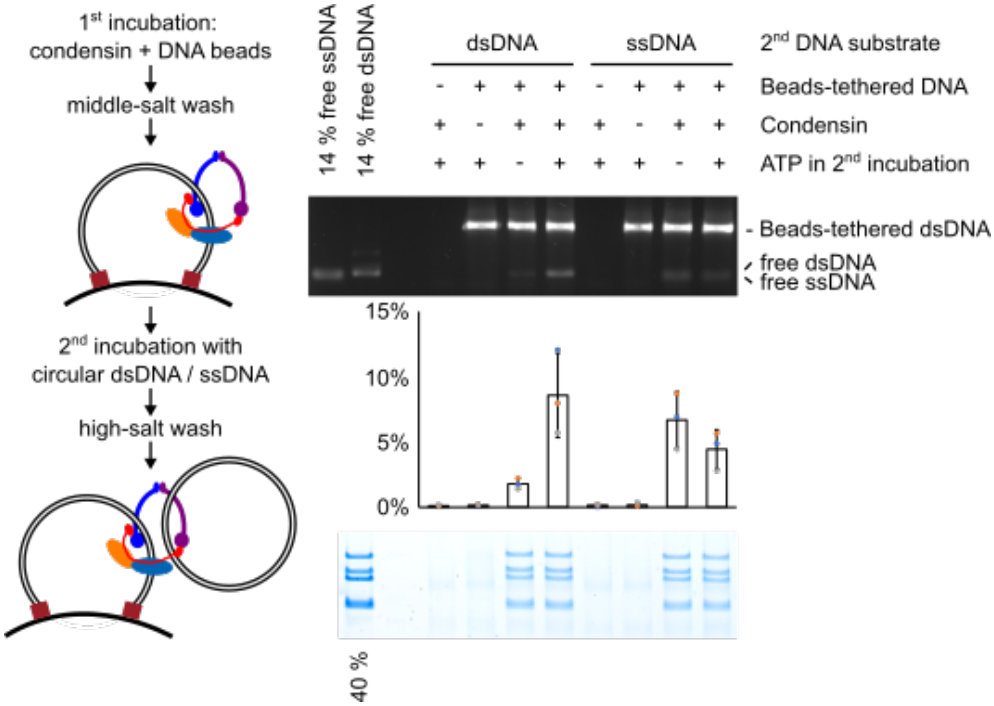

Figure 3.10 DNA loaded condensin can capture a second DNA substrate

Left: Schematic of condensin second DNA capture assay. Condensin was first loaded onto beads-tethered dsDNA using ATP. Following middle-salt wash, the beads was further incubated with either supercoiled pBlueScript plasmid or circular ssDNA in the presence or absence of ATP. The beads were then washed with high-salt buffer and assayed for protein and DNA contents.
Right: DNA contents were analysed by Agarose gel electrophoresis. The free DNA bands was quantified in three independent repeats and the error bar indicates standard deviation of the sample. Protein contents were separated on SDS-PAGE and visualised using Coomassie staining.

biochemically address whether condensin can establish interactions between two DNAs, I performed a condensin “second DNA capture assay” using beads-tethered dsDNA as the first DNA substrate (Figure 3.10 left).

Briefly, condensin was first topologically loaded onto beads-tethered dsDNA using ATP. After washing the beads with middle-salt buffer, the beads were incubated under low-salt loading buffer with a free supercoiled dsDNA plasmid or a circular ssDNA substrate. The beads were finally washed with high-salt buffer and bound protein and DNA were analysed.

In the control experiments, without condensin or beads-tethered dsDNA, neither the free supercoiled dsDNA plasmid nor the condensin was recovered on the beads if condensin or the beads-tethered dsDNA was omitted (Figure 3.10 right). When both condensin and beads-tethered dsDNA were included in the first incubation step, condensin was efficiently loaded onto beads-tethered dsDNA, as shown by the SDS-PAGE. If ATP was left out in the second incubation (*i.e.* the incubation of condensin-dsDNA-beads with the free DNA substrate), less than 2 % of the free dsDNA was recovered. ATP in the second incubation stimulated the recovery of the free dsDNA to around 10 %, suggesting that condensin can capture a second dsDNA, and that this capture requires ATP hydrolysis. Consistently, the time-course of condensin second dsDNA loading showed a time-dependent second dsDNA capture by condensin (Figure 3.11 A). From these results, I conclude that condensin can sequentially capture a second supercoiled dsDNA plasmid in a salt-resistant, ATP-hydrolysis-dependent manner.

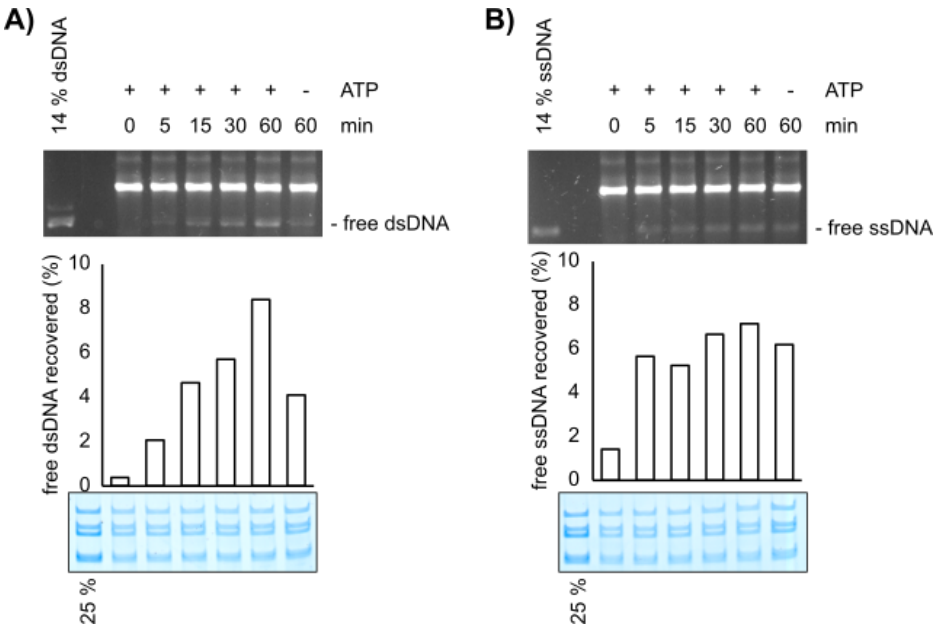

Figure 3.11 Time course of condensin second DNA capture.

A) Time course of the second dsDNA capture by condensin. Condensin was first loaded onto beads-tethered dsDNA using ATP for the same amount of time. Then beads were washed with middle-salt buffer and incubated with free supercoiled dsDNA plasmid and ATP for the indicated amount of time.
B) Time course of the second ssDNA capture by condensin. Same as (A) except the second incubation with circular ssDNA substrate.

To address whether dsDNA-bound condensin can engage not only a second dsDNA, but also a second ssDNA, I repeated the second DNA capture experiment using free circular ssDNA. This showed that condensin that was topologically loaded onto dsDNA can subsequently capture a circular ssDNA substrate (Figure 3.10 right). However, the capture was poorly stimulated by the addition of ATP during the second DNA capture step. Moreover, second ssDNA capture showed less time-dependence (Figure 3.11 B). These observations indicated that although the second ssDNA capture was resistant to high-salt treatment, its mechanism might differ from that of second dsDNA capture.

3.7 Condensin topologically captures second DNA substrates

To investigate whether second DNA capture results in a new topological DNA interactions, after a condensin second DNA capture experiment, either the beads-tethered dsDNA or the free supercoiled dsDNA plasmid was cleaved by restriction enzyme StuI or ScaI treatment, respectively (Figure 3.12).

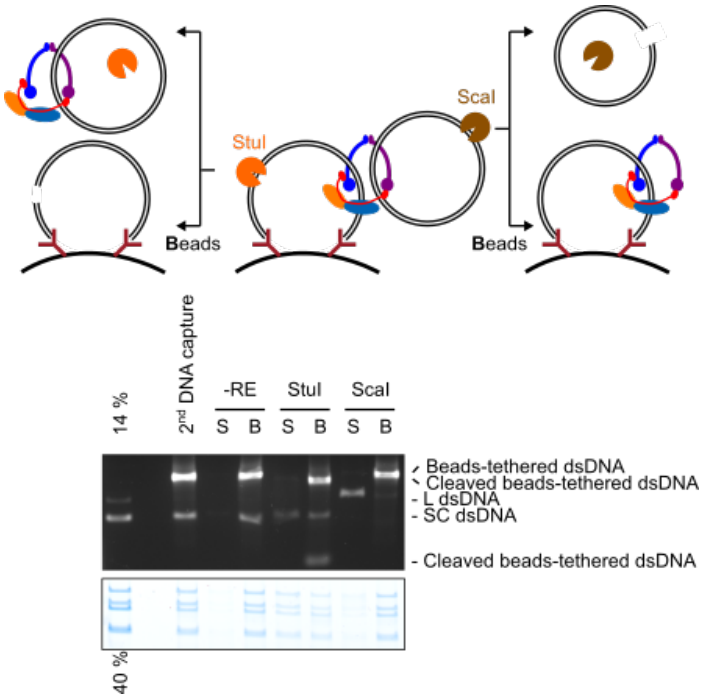

Figure 3.12 Second dsDNA capture by condensin is topological

Top: Schematic of the restriction enzyme specifically cleaving either the beads-tethered DNA or the free plasmid. After condensin second dsDNA capture, the beads were treated with either StuI, which cut specifically the beads-tethered dsDNA, or ScaI, which cut specifically the free supercoiled dsDNA plasmid. Bottom: Restriction digestion after condensin second dsDNA capture showed both plasmids were topologically captured by the condensin.

In the absence of restriction enzyme treatment, both condensin and the free dsDNA plasmids remained stably bound to beads-tethered dsDNA. When the beads-tethered dsDNA was cleaved by StuI, the two pieces of DNA resulting from beads-tethered dsDNA cleavage remained bound to the beads, while

condensin and intact free dsDNA plasmid were released into the supernatant. When only the free supercoiled dsDNA plasmid was cleaved by ScaI, both the intact beads-tethered dsDNA and condensin remained bound to the beads, while the linearised free dsDNA was released into the supernatant. These results suggest that condensin interacted with both the beads-tethered dsDNA and the free dsDNA plasmid in a topological manner.

How about the topology when a second ssDNA is captured by condensin? The topological loading of condensin onto the beads-tethered dsDNA (after capturing a second ssDNA) can again be verified by cleaving the beads-tethered dsDNA, which resulted in the proportionate release of both condensin and ssDNA into the supernatant (Figure 3.13 B). Again, to probe the topology of the captured ssDNA, ssDNA was converted to dsDNA using T4 DNA polymerase. Briefly, after using primer-annealed ssDNA as the DNA substrate for condensin second DNA capture, the captured ssDNA was converted to dsDNA using T4 DNA polymerase. Now the captured DNA became susceptible to restriction enzyme treatment to verify the topology of its interaction with condensin (Figure 3.13 A). In this experiment, no DNA nor condensin was released in the absence of restriction enzyme treatment. When only the beads-tethered dsDNA was cleaved by StuI, condensin and converted free DNA was again released into supernatant proportionally. When the captured and converted second DNA was cleaved by ScaI, only the cleaved free DNA was released while condensin remained bound to the beads-tethered dsDNA. Note that the conversion of the captured second DNA by T4 DNA polymerase did not reach completion and that the resultant products migrated as a partial smear during gel electrophoresis.

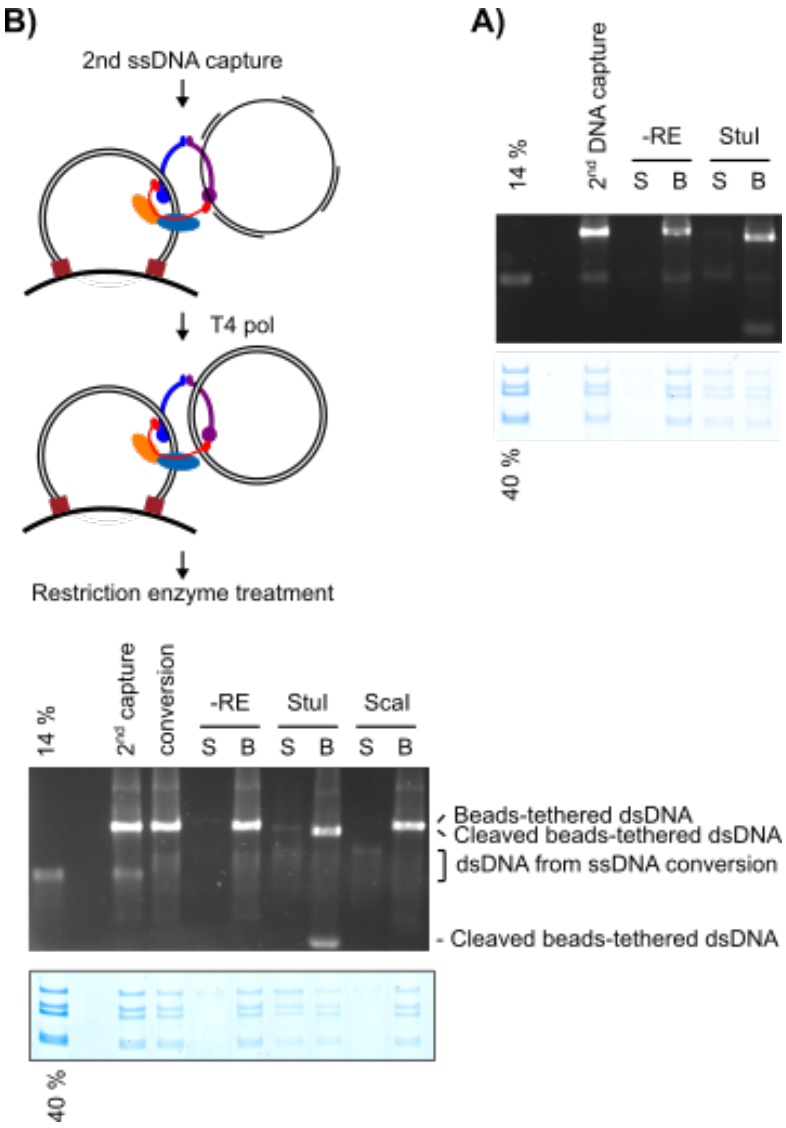

Figure 3.13 Second ssDNA capture by condensin is topological.

A) Conversion of the ssDNA captured by dsDNA loaded condensin to dsDNA followed by restriction enzyme treatment.
B) Direct cleavage of the beads-tethered dsDNA after condensin second ssDNA capture.

To investigate stability and dynamic nature of second DNA capture, I performed condensin unloading reactions after second DNA capture (Figure 3.14 A). As might be expected, the second dsDNA captured by topologically loaded condensin is unloaded from the beads-tethered dsDNA, together with a portion of condensin, in an ATP-dependent manner (Figure 3.14 B). On the other hand, if a second ssDNA was captured by condensin, unloading was ATP-

independent (Figure 3.14 C). This corroborated the previous observation that ssDNA transactions by condensin are less strictly controlled by ATP binding and hydrolysis.

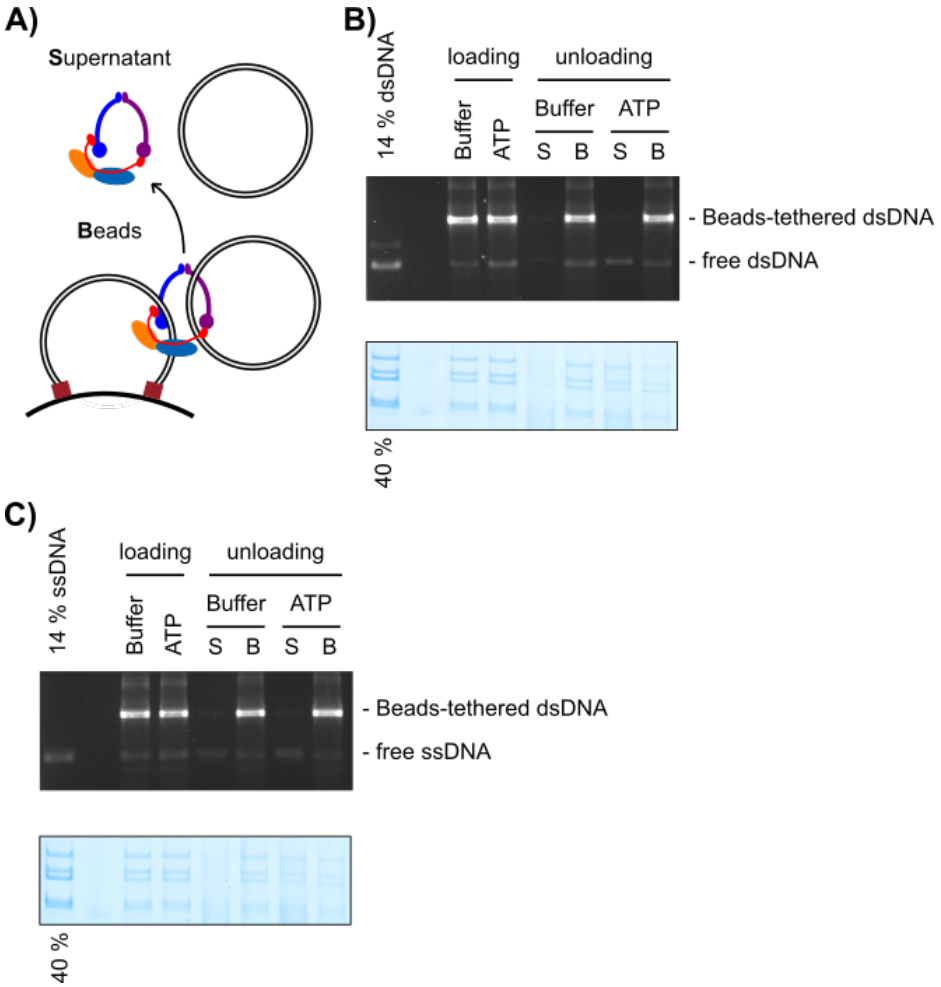

Figure 3.14 Unloading reaction after condensin second DNA reaction.

A) Schematic of the condensin unloading after second DNA capture.
B) Unloading reaction after condensin captures a second dsDNA
C) Unloading reaction after condensin captures a second dsDNA

Taken together, I conclude that condensin, topologically loaded onto one dsDNA, can subsequently topologically capture another dsDNA or ssDNA substrate. While the second dsDNA capture might employ a similar loading mechanism as the first dsDNA loading, the capture of a second ssDNA might be mechanistically different, as judged by the different ATP requirement for both second ssDNA loading and unloading reactions.

3.8 Summary of Chapter 3

To summarise, I established purification protocol of the *S. pombe* condensin in *S. cerevisiae* cells, achieving good stoichiometry, yield, and purity. I confirmed that the purified condensin has basic biochemical activities, such as ATPase activity and DNA binding activity, similar to other condensin complexes reported in the literature. Using an adapted DNA entrapment assay, I demonstrated that condensin can topologically entrap at least one dsDNA or ssDNA. Using a novel beads-tethered DNA substrate, I demonstrated that condensin can load and unload from the DNA in the presence of ATP, recapitulating the previously reported rapid turnover of condensin on chromatin *in vivo*. I also found that , similar to cohesin, condensin forms a DNA-gripping state prior to ATP hydrolysis, which is characterised by tighter linear DNA binding. Importantly, I found that after topologically loading onto one dsDNA, condensin can subsequently entrap an additional dsDNA or ssDNA substrate in a topological manner. These observations provided support for the diffusion capture model of condensin-mediated chromosome formation mentioned in Section 1.2.

Chapter 4. Single molecule visualisation of condensin-DNA interactions

Chapter 3 of my thesis demonstrated the topological DNA entrapment activity by *S. pombe* condensin with one, and two DNA molecules. However, whether a single condensin can perform all the reactions I observe in bulk biochemical experiments is unclear and cannot be easily addressed by additional bulk biochemical experiments. To address whether a single condensin can topologically entrap one or two DNA molecules, I turned to

4.1 Purification and labelling of condensin for single-molecule microscopy

To fluorescently label the condensin for microscopy, a SNAP tag was introduced after the C-terminus of Cut3 for labelling by SNAP-Alexa 647. The purified condensin-Alexa647 behaved like wild-type condensin during the size exclusion chromatography step (Figure 4.1 A). Peak fractions were separated by SDS-PAGE and then analysed by in-gel fluorescence followed by Coomassie staining (Figure 4.1 B). The fractions containing the highest concentration of condensin were collected. Based on the absorption spectrum (Figure 4.1 C), the labelling efficiency of condensin was estimated to be ~93 % a favourable efficiency for quantifying molecule numbers during single-molecule analyses.

To investigate the possibility that SNAP tagging or Alexa 647 labelling altered the activities of condensin, I performed condensin loading assay using both Alexa 647-condensin and wild-type condensin and found that Alexa 647-condensin loaded onto dsDNA in an ATP-dependent manner, indistinguishable from wild-type condensin (Figure 4.1 D). Taken together, the Alexa 647-condensin was efficiently labelled and biochemically equivalent to from wild-type condensin.

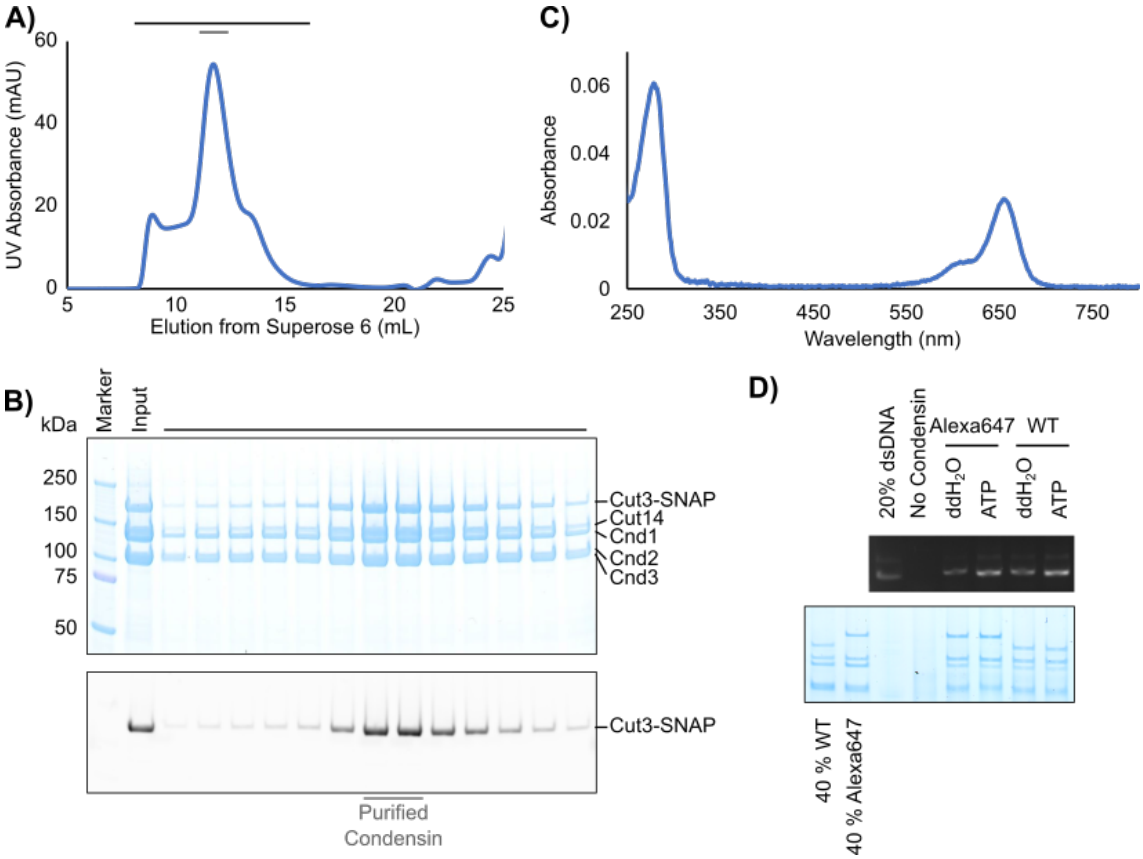

Figure 4.1 Purification of Alexa 647-condensin

A) Chromatogram of the size exclusion chromatography by Superose 6. Black line denotes the fractions taken for SDS-PAGE analyses in (B) and grey line denotes the fractions pooled as the purified Alexa 647-condensin.
B) Coomassie staining and in-gel fluorescence of the SDS-PAGE of Superose 6 elution fractions.
C) Absorbance spectrum for quantification of labelling efficiency.
D) Condensin IP loading assay using Alexa 647-condensin and wild-type condensin

4.2 Single condensin loaded onto and slide along the λ-DNA

For observation of condensin-DNA interactions under the microscope, custom-made microfluid flow cells were prepared using hydrophobic coverslips and then passivated as described in (Molodtsov et al. 2016). λ-DNA with both ends

labelled by digoxygenin was then doubly tethered to the surface using an anti-digoxygenin antibody. Then Alexa 647-condensin was incubated with the λ-DNA in the presence of ATP, before the excess of condensin was washed away

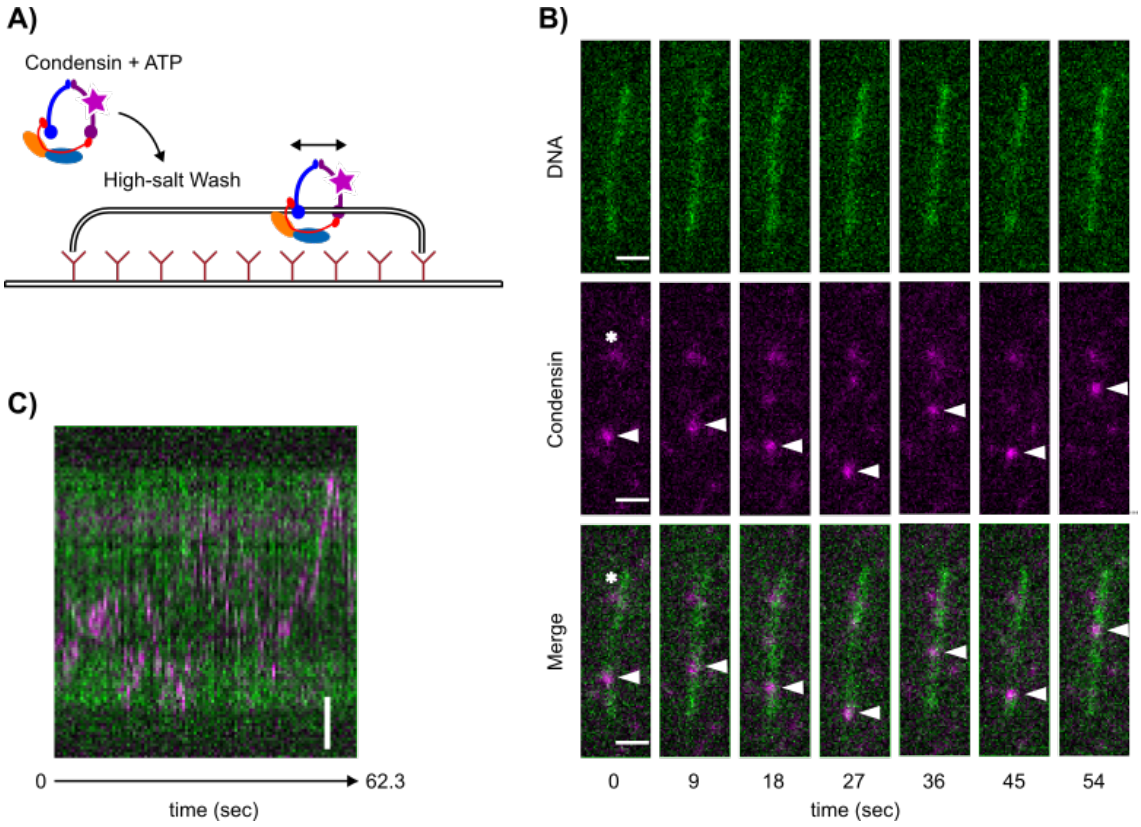

Figure 4.2 Condensin sliding along λ DNA under high-salt conditions

A) Schematic of the reaction in microfluidic flow cells.
B) Snapshots of the condensin sliding along DNA under high-salt conditions. White scale bar is 2 μm. White triangle indicates the sliding condensin molecule. White asterisk indicates a background signal.
C) Kymograph of the entire movie. White scale bar is 2 μm.

using low-salt buffer followed. This was followed by a high-salt buffer wash in the absence of ATP (Figure 4.2 A). Following the high-salt wash, condensin molecules were seen retained on the DNA, that appeared to laterally slide up and down the DNA. A similar behaviour has previously been observed in case of single cohesin complexes, topologically loaded on to λ-DNA. This observation opens the possibility that condensin was topologically loaded onto

DNA in this microscopy setup, able to slide along the lambda DNA (Figure 4.2 B and C).

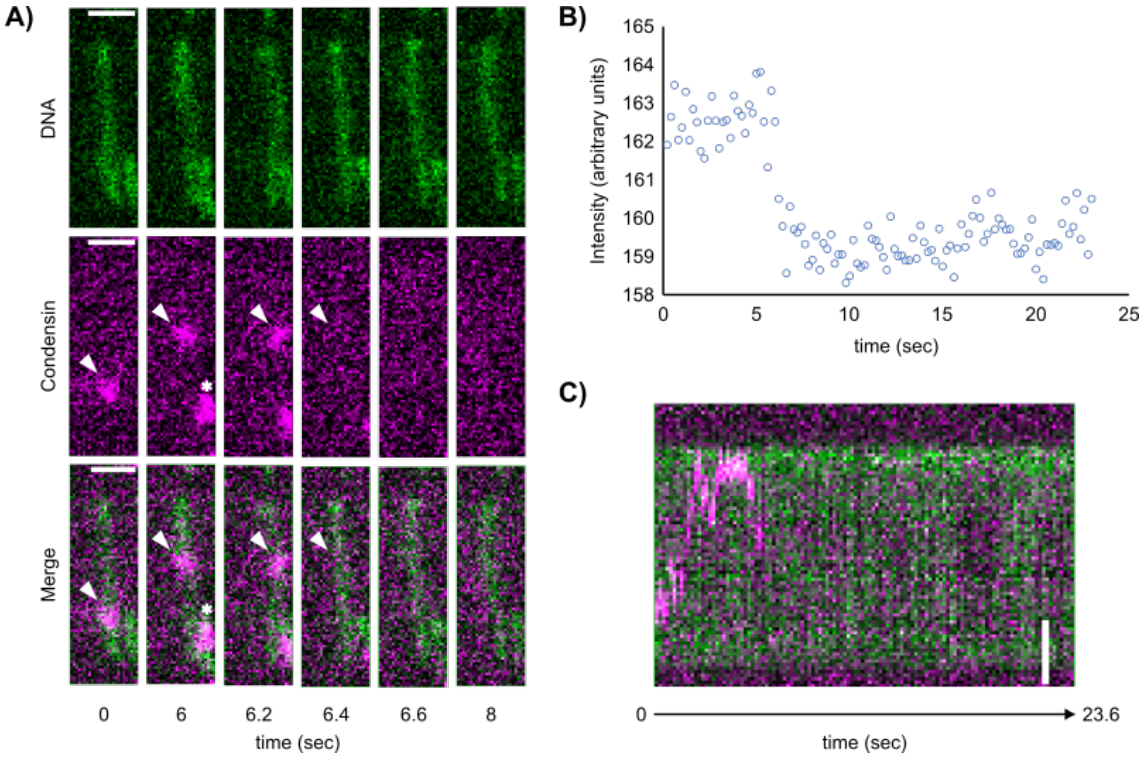

Figure 4.3 Photobleaching of loaded condensin

A) Snapshots of photobleaching experiment, showing a single frame bleaching event. White scale bar is 2 µm. White triangle indicates the sliding condensin molecule. White asterisk indicates another condensin that moved out of the field of view.
B) Quantification of the average condensin signal intensity over time.
C) Kymograph of the photobleaching experiment. White scale bar is 2 µm.

To probe the number of condensin molecules that were visualized by the fluorescent signals on the DNA after loading, the laser power was substantially increased to induce photobleaching. The photobleaching experiment showed single-frame bleaching events in many instances (Figure 4.3 A and C). Quantification of the average signal intensity confirmed uniform intensity of condensin signals, similar to those that led up to one-step bleaching events (Figure 4.3 B). This suggests that single condensin complexes were observed, which slide along the λ DNA. Taken together, a single condensin can load onto

DNA and then resist high-salt treatment, consistent with the condensin loading experiments in Section 3.2. Therefore, it appears likely that individual condensin can slide along DNA, in a high-salt buffer, following topological loading onto the λ DNA.

4.3 Observation of condensin second dsDNA capture using microscopy

To understand whether a single condensin could mediate interactions between two dsDNA, I performed a sequential condensin second dsDNA capture experiment in the microfluidic flow cell. Similar to the bulk second dsDNA

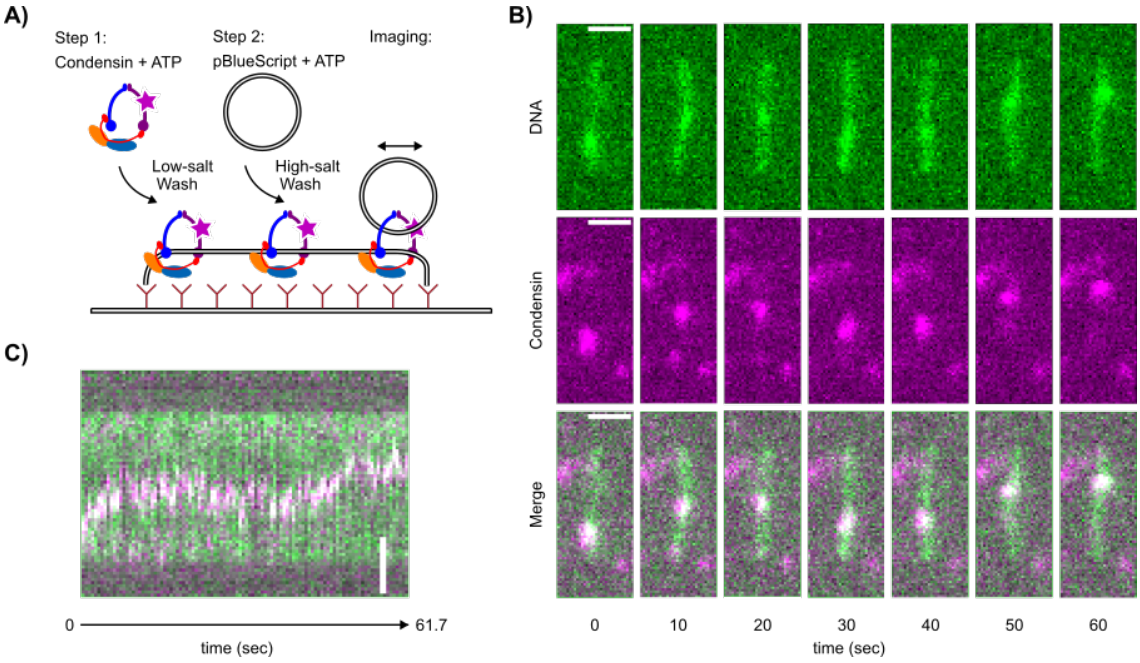

Figure 4.4 Observation of condensin-dependent accumulation of DNA under the microscope

A) The schematic of the sequential condensin second dsDNA capture experiment under the flow cell.
B) Snapshots of the condensin-mediated second dsDNA capture using supercoiled pBlueScript as the second dsDNA. White scale bar is 2 μm.
C) Kymograph of the second dsDNA capture movie. White scale bar is 2 μm.

capture experiment, condensin was first loaded onto λ DNA in the presence of ATP. Excess condensin was then washed away using a low-salt buffer. Then supercoiled pBlueScript plasmid was introduced alongside ATP to stimulate second dsDNA capture. The flow cell was then washed with low-salt buffer followed by high-salt buffer before imaging under high-salt conditions in the absence of ATP (Figure 4.4 A).

After incubation with the second plasmid DNA, an extra DNA density was observed that moved along the λ DNA together with the condensin signal in an apparently stochastic fashion (Figure 4.4 B and C). It is unlikely that the extra DNA density resulted from condensin-mediated DNA compaction or loop extrusion, since DNA structures resulting from either reaction have been reported to dissolve under high-salt buffer conditions and in the absence of ATP (Ganji et al. 2018; Eeftens et al. 2017). As a result, the extra DNA density likely to correspond to the captured supercoiled pBlueScript plasmid.

To confirm that the extra DNA density captured by condensin was the supplied pBlueScript plasmid under the microscope, the second DNA capture substrate was replaced by pBlueScript plasmid covalently labeled with MFP488, which can be distinguished from the general DNA signal from Sytox Orange staining (Figure 4.5 A). As shown, colocalizing with the extra DNA density, the MFP488 labelled pBlueScript was sliding along the λ DNA in the high-salt conditions (Figure 4.5 B and C), consistent with the idea that the extra DNA density observed in earlier experiments was the second plasmid introduced after condensin loading.

Due to optical setup of the microscope, only the two colours of the MFP488 stained plasmid and the Sytox Orange stained overall DNA signal could be simultaneously recorded. To visualize condensin on the same DNA molecule, the microscope filters and laser illumination were switched, and I continued to record the total DNA signal in the Sytox Orange channel, now together with Alexa647 labelled condensin (Figure 4.6 A and C). This revealed a condensin signal that colocalised with the extra DNA intensity while sliding along the λ

DNA, suggesting that condensin was present where the second plasmid DNA was interacting with the λ DNA.

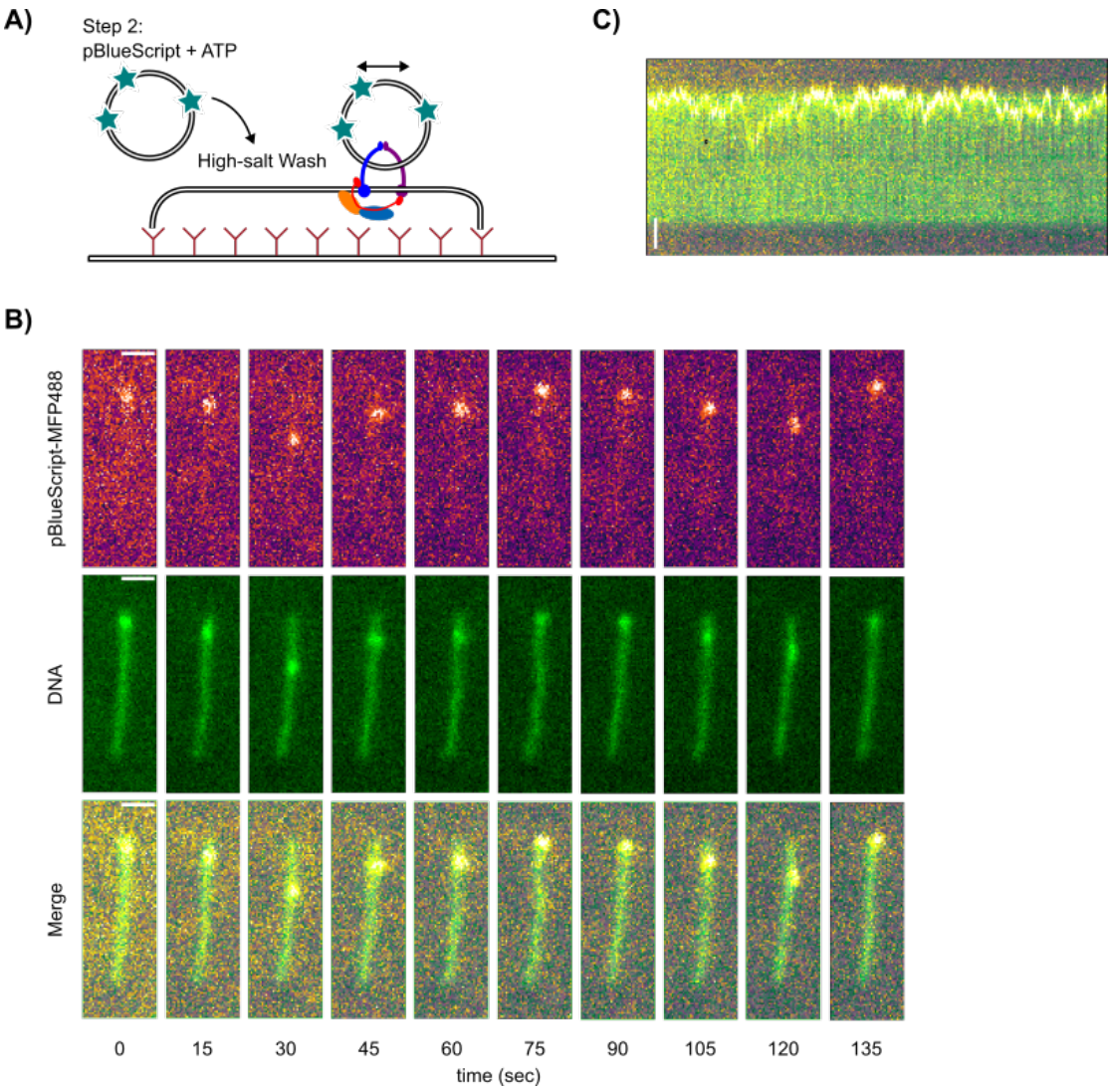

Figure 4.5 Condensin second dsDNA capture experiment using a labelled second DNA substrate

A) Schematic of the second dsDNA capture using MFP488-labelled pBlueScript as the second dsDNA substrate.
B) Snapshots of the MFP488-labelled pBlueScript sliding along the λ DNA, where the corresponding extra DNA density was observed. White scale bar is 2 μm.
C) Kymograph of the movie showing MFP488-labelled pBlueScript sliding along the λ DNA. White scale bar is 2 μm.

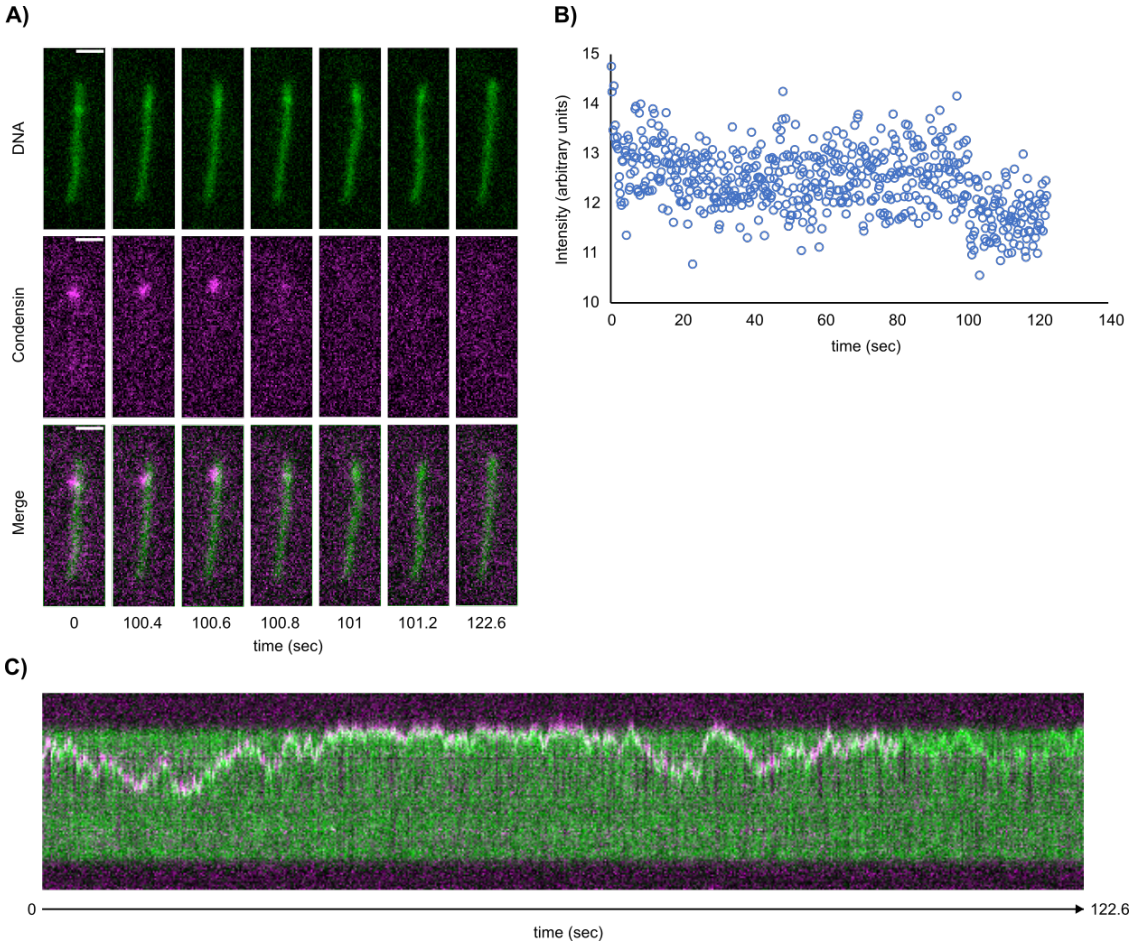

Figure 4.6 Second dsDNA capture observed in single-molecule experiments

A) Snapshots of the movie on the DNA in Figure 4.5, but visualising total DNA and condensin channels. White scale bar is 2 μm.
B) Quantification of the condensin signal intensity over time.
C) Kymograph of the movie in (A). White scale bar is 2 μm.

Assuming the observed condensin signal corresponds to the condensin that mediated the interaction between λ DNA and pBlueScript plasmid, I tried to determine the number of condensin required for the observed second dsDNA capture by measuring the photobleaching profile of condensin signal (Figure 4.6 B). Only one condensin bleaching event was observed around 100 seconds, suggestive of a single condensin mediating the interaction between the two DNA molecules. Among the 20 condensin second DNA capture events recorded, 3 exhibited a single-step photobleaching of condensin complexes. Despite the apparently low frequency of single-condensin events, it is

reasonable to argue that multiple condensin complexes colocalizing on the lambda DNA would cooperatively increase the residence time of the second DNA substrate and thereby increasing the chance of observing the second DNA capture by the single condensin, especially given the dynamic turnover of condensin on DNA. Nevertheless, future experiments will be required to further study second DNA capture at the single molecule level. It will be crucial to investigate whether indeed a single condensin complex is able to sequentially entrap two DNAs.

4.4 Summary of Chapter 4

To summarise this chapter, using Alexa 647 labeled condensin, I successfully reconstituted the condensin loading onto one and two DNA substrates inside a flow cell under the single-molecule microscope. Quantification of the condensin molecules suggests that a single condensin could perform these loading reactions. These observations corroborated the results of bulk biochemical experiments in Chapter 3 and further supported the diffusion capture model of condensin-mediated chromosome formation mentioned in Section 1.2.

Chapter 5. Discussion

This part discusses the implications of the results above in the context of the current views regarding condensin loading onto DNA and condensin-mediated DNA compaction.

5.1 Condensin topologically loads onto DNA in an ATP-dependent manner

Using condensin IP DNA loading assay, condensin loading onto beads-tethered dsDNA assay, DNA cleavage experiments after condensin loading, and the observation of individual condensin loading under the microscope, I demonstrated that a single condensin can topologically load onto DNA in an ATP-dependent, high-salt resistant manner. This is in agreement with the previous data that condensin topologically entraps mini-chromosomes *in vivo* (Cuylen, Metz, and Haering 2011), and that cohesin can topologically entrap DNA *in vitro* and *in vivo* (Murayama and Uhlmann 2014; Ivanov and Nasmyth 2005). On the other hand, a pseudo-topological model of condensin-DNA interactions, where both strands of a DNA loop are captured inside the same condensin ring, was proposed based on the recent observation that condensin with all three interfaces covalently crosslinked cannot recover mini-chromosome from *in vivo* IP experiments (Shaltiel et al. 2021). Challenging the topological model of DNA entry into the tripartite ring formed by Cut14^{Smc2}, Cut3^{Smc4}, and Cnd2^{Brn1}, this model propose that a DNA loop is inserted into the compartment formed by kleisin and is maintained pseudo-topologically by compartments formed between two HEAT repeat subunits and kleisin unstructured regions. In contrast, the non-topological DNA interactions introduced in Section 1.3.5 depict a scenario where DNA loop locates completely outside the condensin ring, and condensin merely interacts with the two strands of the DNA loop via direct protein-DNA interactions (Figure 1.3). Although the pseudo-topological model agrees with the crosslinking data, so does the topological model with the following rationale. Note that the condensin crosslinking data, especially those

involving the kleisin “N-gate”, was collected on Smc2-Brn1 fused condensin. As introduced in Section 1.3.4, the topological loading reaction involves DNA entry at the opened “N-gate”. Now, with a fused condensin “N-gate”, the DNA is trapped either inside the kleisin pocket between “N-gate” and the linker between Smc2 and Brn1, or inside the kleisin pocket between the “N-gate” and Ycs4 binding site, rendering topological DNA entry physically impossible. Since there was no crosslinking at these pockets, the DNA would be naturally lost after SDS treatment. Consequently, the DNA recovery from the Smc2-Brn1 fused condensin could not distinguish between topological and pseudo-topological models of condensin-DNA interaction. Since both of my condensin loading assays also could not directly distinguish between topological and pseudo-topological condensin-DNA interactions, the best experiment would be using non-fusion versions of condensin and then probe DNA recovery after interface crosslinking.

5.2 Condensin forms a DNA-gripping state in the presence of ADP.BeF_3

The DNA-gripping state was first identified and characterised in cohesin and was determined to be the intermediate of loading reaction prior to ATP hydrolysis (Higashi et al. 2020; Shi et al. 2020). Using both the modified condensin IP DNA loading assay and condensin loading onto beads-tethered dsDNA assay, I identified a similar tight DNA-binding state of condensin induced by the ATP transition-state analogue ADP.BeF_3. Comparing the salt-sensitivity of the condensin DNA-gripping state between the two assays, I propose that, in the DNA-gripping state, condensin also forms a topological embracement around the DNA. Consistently, recent condensin DNA-gripping structures showed that DNA is topologically embraced by a channel formed by the ATPase heads, adjacent coiled coils (“neck”), and condensin loader Ycs4 (Shaltiel et al. 2021; Lee, Rhodes, and Löwe 2021). Such DNA-gripping condensin, despite forming a topological embracement around the DNA, behaved differently from the topologically loaded condensin (by ATP).

Compared to the topologically loaded condensin, the DNA-gripping condensin binds DNA in a manner more resistant to middle-salt treatment and cannot be unloaded from the DNA by further incubation with ATP. This potentially means that once condensin grips the DNA, its ATPase heads are tightly engaged so that no nucleotide exchange could occur before ATP hydrolysis and head disengagement. This idea is consistent with the DNA gripping structures for condensin and cohesin, which showed that nucleotides are buried inside the engaged ATPase heads (Higashi et al. 2020; Shi et al. 2020; Shaltiel et al. 2021; Lee, Rhodes, and Löwe 2021). However, this is not compatible with an asymmetric ATPase cycle model, which proposes that the two ATPase heads engages before the second ATP binding (Hassler et al. 2019). Therefore, I propose to modify the asymmetric ATPase cycle model so that the second ATP binding occurs after the dissociation of Cnd1^{Ycs4} from Cut3^{Smc4} induced by the first ATP binding. Then the two heads could engage, resulting in the dissociation of the kleisin N-terminus from the Cut14^{Smc2}.

Overall, the condensin DNA-gripping complex I observed behaved similarly to the cohesin DNA-gripping complex. Since the cohesin DNA-gripping state was proposed to be a loading intermediate, it is reasonable to assume that condensin might follow a similar mechanism for DNA entry. On the other hand, the hinge-Cnd3^{Ycg1} module is still missing from the condensin gripping structure, whereas the cohesin counterpart, hinge-Psc3^{Scc3} module is visible in EM structures, suggesting a more structurally stable conformation of the hinge-Psc3^{Scc3} module in cohesin compared to condensin (Higashi et al. 2020; Shi et al. 2020; Shaltiel et al. 2021; Lee, Rhodes, and Löwe 2021). This difference could be attributed to the flexibility of the Cnd3^{Ycg1} subunit arrangement. Consistently, the condensin Apo structure showed that, due to the “elbow” being closer to the hinge, the hinge cannot reach the ATPase heads even in the folded conformation (Lee et al. 2020), resulting in the hinge-Cnd3^{Scc3} module locating away from the head-Cnd1^{Ycs4}-DNA structure. Alternatively, the missing Cnd3^{Ycg1} could bind elsewhere during DNA-gripping, since a Cnd3^{Ycg1}-head binding mode was also observed in a sub-population of the ATP-bound condensin samples (Lee et al. 2020). The functional significance of this binding

mode requires further confirmation and characterization. Taken together, the missing electron density for the hinge-Cnd3^{Ycg1} module potentially indicated a greater flexibility of Cnd3^{Ycg1} in the DNA-gripping condensin.

5.3 Topologically loaded condensin can unloads from DNA in an ATP-dependent manner

The dynamics of condensin binding to chromatin is important for proper chromosome organisation by condensin (Thadani et al. 2018; Gerlich et al. 2006), but the unloading reaction of condensin is not understood. In contrast to cohesin, which requires different protein factors, Pds5 and Wapl for its unloading (Murayama and Uhlmann 2015), condensin unloading did not require any additional proteins in my condensin unloading assay. This is surprising because cohesin loader Mis4^{Scc2} / Ssl3^{Scc4}, the counterpart of Cnd1^{Ycs4}, cannot support cohesin unloading (Murayama and Uhlmann 2015). Although not confirmed, it is reasonable to assume that the Cnd1^{Ycs4} functions both as the loader and the unloader, given its binding site on condensin kleisin corresponds to that of both cohesin loader and Pds5. On the other hand, the cohesin unloader complex formed by Pds5 and Wapl could support both loading and unloading, and the equilibrium between catalysing loading and unloading reactions depended on salt concentrations (Murayama and Uhlmann 2015). Consistently, I found that condensin loading onto DNA was more efficient in low-salt buffers while unloading dominated at higher salt concentrations. This raises an interesting possibility that Cnd1^{Ycs4} is mechanistically similar to the cohesin loader and unloader complex Pds5/Wapl, rather than the cohesin loader Mis4^{Scc2}/Ssl3^{Scc2}. If so, does condensin have its counterpart of cohesin loader? Alternatively, given that condensin colocalise with cohesin loader (D'Ambrosio et al. 2008), does the cohesin loader also physically interacts with condensin for DNA loading *in vivo*?

Furthermore, compared to the Mis4^{Scc2}/Ssl3^{Scc4} loaded cohesin, where the ATP stimulated loading by 6-fold, the Pds5/Wapl loaded cohesin showed ATP stimulation of only 2.5-fold (Murayama and Uhlmann 2015; 2014). Consistently,

I found that the addition of ATP stimulated condensin loading onto DNA by only 2-fold. Taken together, my reconstituted condensin DNA loading and unloading reactions are biochemically similar to those by cohesin and its unloader complex Pds5/Wapl. Therefore, I propose that Cnd1^{Ycs4} might be the counterpart of the cohesin loader/unloader complex Pds5/Wapl.

5.4 Condensin can sequentially topologically entrap two DNAs

All three models of condensin-mediated mitotic chromosome organisation, namely the torsion-mediated compaction model, the loop extrusion model, and the diffusion capture model, assume that condensin can bind at least two pieces of DNA. Fluorescence microscopy and AFM analyses of condensin on DNA indeed revealed condensin-DNA clusters (Terakawa et al. 2017; J. K. Ryu et al. 2020; Yoshimura et al. 2002). However, the nature of the condensin interaction with two pieces of DNA is poorly understood. By establishing a condensin second DNA capture assay, I demonstrated that condensin can establish interactions between two dsDNA substrates topologically in an ATP-dependent manner. Cohesin, on the other hand, can only topologically entrap a second ssDNA substrate (Murayama et al. 2018). Such difference could potentially reflect on the *in vivo* substrate targeted by these two SMC complexes. Cohesin is loaded onto chromatin in G1 phase and establish sister-chromatid cohesion in G1/S phase; therefore the second DNA substrate that it captures might be the temporarily exposed ssDNA during DNA replication (Murayama et al. 2018). On the other hand, as the cell enters mitosis, condensin is activated and organise chromatin into mitotic chromosome, where dsDNA might be its target.

The single-molecule microscopy revealed that the second dsDNA capture reaction was potentially mediated by a single condensin complex. Given that both the first and second dsDNA loading by condensin are topological, ATP-dependent, and can subsequently be unloaded in an ATP-dependent manner, it is tempting to hypothesize that both the first and second dsDNA substrates

enter the condensin ring via a similar mechanism. On the other hand, considering the proposed loading mechanism based on cohesin DNA-gripping structure, is the same loading mechanism still permissible with one dsDNA already inside the condensin ring? Alternatively, there is some evidence that hinted at the condensin-condensin interactions (Kinoshita et al. 2022).

Both the first and second dsDNA loading by condensin are topological, ATP-dependent, and can subsequently be unloaded in an ATP-dependent manner. Therefore, it is tempting to hypothesize that both the first and second dsDNA substrates enter the condensin ring via a similar mechanism. Given the proposed loading mechanism through sequential kleisin N-gate and ATPase head gate passage, can the same loading mechanism be repeated with one dsDNA already inside the condensin ring? The condensin second dsDNA capture under the microscope revealed that this indeed might be possible and that a single condensin complex sequentially entraps two DNAs. Additional analyses are required to further explore this possibility.

On the other hand, other analyses of condensin-DNA complexes illustrated condensin clusters (Yoshimura et al. 2002; Keenholtz et al. 2017). Such condensin clusters could further promote interactions between more than one DNA. It will be important to investigate whether and how condensin-condensin interactions are formed. One clue comes from *in vitro* mitotic chromosome reconstitution experiments that implied $Cnd1^{Ycs4}$ in an intermolecular interaction with $Cut3^{Smc4}$ from a neighbouring condensin complex (Kinoshita et al. 2022). The mechanism and physiological importance of such interaction requires further characterisation.

Condensin not only topologically entraps dsDNA, but also entraps ssDNA with similar efficiency. While condensin can capture a first or a second ssDNA by topological embrace, these two reactions are biochemically distinct. The first ssDNA capture is ATP-dependent, while second ssDNA capture appears poorly correlated with the availability of ATP. These findings suggest that perhaps the loading mechanism for a second ssDNA substrate differs from that of the first. By its amphipathic and flexible nature, ssDNA might more easily enter and exit

the condensin ring, as compared to a more stiff and highly charged dsDNA. It is also possible that ssDNA uses a fundamentally different entry route into the condensin ring, e.g. during transient opening of the hinge domain (Griese, Witte, and Hopfner 2010). To clarify the mechanism of ssDNA entry into the condensin ring will require further experimentation.

5.5 Diffusion capture as a model for condensin-mediated mitotic chromosome organisation

The torsion-mediated compaction model of how condensin shapes mitotic chromosomes fails to explain how torsional strain is maintained during mitosis in the presence of abundant topoisomerases. The loop extrusion model, although very simplistic at the first sight, makes numerous assumptions on condensin behaviour. These include the required bypass of physical roadblocks while loop extruding, and transforming asymmetric motion into bidirectional compaction. On the other hand, the diffusion capture model assumes only the basic activity of second DNA capture from individual condensin complexes, which I have demonstrated in the presented work. The diffusion capture model can recapitulate mitotic chromosome compaction and individualisation *in silico* and can reproduce the properties of mitotic chromosomes observed *in vivo* (Cheng et al. 2015; Gerguri et al. 2021; Kakui et al. 2020). How does condensin engage in DNA-DNA interactions? My *in vitro* observations of condensin-mediated topological dsDNA-dsDNA capture, and the dynamic condensin turnover that is regulated by ATP, forms a minimal biochemical basis that supports this model. However, many details regarding the diffusion capture model requires further examination. Does the condensin also mediates topological DNA-DNA tethering *in vivo* in the context of chromatin? If so, how do post-translational modifications on condensin regulate its chromatin-chromatin tethering activity *in vivo*? In higher eukaryotes where two versions of condensin exist, does one or both of them engage in second DNA capture? If both condensin I and II can capture a second DNA, then what is the difference that allows condensin II to capture loops about 5 times bigger than condensin I

(Gibcus et al. 2018)? Answers to these questions will help us to further refine the diffusion capture model and hopefully produce a complete picture for condensin-mediated mitotic chromosome organisation.

5.6 Conclusions and outlook

The question of how condensin contributes to mitotic chromosomes formation is still under debate. Using both bulk biochemical experiments and single-molecule fluorescence microscopy, I demonstrated that a single condensin can topologically entrap one or two dsDNA molecules. In addition, I reconstituted the condensin dynamic turnover on the DNA in the presence of ATP. I also discovered that condensin, similar to cohesin, forms a DNA-gripping state prior to ATP hydrolysis using ADP.BeF_3. These observations provide a solid biochemical ground for the diffusion capture model of condensin-mediated mitotic chromosome formation. Now that all three models of chromosome formation, namely the loop extrusion, the torsion-mediated compaction, and the diffusion capture models, are supported by *in vitro* evidence, in the future, it would be crucial to obtain *in vivo* evidence to further support those models. Ideally, separation-of-function mutations of condensin, that disrupts one but not other *in vitro* activities of condensin, could decisively distinguish which model of condensin-mediated chromosome formation is indeed employed *in vivo*. On the other hand, our model of loop extrusion and topological loading by condensin, introduced in Section 1.3.5 and Figure 1.3 suggests that such separation-of-function mutations might be very difficult to construct and possibly very subtle in effect.

Reference List

Alipour, Elnaz, and John F. Marko. 2012. ‘Self-Organization of Domain Structures by DNA-Loop-Extruding Enzymes’. *Nucleic Acids Research* 40 (22): 11202–12. https://doi.org/10.1093/nar/gks925.

Anderson, David E., Ana Losada, Harold P. Erickson, and Tatsuya Hirano. 2002. ‘Condensin and Cohesin Display Different Arm Conformations with Characteristic Hinge Angles’. *Journal of Cell Biology* 156 (3): 419–24. https://doi.org/10.1083/jcb.200111002.

Aono, Nobuki, Takashi Sutani, Takeshi Tomonaga, Satoru Mochida, and Mitsuhiro Yanagida. 2002. ‘Cnd2 Has Dual Roles in Mitotic Condensation and Interphase’. *Nature* 417 (6885): 197–202. https://doi.org/10.1038/417197a.

Banigan, Edward J., Aafke A. van den Berg, Hugo B. Brandão, John F. Marko, and Leonid A. Mirny. 2020. ‘Chromosome Organization by One-Sided and Two-Sided Loop Extrusion’. *ELife* 9 (9): 1–46. https://doi.org/10.7554/eLife.53558.

Banigan, Edward J., and Leonid A. Mirny. 2020. ‘Loop Extrusion: Theory Meets Single-Molecule Experiments’. *Current Opinion in Cell Biology* 64: 124–38. https://doi.org/10.1016/j.ceb.2020.04.011.

Baxter, J., N. Sen, V. López Martínez, M. E. Monturus De Carandini, J. B. Schvartzman, J. F.X. Diffley, and L. Aragón. 2011. ‘Positive Supercoiling of Mitotic DNA Drives Decatenation by Topoisomerase II in Eukaryotes’. *Science* 331 (6022): 1328–32. https://doi.org/10.1126/science.1201538.

Bürmann, Frank, Byung-gil Lee, Thane Than, Ludwig Sinn, Francis J O Reilly, Stanislau Yatskevich, Juri Rappsilber, Bin Hu, Kim Nasmyth, and Jan Löwe. 2019. ‘A Folded Conformation of MukBEF and Cohesin’. *Nature Structural & Molecular Biology* 26 (March): 227–36. https://doi.org/10.1038/s41594-019-0196-z.

Busslinger, Georg A., Roman R. Stocsits, Petra van der Lelij, Elin Axelsson, Antonio Tedeschi, Niels Galjart, and Jan-Michael Peters. 2017. ‘Cohesin Is

Positioned in Mammalian Genomes by Transcription, CTCF and Wapl'. *Nature* 544 (7651): 503–7. https://doi.org/10.1038/nature22063.

Charbin, Adrian, Celine Bouchoux, and Frank Uhlmann. 2014. 'Condensin Aids Sister Chromatid Decatenation by Topoisomerase II'. *Nucleic Acids Research* 42 (1): 340–48. https://doi.org/10.1093/nar/gkt882.

Cheng, Tammy M.K., Sebastian Heeger, Raphaël A.G. Chaleil, Nik Matthews, Aengus Stewart, Jon Wright, Carmay Lim, Paul A. Bates, and Frank Uhlmann. 2015. 'A Simple Biophysical Model Emulates Budding Yeast Chromosome Condensation'. *ELife* 2015 (4): 1–22. https://doi.org/10.7554/eLife.05565.

Csankovszki, Györgyi, Emily L. Petty, and Karishma S. Collette. 2009. 'The Worm Solution: A Chromosome-Full of Condensin Helps Gene Expression Go Down'. *Chromosome Research* 17 (5): 621–35. https://doi.org/10.1007/s10577-009-9061-y.

Cuylen, Sara, Jutta Metz, and Christian H. Haering. 2011. 'Condensin Structures Chromosomal DNA through Topological Links'. *Nature Structural and Molecular Biology* 18 (8): 894–901. https://doi.org/10.1038/nsmb.2087.

D'Ambrosio, Claudio, Christine Katrin Schmidt, Yuki Katou, Gavin Kelly, Takehiko Itoh, Katsuhiko Shirahige, and Frank Uhlmann. 2008. 'Identification of Cis -Acting Sites for Condensin Loading onto Budding Yeast Chromosomes'. *Genes & Development*, 2215–27. https://doi.org/10.1101/gad.1675708.

Davidson, Iain F, Benedikt Bauer, Daniela Goetz, Wen Tang, Gordana Wutz, and Jan-Michael Peters. 2019. 'DNA Loop Extrusion by Human Cohesin.' *Science (New York, N.Y.)* 3418 (November): 1–13. https://doi.org/10.1126/science.aaz3418.

Doughty, Tyler W., Heather E. Arsenault, and Jennifer A. Benanti. 2016. 'Levels of Ycg1 Limit Condensin Function during the Cell Cycle'. *PLoS Genetics* 12 (7): 1–23. https://doi.org/10.1371/journal.pgen.1006216.

Eeftens, Jorine M, Shveta Bisht, Jacob Kerssemakers, Marc Kschonsak, Christian H Haering, and Cees Dekker. 2017. 'Real-time Detection of Condensin-driven DNA Compaction Reveals a Multistep Binding Mechanism'.

The EMBO Journal 36 (23): e201797596. https://doi.org/10.15252/embj.201797596.

Elbatsh, Ahmed M.O., Eugene Kim, Jorine M. Eeftens, Jonne A. Raaijmakers, Robin H. van der Weide, Alberto García-Nieto, Sol Bravo, et al. 2019. 'Distinct Roles for Condensin's Two ATPase Sites in Chromosome Condensation'. *Molecular Cell* 76 (5): 724–37. https://doi.org/10.1016/j.molcel.2019.09.020.

Ganji, Mahipal, Indra A. Shaltiel, Shveta Bisht, Eugene Kim, Ana Kalichava, Christian H. Haering, and Cees Dekker. 2018. 'Real-Time Imaging of DNA Loop Extrusion by Condensin'. *Science* 360: 102–5. https://doi.org/10.1126/science.aar7831.

Gerguri, Tereza, Xiao Fu, Yasutaka Kakui, Bhavin S. Khatri, Christopher Barrington, Paul A. Bates, and Frank Uhlmann. 2021. 'Comparison of Loop Extrusion and Diffusion Capture as Mitotic Chromosome Formation Pathways in Fission Yeast'. *Nucleic Acids Research* 49 (3): 1294–1312. https://doi.org/10.1093/nar/gkaa1270.

Gerlich, Daniel, Toru Hirota, Birgit Koch, Jan Michael Peters, and Jan Ellenberg. 2006. 'Condensin I Stabilizes Chromosomes Mechanically through a Dynamic Interaction in Live Cells'. *Current Biology* 16 (4): 333–44. https://doi.org/10.1016/j.cub.2005.12.040.

Gibcus, Johan H., Kumiko Samejima, Anton Goloborodko, Itaru Samejima, Natalia Naumova, Johannes Nuebler, Masato T. Kanemaki, et al. 2018. 'A Pathway for Mitotic Chromosome Formation'. *Science* 359 (6376): eaao6135. https://doi.org/10.1126/science.aao6135.

Golfier, Stefan, Thomas Quail, Hiroshi Kimura, Jan Brugués, and Jan Brugues. 2020. 'Cohesin and Condensin Extrude DNA Loops in a Cell-Cycle Dependent Manner'. *ELife* 9: e53885. https://doi.org/10.7554/eLife.53885.

Griese, Julia J., Gregor Witte, and Karl Peter Hopfner. 2010. 'Structure and DNA Binding Activity of the Mouse Condensin Hinge Domain Highlight Common and Diverse Features of SMC Proteins'. *Nucleic Acids Research* 38 (10): 3454–65. https://doi.org/10.1093/nar/gkq038.

Gruber, Stephan, Prakash Arumugam, Yuki Katou, Daria Kuglitsch, Wolfgang Helmhart, Katsuhiko Shirahige, and Kim Nasmyth. 2006. ‘Evidence That Loading of Cohesin Onto Chromosomes Involves Opening of Its SMC Hinge’. *Cell* 127 (3): 523–37. https://doi.org/10.1016/j.cell.2006.08.048.

Hassler, Markus, Indra A. Shaltiel, Marc Kschonsak, Bernd Simon, Fabian Merkel, Lena Thärichen, Henry J. Bailey, et al. 2019. ‘Structural Basis of an Asymmetric Condensin ATPase Cycle’. *Molecular Cell*, 1175–88. https://doi.org/10.1016/j.molcel.2019.03.037.

Higashi, Torahiko L., Patrik Eickhoff, Joana S. Sousa, Julia Locke, Andrea Nans, Helen R. Flynn, Ambrosius P. Snijders, et al. 2020. ‘A Structure-Based Mechanism for DNA Entry into the Cohesin Ring’. *Molecular Cell* 79 (6): 917-933.e9. https://doi.org/10.1016/j.molcel.2020.07.013.

Higashi, Torahiko L., Georgii Pobegalov, Minzhe Tang, Maxim I. Molodtsov, and Frank Uhlmann. 2021. ‘A Brownian Ratchet Model for Dna Loop Extrusion by the Cohesin Complex’. *ELife* 10: 1–35. https://doi.org/10.7554/eLife.67530.

Higashi, Torahiko L., and Frank Uhlmann. 2022. ‘SMC Complexes: Lifting the Lid on Loop Extrusion’. *Current Opinion in Cell Biology* 74: 13–22. https://doi.org/10.1016/j.ceb.2021.12.003.

Hirano, Tatsuya. 2012. ‘Condensins: Universal Organizers of Chromosomes with Diverse Functions’. *Genes and Development* 26 (15): 1659–78. https://doi.org/10.1101/gad.194746.112.

———. 2014. ‘Condensins and the Evolution of Torsion-Mediated Genome Organization’. *Trends in Cell Biology* 24 (12): 727–33. https://doi.org/10.1016/j.tcb.2014.06.007.

Hirota, Toru, Daniel Gerlich, Birgit Koch, Jan Ellenberg, and Jan Michael Peters. 2004. ‘Distinct Functions of Condensin I and II in Mitotic Chromosome Assembly’. *Journal of Cell Science* 117 (26): 6435–45. https://doi.org/10.1242/jcs.01604.

Ivanov, Dmitri, and Kim Nasmyth. 2005. ‘A Topological Interaction between Cohesin Rings and a Circular Minichromosome’. *Cell* 122 (6): 849–60. https://doi.org/10.1016/j.cell.2005.07.018.

Jeppsson, Kristian, Takaharu Kanno, Katsuhiko Shirahige, and Camilla Sjögren. 2014. ‘The Maintenance of Chromosome Structure: Positioning and Functioning of SMC Complexes’. *Nature Reviews Molecular Cell Biology* 15 (9): 601–14. https://doi.org/10.1038/nrm3857.

Kakui, Yasutaka, Christopher Barrington, David J. Barry, Tereza Gerguri, Xiao Fu, Paul A. Bates, Bhavin S. Khatri, and Frank Uhlmann. 2020. ‘Fission Yeast Condensin Contributes to Interphase Chromatin Organization and Prevents Transcription-Coupled DNA Damage’. *Genome Biology* 21 (1): 1–25. https://doi.org/10.1186/s13059-020-02183-0.

Keenholtz, Ross A, Thillaivillalan Dhanaraman, Roger Palou, Jia Yu, Damien D ’amours, and John F Marko. 2017. ‘Oligomerization and ATP Stimulate Condensin-Mediated DNA Compaction’. *Scientific Reports*, no. May: 1–13. https://doi.org/10.1038/s41598-017-14701-5.

Kim, Eugene, Jacob Kerssemakers, Indra A. Shaltiel, Christian H. Haering, and Cees Dekker. 2020. ‘DNA-Loop Extruding Condensin Complexes Can Traverse One Another’. *Nature* 579 (7799): 438–42. https://doi.org/10.1038/s41586-020-2067-5.

Kim, Yoori, Zhubing Shi, Hongshan Zhang, Ilya J. Finkelstein, and Hongtao Yu. 2019. ‘Human Cohesin Compacts DNA by Loop Extrusion’. *Science* 366 (6471): 1345–49. https://doi.org/10.1126/science.aaz4475.

Kimura, Keiji, Michiko Hirano, Ryuji Kobayashi, and Tatsuya Hirano. 1998. ‘Phosphorylation and Activation of 13 S Condensin by Cdc2 in Vitro’. *Science* 282 (October): 487–91.

Kimura, Keiji, and Tatsuya Hirano. 1997. ‘ATP-Dependent Positive Supercoiling of DNA by 13S Condensin: A Biochemical Implication for Chromosome Condensation’. *Cell* 90 (4): 625–34. https://doi.org/10.1016/S0092-8674(00)80524-3.

Kimura, Keiji, Valentin V. Rybenkov, Nancy J. Crisona, Tatsuya Hirano, and Nicholas R. Cozzarelli. 1999. '13S Condensin Actively Reconfigures DNA by Introducing Global Positive Writhe: Implications for Chromosome Condensation'. *Cell* 98 (2): 239–48. https://doi.org/10.1016/S0092-8674(00)81018-1.

Kinoshita, Kazuhisa, Tetsuya J. Kobayashi, and Tatsuya Hirano. 2015. 'Balancing Acts of Two HEAT Subunits of Condensin I Support Dynamic Assembly of Chromosome Axes'. *Developmental Cell* 33 (1): 94–107. https://doi.org/10.1016/j.devcel.2015.01.034.

Kinoshita, Kazuhisa, Yuko Tsubota, Shoji Tane, Yuuki Aizawa, Ryota Sakata, Kozo Takeuchi, Keishi Shintomi, Tomoko Nishiyama, and Tatsuya Hirano. 2022. 'A Loop Extrusion–Independent Mechanism Contributes to Condensin I–Mediated Chromosome Shaping'. *Journal of Cell Biology* 221 (3): e202109016. https://doi.org/10.1083/jcb.202109016.

Kong, Muwen, Erin E. Cutts, Dongqing Pan, Fabienne Beuron, Thangavelu Kaliyappan, Chaoyou Xue, Edward P. Morris, Andrea Musacchio, Alessandro Vannini, and Eric C. Greene. 2020. 'Human Condensin I and II Drive Extensive ATP-Dependent Compaction of Nucleosome-Bound DNA'. *Molecular Cell* 79 (1): 99-114.e9. https://doi.org/10.1016/j.molcel.2020.04.026.

Kschonsak, Marc, Fabian Merkel, Shveta Bisht, Jutta Metz, Vladimir Rybin, Markus Hassler, and Christian H. Haering. 2017. 'Structural Basis for a Safety-Belt Mechanism That Anchors Condensin to Chromosomes'. *Cell* 0 (0): 588-600.e24. https://doi.org/10.1016/j.cell.2017.09.008.

Lancaster, Lucy, Harshil Patel, Gavin Kelly, and Frank Uhlmann. 2021. 'A Role for Condensin in Mediating Transcriptional Adaptation to Environmental Stimuli'. *Life Science Alliance* 4 (7): 1–18. https://doi.org/10.26508/lsa.202000961.

Laura Vian, Authors, Aleksandra Pe, Suhas SP Rao, David Levens, Erez Lieberman Aiden, Rafael Casellas, Laura Vian, et al. 2018. 'The Energetics and Physiological Impact of Cohesin Extrusion'. *Cell* 173: 1–14. https://doi.org/10.1016/j.cell.2018.03.072.

Lee, Byung-Gil, Fabian Merkel, Matteo Allegretti, Markus Hassler, Christopher Cawood, Léa Lecomte, Francis J. O'Reilly, et al. 2020. 'Cryo-EM Structures of Holo Condensin Reveal a Subunit Flip-Flop Mechanism'. *Nature Structural & Molecular Biology*, July. https://doi.org/10.1038/s41594-020-0457-x.

Lee, Byung-Gil, James Rhodes, and Jan Löwe. 2021. 'Clamping of DNA Shuts the Condensin Neck Gate'. *BioRxiv* 44 (0): 2021.10.29.466484.

Lengronne, Armelle, Yuki Katou, Saori Mori, Shihori Yokabayashi, Gavin P. Kelly, Takehiko Ito, Yoshinori Watanabe, Katsuhiko Shirahige, and Frank Uhlmann. 2004. 'Cohesin Relocation from Sites of Chromosomal Loading to Places of Convergent Transcription'. *Nature* 430 (6999): 573–78. https://doi.org/10.1038/nature02742.

Maeshima, Kazuhiro, and Ulrich K. Laemmli. 2003. 'A Two-Step Scaffolding Model for Mitotic Chromosome Assembly'. *Developmental Cell* 4 (4): 467–80. https://doi.org/10.1016/S1534-5807(03)00092-3.

Minamino, Masashi, Torahiko L Higashi, Céline Bouchoux, and Frank Uhlmann. 2018. 'Topological in Vitro Loading of the Budding Yeast Cohesin Ring onto DNA'. *Life Science Alliance* 1 (5): e201800143. https://doi.org/10.26508/lsa.201800143.

Molodtsov, Maxim I., Christine Mieck, Jeroen Dobbelaere, Alexander Dammermann, Stefan Westermann, and Alipasha Vaziri. 2016. 'A Force-Induced Directional Switch of a Molecular Motor Enables Parallel Microtubule Bundle Formation'. *Cell* 167 (2): 539-552.e14. https://doi.org/10.1016/j.cell.2016.09.029.

Muñoz, Sofía, Masashi Minamino, Corella S. Casas-Delucchi, Harshil Patel, and Frank Uhlmann. 2019. 'A Role for Chromatin Remodeling in Cohesin Loading onto Chromosomes'. *Molecular Cell* 74 (4): 664-673.e5. https://doi.org/10.1016/j.molcel.2019.02.027.

Muñoz, Sofía, Francesca Passarelli, and Frank Uhlmann. 2020. 'Conserved Roles of Chromatin Remodellers in Cohesin Loading onto Chromatin'. *Current Genetics* 66 (5): 951–56. https://doi.org/10.1007/s00294-020-01075-x.

Murayama, Yasuto, Catarina P. Samora, Yumiko Kurokawa, Hiroshi Iwasaki, and Frank Uhlmann. 2018. 'Establishment of DNA-DNA Interactions by the Cohesin Ring'. *Cell* 172 (3): 465-469.e15. https://doi.org/10.1016/j.cell.2017.12.021.

Murayama, Yasuto, and Frank Uhlmann. 2014. 'Biochemical Reconstitution of Topological DNA Binding by the Cohesin Ring'. *Nature* 505 (7483): 367–71. https://doi.org/10.1038/nature12867.

———. 2015. 'DNA Entry into and Exit out of the Cohesin Ring by an Interlocking Gate Mechanism'. *Cell* 163 (7): 1628–40. https://doi.org/10.1016/j.cell.2015.11.030.

Nakazawa, Norihiko, Rajesh Mehrotra, Masahiro Ebe, and Mitsuhiro Yanagida. 2011. 'Condensin Phosphorylated by the Aurora-B-like Kinase Ark1 Is Continuously Required until Telophase in a Mode Distinct from Top2'. *Journal of Cell Science* 124 (11): 1795–1807. https://doi.org/10.1242/jcs.078733.

Nasmyth, Kim. 2001. 'Disseminating the Genome: Joining, Resolving, and Separating Sister Chromatids During Mitosis and Meiosis'. *Annual Review of Genetics* 35 (1): 673–745. https://doi.org/10.1146/annurev.genet.35.102401.091334.

Nichols, Michael H., and Victor G. Corces. 2018. 'A Tethered-Inchworm Model of SMC DNA Translocation'. *Nature Structural and Molecular Biology* 25 (10): 906–10. https://doi.org/10.1038/s41594-018-0135-4.

Niki, Hironori, Aline Jaffe, Ryu Imamura, Teru Ogura, and Sota Hiraga. 1991. 'The New Gene MukB Codes for a 177 Kd Protein with Coiled-Coil Domains Involved in Chromosome Partitioning of E.Coli'. *The EMBO Journal* 10 (1): 183–93.

Ono, Takao, Yuda Fang, David L Spector, and Tatsuya Hirano. 2004. 'Spatial and Temporal Regulation of Condensins I and II in Mitotic Chromosome Assembly in Human Cells □ D'. *Molecular Biology of the Cell* 15: 3296–3308. https://doi.org/10.1091/mbc.E04.

Ono, Takao, Ana Losada, Michiko Hirano, Michael P. Myers, Andrew F. Neuwald, and Tatsuya Hirano. 2003. 'Differential Contributions of Condensin I and Condensin II to Mitotic Chromosome Architecture in Vertebrate Cells'. *Cell* 115 (1): 109–21. https://doi.org/10.1016/S0092-8674(03)00724-4.

Palou, Roger, Thillaivillalan Dhanaraman, Rim Marrakchi, Mirela Pascariu, Mike Tyers, and Damien D'Amours. 2018. *Condensin ATPase Motifs Contribute Differentially to the Maintenance of Chromosome Morphology and Genome Stability*. *PLOS Biology*. Vol. 16. https://doi.org/10.1371/journal.pbio.2003980.

Poirier, Michael G, and John F Marko. 2002. 'Mitotic Chromosomes Are Chromatin Networks without a Mechanically Contiguous Protein Scaffold.' *Proceedings of the National Academy of Sciences of the United States of America* 99 (24): 15393–97. https://doi.org/10.1073/pnas.232442599.

Pradhan, Biswajit, Roman Barth, Eugene Kim, Iain F. Davidson, Benedikt Bauer, Theo van Laar, Wayne Yang, et al. 2021. 'SMC Complexes Can Traverse Physical Roadblocks Bigger than Their Ring Size'. *BioRxiv*.

Rhodes, James DP D.P., Davide Mazza, Kim A. Nasmyth, and Stephan Uphoff. 2017. 'Scc2/Nipbl Hops between Chromosomal Cohesin Rings after Loading'. *ELife* 6: e30000. https://doi.org/10.7554/ELIFE.30000.

Ryu, Je Kyung, Allard J. Katan, Eli O. van der Sluis, Thomas Wisse, Ralph de Groot, Christian H. Haering, and Cees Dekker. 2020. 'The Condensin Holocomplex Cycles Dynamically between Open and Collapsed States'. *Nature Structural and Molecular Biology* 27 (12): 1134–41. https://doi.org/10.1038/s41594-020-0508-3.

Ryu, Je-kyung, Sang-hyun Rah, Richard Janissen, Jacob W J Kerssemakers, Andrea Bonato, Davide Michieletto, and Cees Dekker. 2021. 'Condensin Extrudes DNA Loops in Steps up to Hundreds of Base Pairs That Are Generated by ATP Binding Events'. *Nucleic Acids Research*, 1–13.

Ryu, Je-Kyung, Sang-Hyun Rah, Richard Janissen, Jacob W. J. Kerssemakers, and Cees Dekker. 2020. 'Resolving the Step Size in Condensin-Driven DNA

Loop Extrusion Identifies ATP Binding as the Step-Generating Process'. *BioRxiv*. https://doi.org/10.2139/ssrn.3728949.

Saka, Yasushi, Takashi Sutani, Yukiko Yamashita, Shigeaki Saitoh, Masahiro Takeuchi, Yukinobu Nakaseko, and Mitsuhiro Yanagida. 1994. 'Fission Yeast Cut3 and Cut14, Members of a Ubiquitous Protein Family, Are Required for Chromosome Condensation and Segregation in Mitosis'. *EMBO Journal* 13 (20): 4938–52. https://doi.org/10.1002/j.1460-2075.1994.tb06821.x.

Sawitzke, James A., and Stuart Austin. 2000. 'Suppression of Chromosome Segregation Defects of Escherichia Coli Muk Mutants by Mutations in Topoisomerase I'. *Proceedings of the National Academy of Sciences of the United States of America* 97 (4): 1671–76. https://doi.org/10.1073/pnas.030528397.

Schalch, Thomas, Sylwia Duda, David F. Sargent, and Timothy J. Richmond. 2005. 'X-Ray Structure of a Tetranucleosome and Its Implications for the Chromatin Fibre.' *Nature* 436 (7047): 138–41. https://doi.org/10.1038/nature03686.

Shaltiel, Indra A, Sumanjit Datta, Léa Lecomte, Markus Hassler, Marc Kschonsak, Sol Bravo, Catherine Stober, Sebastian Eustermann, and Christian H Haering. 2021. 'A Hold-and-Feed Mechanism Drives Directional DNA Loop Extrusion by Condensin'. *BioRxiv* 50: 2021.10.29.466147.

Shi, Zhubing, Haishan Gao, Xiao-chen Bai, and Hongtao Yu. 2020. 'Cryo-EM Structure of the Human Cohesin-NIPBL-DNA Complex'. *Science* 368: 1454–59.

Shintomi, Keishi, Hirano, Tatsuya, Keishi Shintomi, and Tatsuya Hirano. 2011. 'The Relative Ratio of Condensin I to II Determines Chromosome Shapes'. *Genes & Development* 25: 1464–69. https://doi.org/10.1101/gad.2060311.

Shintomi, Keishi, Fukashi Inoue, Hiroshi Watanabe, Keita Ohsumi, Miho Ohsugi, and Tatsuya Hirano. 2017. 'Mitotic Chromosome Assembly despite Nucleosome Depletion in Xenopus Egg Extracts'. *Science* 356 (6344): 1284–87. https://doi.org/10.1126/science.aam9702.

Shintomi, Keishi, Tatsuro S. Takahashi, and Tatsuya Hirano. 2015. 'Reconstitution of Mitotic Chromatids with a Minimum Set of Purified Factors'. *Nature Cell Biology*. https://doi.org/10.1038/ncb3187.

Srinivasan, Madhusudhan, Johanna C. Scheinost, Naomi J. Petela, Thomas G. Gligoris, Maria Wissler, Sugako Ogushi, James E. Collier, et al. 2018. 'The Cohesin Ring Uses Its Hinge to Organize DNA Using Non-Topological as Well as Topological Mechanisms'. *Cell* 173 (6): 1508-1519.e18. https://doi.org/10.1016/j.cell.2018.04.015.

St-Pierre, Julie, Mélanie Douziech, Franck Bazile, Mirela Pascariu, Éric Bonneil, Véronique Sauvé, Hery Ratsima, and Damien D'Amours. 2009. 'Polo Kinase Regulates Mitotic Chromosome Condensation by Hyperactivation of Condensin DNA Supercoiling Activity'. *Molecular Cell* 34 (4): 416–26. https://doi.org/10.1016/j.molcel.2009.04.013.

Sutani, Takashi, Toyonori Sakata, Ryuichiro Nakato, Koji Masuda, Mai Ishibashi, Daisuke Yamashita, Yutaka Suzuki, Tatsuya Hirano, Masashige Bando, and Katsuhiko Shirahige. 2015. 'Condensin Targets and Reduces Unwound DNA Structures Associated with Transcription in Mitotic Chromosome Condensation'. *Nature Communications* 6: 1–13. https://doi.org/10.1038/ncomms8815.

Terakawa, Tsuyoshi, Shveta Bisht, Jorine M. Eeftens, Cees Dekker, Christian H. Haering, and Eric C. Greene. 2017. 'The Condensin Complex Is a Mechanochemical Motor That Translocates along DNA'. *Science* 6516 (September): eaan6516. https://doi.org/10.1101/137711.

Thadani, Rahul, Julia Kamenz, Sebastian Heeger, Sofia Munoz, and Frank Uhlmann. 2018. 'Cell-Cycle Regulation of Dynamic Chromosome Association of the Condensin Complex'. *Cell Reports*, 2308–17. https://doi.org/10.1016/j.celrep.2018.04.082.

Toselli-Mollereau, Esther, Xavier Robellet, Lydia Fauque, Sébastien Lemaire, Christoph Schiklenk, Carlo Klein, Clémence Hocquet, et al. 2016. 'Nucleosome Eviction in Mitosis Assists Condensin Loading and Chromosome

Condensation'. *The EMBO Journal* 35 (14): 1565–81. https://doi.org/10.15252/embj.201592849.

Uhlmann, Frank. 2016. 'SMC Complexes: From DNA to Chromosomes'. *Nature Reviews Molecular Cell Biology* 17 (7): 399–412. https://doi.org/10.1038/nrm.2016.30.

Wang, Bi-Dar, David Eyre, Munira Basrai, Michael Lichten, and Alexander Strunnikov. 2005. ' Condensin Binding at Distinct and Specific Chromosomal Sites in the Saccharomyces Cerevisiae Genome '. *Molecular and Cellular Biology* 25 (16): 7216–25. https://doi.org/10.1128/mcb.25.16.7216-7225.2005.

Wang, Xindan., Hugo B. Brandão, Tung B. K. Le, Michael T. Laub, and David Z. Rudner. 2017. 'Bacillus Subtilis SMC Complexes Juxtapose Chromosome Arms as They Travel from Origin to Terminus'. *Science* 355 (6324): 524–27. https://doi.org/10.1126/science.aai8982.

Woodcock, Christopher L, and Rajarshi P Ghosh. 2010. 'Chromatin Higher-Order Structure and Dynamics'. *Cold Spring Harbor Perspectives in Biology* 2: a000596.

Yoshimura, Shige H., Kohji Hizume, Akiko Murakami, Takashi Sutani, Kunio Takeyasu, and Mitsuhiro Yanagida. 2002. 'Condensin Architecture and Interaction with DNA: Regulatory Non-SMC Subunits Bind to the Head of SMC Heterodimer'. *Current Biology* 12 (6): 508–13. https://doi.org/10.1016/S0960-9822(02)00719-4.